Observatório Nacional

Divisão de Programas de Pós-Graduação

MÉTODOS DE REDES COMPLEXAS MONO E MULTICAMADAS APLICADOS À SISMOLOGIA

Jennifer Ribeiro Silvério da Conceição

Dissertação apresentada ao Programa de Pós-graduação em Geofísica do Observatório Nacional, como parte dos requisitos necessários à obtenção do título de Mestre em Geofísica.

Orientador(a): Dr. Douglas Santos Rodrigues Ferreira

Coorientador(a): Dr. Andrés Reinaldo Rodriguez Papa

Rio de Janeiro
Agosto de 2023

“MÉTODOS DE REDES COMPLEXAS MONO E MULTICAMADAS APLICADOS À SISMOLOGIA”

Jennifer Ribeiro Silvério da Conceição

DISSERTAÇÃO SUBMETIDA AO CORPO DOCENTE DO PROGRAMA DE PÓS-GRADUAÇÃO EM GEOFÍSICA DO OBSERVATÓRIO NACIONAL COMO PARTE DOS REQUISITOS NECESSÁRIOS PARA A OBTENÇÃO DO GRAU DE MESTRA EM GEOFÍSICA.

Aprovada por:

Douglas Santos Rodrigues Ferreira

Dr. Douglas Santos Rodrigues Ferreira - (Orientador) - (ON)

Diogo Luiz de Oliveira Coelho

Dr. Diogo Luiz de Oliveira Coelho – (ON)

Dr. Ronaldo Menezes - (University of Exeter - Inglaterra)

RIO DE JANEIRO – BRASIL

04 DE AGOSTO DE 2023

Ribeiro Silvério da Conceição, Jennifer

Métodos de Redes Complexas Mono e Multicamadas Aplicados à Sismologia/Jennifer Ribeiro Silvério da Conceição. – Rio de Janeiro: ON, 2023.

111 p. 29, 7cm.

Orientador(a): Douglas Santos Rodrigues Ferreira

Coorientador(a): Andrés Reinaldo Rodriguez Papa

Dissertação (mestrado) – ON/Programa de Pós-graduação em Geofísica, 2023.

1. Terremotos. 2. Sistemas Complexos. 3. Mecânica Estatística Não-Extensiva. 4. Redes Complexas. 5. Modelo Olami-Feder-Christensen. I. Reinaldo Rodriguez Papa, Andrés. II. Observatório Nacional, Programa de Pós-graduação em Geofísica. III. Título.

Agradecimentos

- Em primeiro lugar, a Deus, pelo dom da vida e por todas as belezas nesse mundo fascinante. Pela força e perseverança nos momentos difíceis, e pela alegria ao superá-los.

- Ao Douglas, que mais do que um orientador, sempre foi um grande amigo. Agradeço por ter me proporcionado oportunidades únicas, por ter me ensinado lições valiosas, tanto acadêmicas quanto pessoais, e por ser um exemplo de profissional e de pessoa. Por ter acreditado em mim desde o início, quando eu ainda estava no ensino médio. Se não fosse isso, sem dúvidas, não estaria aqui agora. Saiba que é um privilégio ser sua aluna, e que levarei seus ensinamentos por toda a vida.

- À minha mãe, que, apesar de todas as dificuldades que passou em toda sua vida, jamais deixou de ser companheira e amiga. Agradeço também pela paciência nos momentos em que estive ausente. Você é o exemplo de mãe guerreira e excepcional, e tenho muito orgulho de ser sua filha.

- Aos meus irmãos, que tanto acreditam no meu potencial e sempre demonstraram muito carinho por mim.

- Ao meu coorientador Papa, por ter aceitado me coorientar e sempre estar à disposição para me ajudar.

- À Coordenação de Pós-Graduação em Geofísica do ON, que prontamente me ajudou sempre que precisei.

Resumo da Dissertação apresentada ao Programa de Pós-Graduação em Geofísica do Observatório Nacional como parte dos requisitos necessários para a obtenção do título de Mestre em Geofísica.

MÉTODOS DE REDES COMPLEXAS MONO E MULTICAMADAS APLICADOS À SISMOLOGIA

Jennifer Ribeiro Silvério da Conceição

Agosto/2023

Neste projeto, foram estudados dados de terremotos globais reais e sintéticos sob a perspectiva de Redes Complexas e da Mecânica Estatística Não-Extensiva (MENE). Através da análise de distribuições de probabilidade espaciais e temporais entre terremotos sucessivos, foi investigado o comportamento de sistemas complexos no fenômeno sismológico, sendo observada concordância entre essas distribuições e funções não tradicionais, q-exponenciais, presentes na teoria da MENE. Essas funções surgem em sistemas que possuem fortes correlações de longo alcance temporal e espacial entre os seus elementos, e foram encontradas em trabalhos anteriores para terremotos regionais e globais. Além disso, encontrou-se relações que proporcionaram invariância de escala nos eventos sísmicos observados e simulados, de forma a ser mais uma evidência da característica complexa presente no fenômeno sismológico. Ademais, foram construídas redes complexas de epicentros utilizando duas abordagens: mono e multicamadas. No primeiro caso, foram considerados dois modelos de ligação, sucessivo e de janela de tempo, para estabelecer relações entre locais distintos do mundo. Através da análise de propriedades topológicas das redes criadas, como a função de correlação de grau e o coeficiente de correlação de grau, revelou-se que terremotos rasos (profundidade de até 70 km) apresentam comportamento assortativo, com regiões onde ocorreram terremotos de grande magnitude mostrando fortes correlações entre si. Em contraste, redes de terremotos profundos (profundidade maior que 70 km) exibem comportamento neutro (aleatório) sem correlação específica entre si. Também foram criadas redes temporais *multiplex* sucessivas de terremotos globais, revelando propriedades únicas em redes de terremotos, que não são visíveis em redes simples. Foi encontrado que as distribuições de *strength* dessas redes seguem um comportamento de lei de potência com corte exponencial. O coeficiente de aglomeração global das redes *multiplex* de eventos rasos possui invariância de escala, enquanto redes *multiplex* de terremotos profundos

exibem comportamento semelhante aos das redes aleatórias similares. Os resultados indicam semelhanças e diferenças entre terremotos rasos e profundos em vários contextos. Ademais, fortalecem a hipótese de que a Terra se encontra em um estado crítico e da possível existência de relações entre eventos espacial e temporalmente afastados.

Abstract of the Dissertation presented to the National Observatory's Graduate Program in Geophysics as a partial fulfillment of the requirements for the degree of Master in Geophysics.

MONO AND MULTILAYER COMPLEX NETWORK METHODS APPLIED TO SEISMOLOGY

Jennifer Ribeiro Silvério da Conceição

August/2023

In this work, we studied real and synthetic earthquake data from the viewpoint of Complex Networks and Nonextensive Statistical Mechanics (NESM). Through the analysis of spatial and temporal probability distributions between successive earthquakes, the behavior of complex systems in the seismological phenomenon was investigated, being observed agreement between these distributions and non-traditional functions, q-exponential, present in the theory of NESM. These functions arise in systems that have strong long-range temporal and spatial correlations between their elements, and have been found in previous works for regional and global earthquakes. In addition, we found relationships that provided scale invariance in the observed and simulated seismic events, being one more evidence of the presence of complex characteristics in the seismological phenomenon. Furthermore, complex networks of epicenters were constructed using two approaches: monolayer and multilayer. In the first case, we considered two models of connection, successive and time window, to establish relationships between different locations in the world. Through the analysis of topological properties of the created networks, such as the degree correlation function and the degree correlation coefficient, it was revealed that shallow earthquakes (depth of up to 70 km) has assortative behavior, which means regions where occurred earthquakes with great magnitude are strongly correlated to each other. In contrast, networks of deep earthquake (depth greater than 70 km) exhibit neutral (random) behavior with no specific correlation between them. We also created temporal *multiplex* networks of successive connections for global earthquakes, and they revealed unique properties in earthquake networks that were not visible in simple networks. We observed the distributions of *strength* of these networks follow a power law with exponential cutoff behavior. The global clustering coefficient of the *multiplex* networks of shallow earthquakes presents scale invariance, while networks

of deep events exhibit behavior similar to random networks. The results indicate similarities and differences between shallow and deep earthquakes in various contexts. Furthermore, they strengthen the hypothesis that the Earth is in a critical state and the possible existence of relationships between spatially and temporally distant events.

Sumário

Lista de Figuras

Capítulo 1

Introdução

1.1 Considerações Gerais

Nos últimos 20 anos, observamos a ocorrência de terremotos de grandes magnitudes, dentre os quais podem ser destacados: o terremoto de magnitude 9,1 (M_W) em Sumatra (2004), de magnitude 8,8 (M_W) no Chile (2010) e o de magnitude 9,1 (M_W) no Japão (2011)[1]. Somados, esses eventos ocasionaram a perda de centenas de milhares de vidas e enormes danos econômicos. Entretanto, a ocorrência de eventos catastróficos não está relacionada necessariamente a esses terremotos de magnitude acima de 8,0 (M_W). Um exemplo a ser citado é o terremoto de magnitude 7,0 (M_W) ocorrido no Haiti, em 2010, que culminou com a morte de mais de 217 000 pessoas [1] e o colapso de diversas estruturas.

Recentemente, no dia 06 de fevereiro de 2023, mais um desastre humanitário de proporções insondáveis ocorreu, desta vez na região entre a Turquia e a Síria, em razão de um tremor de magnitude 7,8 (M_W) e suas réplicas, que provocaram a morte de mais de 50 000 pessoas. Assim, a melhor compreensão sobre a dinâmica responsável pelos fenômenos sismológicos é de extrema importância para diversas áreas do conhecimento, tais como engenharia e as ciências social, geofísica e geológica.

Atualmente, sabemos que dinâmica de falhas é o mecanismo responsável pela maioria dos eventos sísmicos: o atrito de falhas é frequentemente instável, de forma que deslizamentos ocorrem rapidamente enquanto uma ruptura se propaga dinamicamente pela superfície da falha. Esses movimentos repentinos geram ondas sísmicas [2]. O ponto onde ocorre a fratura e a consequente liberação de energia na forma de ondas sísmicas é chamado de hipocentro (ou foco) e o local logo acima do foco, na superfície terrestre, é denominado epicentro. Como pode ser observado na Fig. 1.1, os limites de placas tectônicas são as regiões mais sismicamente ativas.

Apesar dos conhecimentos existentes, a dinâmica envolvida no processo de produção

[1] https://www.usgs.gov/programs/earthquake-hazards/science/20-largest-earthquakes-world

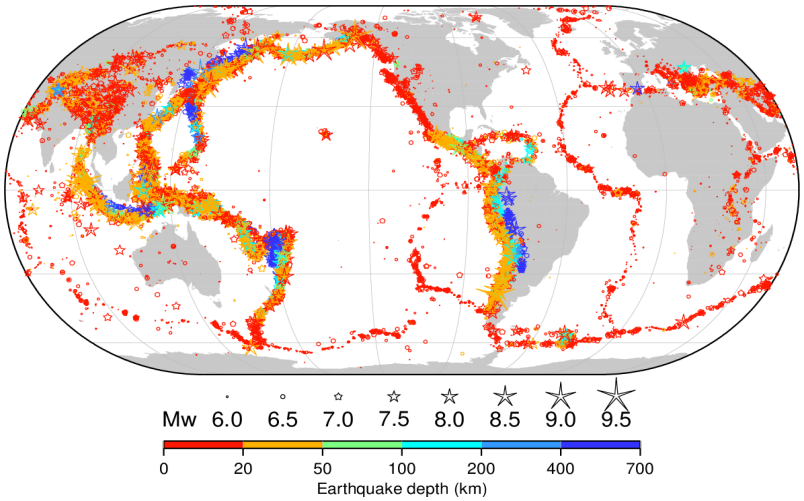

Fig. 1.1: Mapa mostrando cerca de 49 000 terremotos que ocorreram entre 1904 e 2018. Os tamanhos dos símbolos representam as diferentes magnitudes e as cores as diferentes profundidades, de acordo com a escala apresentada na figura. Podemos observar a concentração de terremotos nas delimitações das placas tectônicas. Fonte: extraído de http://www.isc.ac.uk/iscgem/overview.php. Acesso em 27 de fevereiro de 2023.

de eventos sísmicos em todo o planeta permanece um aspecto intrigante e estudado por diversos cientistas por meio de diferentes ferramentas e metodologias.

Dentre as mais variadas metodologias utilizadas para estudar os terremotos, a análise de suas propriedades estatísticas possui grande destaque, sendo a lei de Gutenberg-Richter (GR) [3], que descreve a frequência dos terremotos em razão de sua magnitude, e a lei de Omori [4], para a evolução temporal da frequência de réplicas, resultados estatísticos amplamente conhecidos e utilizados na sismologia. Uma característica interessante dessas leis é o fato de serem caracterizadas por distribuições que seguem leis de potência (no caso da lei de GR, esse comportamento surge quando a escrevemos na forma de energia, ao invés da magnitude dos terremotos), o que leva à hipótese de que o fenômeno sismológico se comporta como um sistema complexo.

Apesar de não haver uma definição teórica precisa de sistemas complexos e complexidade, esses conceitos podem ser estabelecidos a partir de um conjunto de características. Assim, sistemas complexos podem ser entendidos como sistemas auto-organizados constituídos por um elevado número de elementos que interagem entre si de maneira não-linear, de modo que a complexidade surge como resultado dos padrões de interação [5, 6]. Nesses tipos de sistemas, sua evolução é muito sensível a pequenas perturbações ou a condições iniciais. Um fenômeno peculiar observado em vários sistemas complexos é o aparecimento de funções de distribuições em lei de potência de grandezas medidas. Essas distribuições possuem a mesma forma quando a quantidade medida é redimensionada, por essa razão, são ditas invariantes

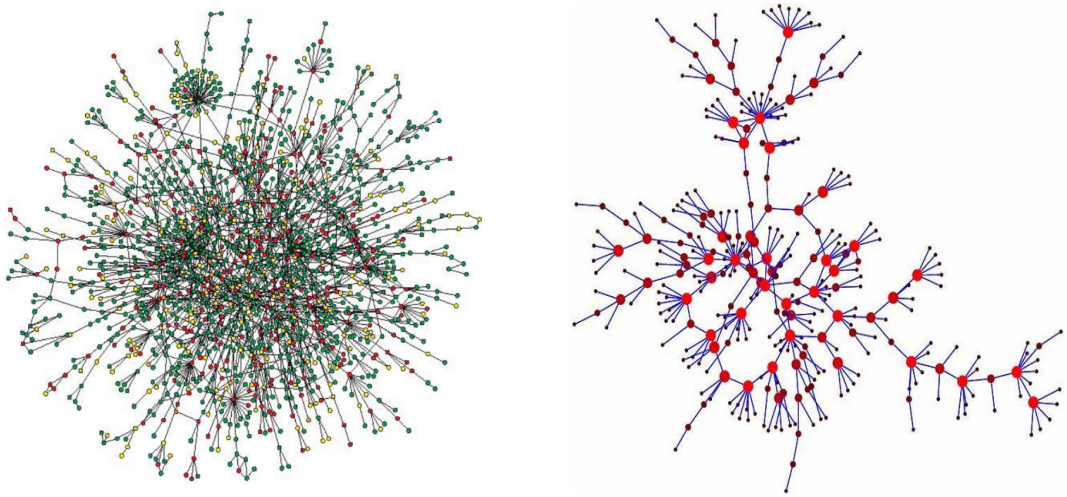

(a) (b)

Fig. 1.2: Exemplos de redes complexas. (a) Rede de interações proteína-proteína [8] e (b) rede de contatos sexuais entre indivíduos [9]. Os vértices estão representados por círculos coloridos e as arestas por linhas retas.

por escala [7].

Dessa forma, tendo em vista o comportamento complexo dos terremotos, precisamos buscar métodos de análise que sejam adequados para esse tipo de sistema. Nesse sentido, a teoria de Redes Complexas é uma ferramenta muito promissora no estudo de sistemas formados por um grande número de constituintes que interagem entre si de forma não linear. Essa teoria utiliza conceitos provenientes da teoria dos grafos, em que os vértices (ou nós) representam os elementos da rede, e as relações entre esses elementos são representadas por arestas (ou ligações) que os conectam (Fig. 1.2).

Através da construção de uma rede, podemos entender diversos sistemas reais, variando desde os tecnológicos aos biológicos. Por exemplo, o cérebro humano é constituído de um enorme conjunto de neurônios conectados por sinapses; a Internet é formada por roteadores e cabos de computador; a sociedade é composta de pessoas que interagem entre si por diferentes relações sociais [10, 11, 12]. Além disso, redes complexas também têm sido aplicadas ao estudo de geociências, como teleconexões de chuvas extremas [13], ciclones tropicais [14] e erupções solares [15].

É interessante notar que, apesar de existirem diferenças entre os variados sistemas complexos encontrados na natureza, as estruturas dessas redes são muito semelhantes, visto que eles são regidos pelos mesmos princípios. Por essa razão, a mesma abordagem matemática e computacional pode ser utilizada para estudá-los. No caso dos terremotos, nosso sistema de interesse, após os trabalhos de Abe e Suzuki [16, 17] que introduziram a ideia de redes de terremotos, diversos estudos têm utilizado esse método para analisar a estrutura desse sitema complexo [18, 19, 20, 21, 22, 23, 24],

obtendo resultados muito promissores.

Neste trabalho, iremos analisar redes de epicentros de dois tipos: monocamadas e multicamadas. A teoria de redes multicamadas é uma área recente, que nasceu com o intuito de melhor modelar e caracterizar sistemas que apresentam diferentes tipos de correlação, chamados "aspectos" [25, 26]. Um exemplo de aplicação de redes multicamadas são redes temporais *multiplex*, a partir das quais é possível estabelecer um melhor entendimento sobre a dinâmica temporal dos eventos de um sistema [25, 27].

Além disso, ainda dentro do estudo de sistemas complexos, outra teoria que apresenta resultados interessantes é a Mecânica Estatística Não-Extensiva (MENE). Essa teoria foi proposta por Constantino Tsallis [28], sendo capaz de analisar sistemas que apresentam interações e memória de longo alcance e condições de contorno (multi)fractais [29], casos em que a mecânica estatística de Boltzmann-Gibbs (BG) não se aplica [30, 31, 32, 33]. A MENE possibilita o estudo de sistemas com propriedades como interação de longo alcance entre seus elementos, memória temporal de longo alcance, evolução fractal do espaço de fase e certos tipos de dissipação de energia, sendo aplicada a diversos fenômenos distintos, incluindo fenômenos geofísicos, como reversão do campo geomagnético, emissões pré-sismicas, erupções solares e fratura em rochas [34, 35, 32, 36].

Na sismologia, diversos trabalhos aplicaram a teoria da MENE para analisar distribuições de probabilidade de propriedades tais como magnitude, diferenças de magnitude, intervalo de tempo entre terremotos subsequentes e distância entre eventos consecutivos [37, 38, 39, 22, 40, 41]. Além disso, a MENE também já foi aplicada em vários estudos de redes de epicentros [42, 23, 24], mostrando evidência da relação entre a MENE e as redes complexas [43, 44].

1.2 Motivação

Diversos trabalhos apontam para a existência de interações devidas a correlações de longo alcance no fenômeno sismológico [39, 38, 23, 24]. Assim, é evidente procurar por esses tipos de interações para que se tenha um melhor entendimento da dinâmica dos terremotos e de possíveis correlações entre diferentes terremotos e locais. Ademais, através da transformação de uma série temporal em uma rede, de acordo com algum algoritmo de mapeamento específico, é possível extrair informações sobre a série temporal através da análise da rede derivada.

Dessa forma, neste trabalho consideramos essas propriedades dos terremotos para estudar e caracterizar estatisticamente os eventos sísmicos, e investigar as correlações existentes entre eles, considerando parâmetros como magnitude, distância e intervalo de tempo de ocorrência, de terremotos globais e terremotos simulados

computacionalmente. Buscamos encontrar, dentre outras coisas, distribuições de probabilidade em lei de potência, características fractais, como invariância de escala espacial e temporal, e expoentes críticos universais.

1.3 Objetivos

O presente trabalho tinha por objetivo contribuir para um entendimento mais aprofundado acerca dos processos dinâmicos envolvidos no desencadeamento de terremotos pelo planeta, através da aplicação da teoria de sistemas complexos. Para tanto, foram realizados os seguintes itens:

- Construção de distribuições de probabilidade de intervalo de tempo e distância entre terremotos sucessivos reais e terremotos simulados com o modelo de Olami-Feder-Christensen (OFC) com topologia mundo-pequeno;
- Análise das distribuições de probabilidade espaço-temporais sob a perspectiva da Mecânica Estatística Não-Extensiva;
- Busca de relações de escala para as distribuições de probabilidade espaço-temporais dos terremotos e investigação da influência de parâmetros, como a magnitude dos eventos, nessas distribuições.
- Construção de redes de epicentros globais rasos e profundos seguindo dois modelos de criação: o modelo sucessivo e o modelo de "janela de tempo";
- Construção de redes de epicentros sucessivos utilizando dados de terremotos sintéticos gerados com o modelo de OFC com topologia mundo-pequeno;
- Análise da assortatividade das redes construídas utilizando dois métodos: a distribuição de conectividade dos vizinhos mais próximos dos vértices e o coeficiente de correlação de grau;
- Construção de redes temporais *multiplex* com os dados de terremotos globais rasos e profundos seguindo o modelo de conexões sucessivas;
- Análise das propriedades topológicas dessas redes e sua variação com o número de camadas (anos) considerados.

1.4 Estrutura e Organização da Dissertação

A estrutura e organização dos capítulos que integram a presente dissertação são apresentadas a seguir.

Este capítulo (Capítulo 1), sendo a Introdução, expressa as ideias gerais sobre o tema do trabalho.

O Capítulo 2 discorre sobre a investigação de relações de escala em distribuições de probabilidade da distância e do intervalo de tempo entre terremotos sucessivos, considerando tanto catálogos de terremotos sintéticos (gerados com o modelo OFC modeficado) quanto dados de catálogos reais obtidos a partir de observatórios sismológicos. O artigo a que esse capítulo se refere foi publicado em *Chaos, Solitons & Fractals, v. 165, pp. 112814. DOI:10.1016/j.chaos.2022.112814.*

No Capítulo 3 foram implementados métodos de construção de redes (monocamadas) de epicentros seguindo o modelo de ligações sucessivas e o modelo de "janela de tempo". As análises foram realizadas para terremotos globais e terremotos simulados com o modelo OFC com topologia mundo-pequeno. Os resultados desse estudo foram publicados em *Brazilian Journal of Geophysics, v.40, n.1. DOI: 10.22564/brjg.v40i1.2134.*

No Capítulo 4 foi aplicada a abordagem de redes multicamadas para estudar terremotos de todo o mundo. Foram construídas redes temporais *multiplex* para buscar variações na atividade sísmica global ao longo dos anos.

A dissertação termina no Capítulo 5, onde as considerações finais sobre o trabalho são realizadas e, além disso, são apresentadas perspectivas futuras de análises e investigações.

Referências Bibliográficas

[1] Marc O Eberhard, Steven Baldridge, Justin Marshall, Walter Mooney, and Glenn J Rix. The mw 7.0 haiti earthquake of january 12, 2010: Usgs/eeri advance reconnaissance team report. *US Geological Survey Open-File Report*, 1048(2013):64, 2010.

[2] Christopher H Scholz. *The mechanics of earthquakes and faulting*. Cambridge university press, 2019.

[3] Beno Gutenberg and Carl F Richter. Earthquake magnitude, intensity, energy, and acceleration: (second paper). *Bulletin of the seismological society of America*, 46(2):105–145, 1956.

[4] Fusakichi Omori. On the aftershocks of earthquakes. *Journal of the College of Science*, 7:111–120, 1894.

[5] Sunny Y Auyang. *Foundations of complex-system theories: in economics, evolutionary biology, and statistical physics*. Cambridge University Press, 1998.

[6] Paul Cilliers. *Complexity and postmodernism: Understanding complex systems*. routledge, 2002.

[7] Iram Gleria, Raul Matsushita, and Sergio Da Silva. Sistemas complexos, criticalidade e leis de potência. *Revista Brasileira de Ensino de Física*, 26:99–108, 2004.

[8] Hawoong Jeong, Sean P Mason, A-L Barabási, and Zoltan N Oltvai. Lethality and centrality in protein networks. *Nature*, 411(6833):41–42, 2001.

[9] Mark EJ Newman. The structure and function of complex networks. *SIAM review*, 45(2):167–256, 2003.

[10] Réka Albert and Albert-László Barabási. Statistical mechanics of complex networks. *Reviews of modern physics*, 74(1):47, 2002.

[11] Alain Barrat, Marc Barthelemy, and Alessandro Vespignani. *Dynamical processes on complex networks*. Cambridge university press, 2008.

[12] Sergei N Dorogovtsev and José FF Mendes. *Evolution of networks: From biological nets to the Internet and WWW*. Oxford university press, 2003.

[13] Niklas Boers, Bedartha Goswami, Aljoscha Rheinwalt, Bodo Bookhagen, Brian Hoskins, and Jürgen Kurths. Complex networks reveal global pattern of extreme-rainfall teleconnections. *Nature*, 566(7744):373–377, 2019.

[14] Shraddha Gupta, Niklas Boers, Florian Pappenberger, and Jürgen Kurths. Complex network approach for detecting tropical cyclones. *Climate Dynamics*, 57:3355–3364, 2021.

[15] Akbar Gheibi, Hossein Safari, and Mohsen Javaherian. The solar flare complex network. *The Astrophysical Journal*, 847(2):115, 2017.

[16] Sumiyoshi Abe and Norikazu Suzuki. Scale-free network of earthquakes. *EPL (Europhysics Letters)*, 65(4):581, 2004.

[17] Sumiyoshi Abe and Norikazu Suzuki. Small-world structure of earthquake network. *Physica A: Statistical Mechanics and its Applications*, 337(1-2):357–362, 2004.

[18] Sumiyoshi Abe and Norikazu Suzuki. Complex-network description of seismicity. *Nonlinear Processes in Geophysics*, 13(2):145–150, 2006.

[19] Soghra Rezaei, Hanieh Moghaddasi, and Amir Hossein Darooneh. Preferential attachment in evolutionary earthquake networks. *Physica A: Statistical Mechanics and its Applications*, 495:172–179, 2018.

[20] Denisse Pastén, Felipe Torres, Benjamín A Toledo, Víctor Muñoz, José Rogan, and Juan Alejandro Valdivia. Non-universal critical exponents in earthquake complex networks. *Physica A: Statistical Mechanics and its Applications*, 491: 445–452, 2018.

[21] Sumiyoshi Abe and Norikazu Suzuki. Complex earthquake networks: Hierarchical organization and assortative mixing. *Physical Review E*, 74(2):026113, 2006.

[22] Douglas SR Ferreira, Andrés RR Papa, and Ronaldo Menezes. Small world picture of worldwide seismic events. *Physica A: Statistical Mechanics and its Applications*, 408:170–180, 2014.

[23] Douglas Ferreira, Jennifer Ribeiro, Andrés Papa, and Ronaldo Menezes. Towards evidence of long-range correlations in shallow seismic activities. *EPL (Europhysics Letters)*, 121(5):58003, 2018.

[24] Douglas SR Ferreira, Jennifer Ribeiro, Paulo SL Oliveira, André R Pimenta, Renato P Freitas, and Andrés RR Papa. Long-range correlation studies in deep earthquakes global series. *Physica A: Statistical Mechanics and its Applications*, 560:125146, 2020.

[25] Mikko Kivelä, Alex Arenas, Marc Barthelemy, James P Gleeson, Yamir Moreno, and Mason A Porter. Multilayer networks. *Journal of complex networks*, 2(3): 203–271, 2014.

[26] Zaynab Hammoud and Frank Kramer. Multilayer networks: aspects, implementations, and application in biomedicine. *Big Data Analytics*, 5(1):1–18, 2020.

[27] Nastaran Lotfi, Amir Hossein Darooneh, and Francisco A Rodrigues. Centrality in earthquake multiplex networks. *Chaos: An Interdisciplinary Journal of Nonlinear Science*, 28(6):063113, 2018.

[28] Constantino Tsallis. Possible generalization of boltzmann-gibbs statistics. *Journal of statistical physics*, 52(1):479–487, 1988.

[29] Constantino Tsallis. Nonextensive statistics: theoretical, experimental and computational evidences and connections. *Brazilian Journal of Physics*, 29: 1–35, 1999.

[30] Ioannis Koutalonis and Filippos Vallianatos. Evidence of non-extensivity in earth's ambient noise. *Pure and Applied Geophysics*, 174(12):4369–4378, 2017.

[31] Filippos Vallianatos and Peter Sammonds. Evidence of non-extensive statistical physics of the lithospheric instability approaching the 2004 sumatran–andaman and 2011 honshu mega-earthquakes. *Tectonophysics*, 590:52–58, 2013.

[32] Cleiton S Barbosa, Douglas SR Ferreira, Marco A do Espírito Santo, and Andrés RR Papa. Statistical analysis of geomagnetic field reversals and their consequences. *Physica A: Statistical Mechanics and its Applications*, 392(24): 6554–6560, 2013.

[33] Josef Ludescher, Constantino Tsallis, and Armin Bunde. Universal behaviour of interoccurrence times between losses in financial markets: An analytical description. *EPL (Europhysics Letters)*, 95(6):68002, 2011.

[34] Maria Kalimeri, Constantinos Papadimitriou, Georgios Balasis, and Konstantinos Eftaxias. Dynamical complexity detection in pre-seismic emissions using nonadditive tsallis entropy. *Physica A: Statistical Mechanics and its Applications*, 387(5-6):1161–1172, 2008.

[35] Filippos Vallianatos, Philip Benson, Philip Meredith, and Peter Sammonds. Experimental evidence of a non-extensive statistical physics behaviour of fracture in triaxially deformed etna basalt using acoustic emissions. *EPL (Europhysics Letters)*, 97(5):58002, 2012.

[36] Leonidas P Karakatsanis, Georgios P Pavlos, and Markos N Xenakis. Tsallis non-extensive statistics, intermittent turbulence, soc and chaos in the solar plasma. part two: Solar flares dynamics. *Physica A: Statistical Mechanics and its Applications*, 392(18):3920–3944, 2013.

[37] Amir H Darooneh and Cyruse Dadashinia. Analysis of the spatial and temporal distributions between successive earthquakes: Nonextensive statistical mechanics viewpoint. *Physica A: Statistical Mechanics and its Applications*, 387(14): 3647–3654, 2008.

[38] Sumiyoshi Abe and Norikazu Suzuki. Scale-free statistics of time interval between successive earthquakes. *Physica A: Statistical Mechanics and its Applications*, 350(2-4):588–596, 2005.

[39] Sumiyoshi Abe and Norikazu Suzuki. Law for the distance between successive earthquakes. *Journal of Geophysical Research: Solid Earth*, 108(B2), 2003.

[40] Thais Machado Scherrer, George Sand França, Raimundo Silva, Daniel Brito de Freitas, and Carlos da Silva Vilar. Analysis of four brazilian seismic areas using a nonextensive approach. *Europhysics Letters*, 109(4):49001, 2015.

[41] Filippo Caruso, Alessandro Pluchino, Vito Latora, Sergio Vinciguerra, and Andrea Rapisarda. Analysis of self-organized criticality in the olami-feder-christensen model and in real earthquakes. *Physical Review E*, 75(5):055101, 2007.

[42] Douglas SR Ferreira, Andrés RR Papa, and Ronaldo Menezes. On the agreement between small-world-like ofc model and real earthquakes. *Physics Letters A*, 379(7):669–675, 2015.

[43] Stefan Thurner. Nonextensive statistical mechanics and complex scale-free networks. *Europhysics News*, 36(6):218–220, 2005.

[44] Qi Zhang, Meizhu Li, and Yong Deng. A new structure entropy of complex networks based on nonextensive statistical mechanics. *International Journal of Modern Physics C*, 27(10):1650118, 2016.

Chapter 2

Spatiotemporal Analysis of Earthquake Occurrence in Synthetic and Worldwide Data

Artigo publicado - *FERREIRA, D., RIBEIRO, J., OLIVEIRA JR, P., et al., 2022, "Spatiotemporal analysis of earthquake occurrence in synthetic and worldwide data", Chaos, Solitons & Fractals, v. 165, pp. 112814. DOI: 10.1016/j.chaos.2022.112814.*

Abstract

The present work presents spatiotemporal analyses of distributions between successive earthquakes. This study comprehends data produced by a modified version of the Olami-Feder-Christensen model with a *small-world* topology and actual worldwide earthquakes from 2000 to 2019. The distributions were studied from the nonextensive statistical mechanic's viewpoint, which was shown to be a suitable approach since q-exponential functions produced better fittings to data than pure power laws. Our results show that, by applying scaling relationships, the probability distributions have data collapses in all cases. It reinforces the conception of a critical behavior in the seismological phenomenon and that there is no differentiation between the spatiotemporal statistical features of earthquakes, whether small or large in size or magnitude. In addition, the presence of q-exponential distributions and the ability of a *small-world-like* OFC model to reproduce spatiotemporal features of real worldwide earthquakes indicate self-organized criticality and long-range spatiotemporal correlations between earthquakes.

2.1 Introduction

Earthquakes are, at the same time, one of the most dangerous and intriguing phenomena in nature. Its consequences in society are, on several occasions, devastating and irreversible. It makes the study of that phenomenon so crucial for society. However, the complexity involved in earthquake dynamics makes its comprehension a challenge for scientists. Researchers from several areas have studied the seismic phenomenon from different points of view, with the statistical approach being one of these points. The Gutenberg-Richter (GR) law [1] for the frequencies of the earthquake magnitudes, and Omori's law [2] for the temporal decay of frequency of aftershocks, are two well-known examples.

In the past decades, many scientists have applied complex systems theories and concepts to study several subjects in Earth Sciences [3, 4, 5], including the behavior and dynamics of earthquakes. Complex systems have peculiar characteristics such as the emergency of global patterns from individual interactions, power-law distributions, and nonlinear behavior. Following this perspective, previous works have found complex features in several spatiotemporal properties of earthquakes [6, 7, 8, 9, 10, 11].

In this context, an important phenomenon in numerous complex systems is Self-organized Criticality (SOC). First introduced by Bak, Tang, and Wiesenfeld in their 1987 paper [12], SOC can be seen as a property of dynamic systems where complexity emerges without the need to adjust system control parameters. In many systems, to achieve criticality, it is usual to fine-tune some external control parameters; however, there are natural systems where such adjustments are not necessary, as they self-organize for criticality. These systems are known as *self-organized systems*. Such systems naturally evolve to critical states where the slightest disturbance can lead to "avalanche events", with spatiotemporal invariance, power-law distributions, and fractal dimensions as frequent features [13, 14, 15, 16]. Since earthquake data present these features and the configuration of earthquake occurrence in space-time and magnitude should reflect the complex interactions in the lithosphere, the seismological literature has continuously reported the study of earthquakes under the SOC perspective [17, 18, 19, 20, 21, 22, 23].

The self-organized criticality idea has always been extensively discussed by using many models, being "sandpile" [24], "forest-fire" [25], and "slider-block" [26] some of the most studied. Within this scenario, a very suitable tool is the use of theoretical-computational models that can describe and reproduce the statistical characteristics of earthquakes. Among the various models created, the one by Olami, Feder, and Christensen (OFC model) stands out because, despite its apparent simplicity, it can reproduce several statistical properties of earthquakes [27, 28, 29]. Introduced in

1992, the OFC model incorporates various SOC features, and since its inception, it has been used by several researchers in studies on the dynamics of earthquakes. A more detailed explanation of the model, and some of its achievements, is presented in section 2.3.2.

Another relevant point to highlight is that many authors have also found long-range effects in space and time for earthquakes based on time series obtained from seismological catalogs. Those studies were conducted using different mathematical approaches for real data from various regions and synthetic data produced by computational models [30, 31, 32, 33, 34, 35].

One approach that deserves our attention is using nonextensive statistical mechanics (NESM) formalism to investigate correlations in earthquake data series. Constantino Tsallis proposed NESM in 1988 as a generalization of the Boltzmann-Gibbs statistics [36]. Since then, it has been widely used to produce better comprehensions of various complex systems. In geosciences, we can cite some examples of applications in geomagnetism [37, 38], geological structures [39, 40], volcanology [41, 40], and tectonics [42, 43]. Specifically, in seismology, which is the subject of the present paper, NESM was applied to many earthquakes features, such as magnitude frequencies [44, 45, 46], time distributions [47, 48, 49], distances between successive events [50, 51, 52], spatial seismicity distributions [53, 54], differences of magnitudes [55], and earthquakes networks [56, 57, 58, 59, 60], only to mention a few. In section 2.2, we present a brief introduction to NESM formalism.

As seen in the previously mentioned references, the NESM concepts have been applied to seismological statistical studies for data catalogs from numerous regions of the globe. However, the number of works combining critical models and nonextensive statistical mechanics to reproduce and study spatiotemporal characteristics of earthquakes is still very small. In this paper, we implement the modified version of the OFC model proposed in [61, 48] to conduct simulations to create synthetic data catalogs of earthquakes under different limits and sizes. These results were used to verify the nonextensive behavior of spatial and temporal distributions and compare them to those obtained for data catalogs from worldwide earthquakes. Moreover, we have found scaling relationships that collapse the spatiotemporal probability distributions for synthetic and worldwide earthquakes. The data collapse obtained in our results reinforces the critical behavior of the seismological phenomenon. Therefore, the approach performed in the present work aims to collaborate with the idea of long-range spatiotemporal correlations between earthquakes and strengthen the statistical physics interpretation of the earthquake phenomenon.

2.2 Nonextensive formalism

Statistical mechanics constitutes one of the foundations of contemporary physics, and its standard concepts, based on Boltzmann-Gibbs (BG) theory, have uncountable applications, from microscopic to macroscopic systems. However, in systems whose elements are strongly correlated or with long-range interactions, BG statistics does not seem to be appropriate.

With this frame, the work published by Tsallis in 1988 [36] initiated the nonextensive statistical mechanics' principles by introducing a generalization of the Boltzmann–Gibbs statistical mechanics. In his work, Tsallis proposes an entropy that can explain the statistical properties of a variety of complex systems at their quasi-equilibrium states. Tsallis' entropy is given by

$$S_q = k\frac{1-\sum_{i=1}^{W} p_i^q}{q-1}, \tag{2.1}$$

where W is the total number of possible configurations, q is the entropic index, p_i are the associated probabilities, and k is a conventional positive constant.

Even though that entropy has many properties in common with the entropy of the classical statistical mechanics of Boltzmann–Gibbs, the additivity property is violated in Tsallis' entropy, which means that the entropy of the whole system may be different from the sum of the entropies of its parts, i.e., for any two probabilistically independent systems, A and B, the Tsallis' entropy satisfies the equation

$$S_q(A+B) = S_q(A) + S_q(B) + \frac{(1-q)}{k} S_q(A) S_q(B), \tag{2.2}$$

where the entropic index q indicates the degree of nonadditivity of the system.

Taking the limit $q \to 1$ in Eqs. 2.1 and 2.2, we recover the standard Boltzmann–Gibbs entropy, $S_{BG} = -k\sum_{i=1}^{W} p_i \ln p_i$, and the additivity principle, respectively.

By applying the maximum entropy principle to the Tsallis' entropy under appropriate constraints, the nonextensive probability distribution obtained has a q-exponential form [62, 63], defined by

$$e_q(x) = \begin{cases} [1+(1-q)x]^{1/(1-q)} & \text{if} \quad [1+(1-q)x] \geq 0 \\ 0 & \text{otherwise.} \end{cases} \tag{2.3}$$

From Eq. 2.3 it is possible to check that, for a distribution $f(x) = e_q(-\beta x)$, if $q > 1$ and $x \gg [-\beta(1-q)]^{-1}$, then the distribution can be approximated to a power-law given by

$$f(x) \sim x^{1/(1-q)}. \tag{2.4}$$

The inverse function of the q-exponential is the q-logarithmic function,

$$ln_q(x) = \frac{x^{1-q} - 1}{1 - q}. \tag{2.5}$$

Eqs. 2.3 and 2.5 are generalizations of the usual exponential and logarithmic functions, respectively, i.e., taking the limit $q \to 1$ in Eqs. 2.3 and 2.5, we get back the standard functions. Thus, similarly to BG entropy, for the particular case of equal probabilities, it is straightforwardly verified that Tsallis' entropy takes the form

$$S_q = k \ln_q W. \tag{2.6}$$

2.3 Method

For the present study, we have used NESM concepts applied to both real and synthetic earthquake data catalogs, intending to take another step toward better understanding the complex seismological system. The synthetic catalogs were created using a modified version of the well-known Olami-Feder-Christensen model, and the results were compared to the real ones.

NESM approach and the modified OFC model are explained in the following two subsections.

2.3.1 Nonextensive approach

Nonextensive statistical mechanics have been used to study probability distributions for different earthquake parameters. In that context, two important approaches were made by Abe and Suzuki concerning distances between successive earthquakes and inter-event times. In [50], Abe and Suzuki performed the probability of finding the distances in the range [r, r + dr], starting from the integral form of Tsallis' entropy,

$$S_q[p] = \frac{1}{1 - q} \left(\int_0^\infty \frac{dr}{\sigma} [\sigma p(r)]^q - 1 \right), \tag{2.7}$$

where σ is a scale factor with dimension of length. Applying the maximization entropy principle under the constraints on the normalization condition, $\int_0^\infty p(r)dr = 1$, and the q-expectation value of the distance, $\langle r \rangle_q = \int_0^\infty r P_q(r)dr$, they have found, after some mathematical manipulations, the cumulative distribution,

$$P_{\geq}(r) = \int_r^\infty P_q(r')dr' = e_q(-\beta_s r) \tag{2.8}$$

where β_s is a scale constant.

Similarly, in [64] the authors have found the cumulative distribution for the time interval between two earthquakes (calm time),

$$P_{\geq}(t) = \int_t^{\infty} P_q(t')dt' = e_q(-\beta_t t) \tag{2.9}$$

where β_t is also a scale constant.

Those approaches will be adopted in our analysis for probability distributions in space and time.

2.3.2 The modified OFC model

The OFC model is considered one of the most studied spring-block models to reproduce statistical properties of earthquakes, exhibiting a rich phenomenology of actual earthquakes. Based on a two-dimensional version of the Burridge-Knopoff spring-block model [26], the OFC model can consider different conservation levels in its dynamics. The original version of the model can be described as follows.

The model's arrangement simulates a two-dimensional discrete regular $L \times L$ squared lattice containing $N = L^2$ blocks. Each block is attached to its first neighbors by springs, and all blocks are rested on a rigidly fixed plate connected by friction. Furthermore, each block is also bonded by a spring to an upper rigid driven plate. The slowly relative movement of the upper plate in relation to the lower one makes the blocks subject to elastic forces opposite the frictional ones. When the force on one of the blocks is larger than an initially set frictional force threshold, then the block slips. After the slipping, the block is assumed to relax to the zero-force position, and there is a rearrangement in the nearest neighbor's forces. Such force redefinition can result in further block slides, evolving into a chain reaction.

The OFC dynamics is simulated considering a cellular automaton model, where an $L \times L$ array is defined, and each site (i, j) carries a seismogenic force represented by $F_{i,j}$. Initially, all sites are designated with random values within the $[0, F_{th}[$ range, with F_{th} being a threshold that simulates the limit value for the friction force. Trying to mimic a uniform motion of tectonic plates, the forces in all blocks increase simultaneously and uniformly until one of the blocks reaches the threshold value (i.e., $F_{i,j} \geqslant F_{th}$), becoming unstable and slipping (at this point, the driving stops and the earthquake process starts). After the block slips, a fraction of its tension is equally redistributed between its nearest neighbors and then taken to zero, as shown by the following relaxation rule:

$$F_{i,j} \geqslant F_{th} \Rightarrow \begin{cases} F_{n,n} \rightarrow F_{n,n} + \alpha F_{i,j} \\ F_{i,j} \rightarrow 0, \end{cases} \tag{2.10}$$

where $F_{n,n}$ are forces in the (n, n) nearest neighbors and α is the dissipation parameter, controlling the level of conservation of the dynamics, being $\alpha = 1/4$ the conservative case. If the redistributing process makes other sites unstable, these steps are repeated until there are no more unstable sites, and then the earthquake is considered to be completed evolved. The earthquake's size, s, is defined by the total number of relaxations, which is proportional to the energy released during the earthquake.

An important feature to be defined in the OFC model is the boundary condition related to the dissipation parameter of the sites located on the lattice's boundaries. We use the *open boundary* (non-periodic) condition in the present study, where α is the same for all blocks, regardless of your location on the lattice. This condition implies that sites on boundaries have a higher dissipation level per relaxation than those in bulk.

When an earthquake finishes, the relative movement between the plates returns, and the system accumulates tension in all sites again. In this way, an $F_{th} - F_{max}$ quantity is added to all sites, making unstable the site with the highest tension, F_{max}, thereby starting a new earthquake process. As the time interval between two seismic events is much longer than the duration of an event, earthquakes will be considered instantaneous events. It means that during the redistribution of forces, it is considered that the uniform-driving stops, and, consequently, no extra time are added during this process.

However, as verified in [48], a better agreement with real data is obtained when the lattice topology in the OFC model is not regular, as considered in the original model. Following the idea proposed by Caruso et al. [61], the connections between the sites (blocks) in the lattice will obey the Watts–Strogatz mechanism to construct *small-world networks* [65]. This improvement in the OFC model is expected to make it more realistic, as it considers the long-range interactions between the elements more effectively, corroborating with several works which indicate long-range spatiotemporal connections between earthquakes [66, 67, 68, 69, 70, 71]. To create the *small-world-like topology* in the OFC model, we start from the standard two-dimensional regular lattice. Then, the link between every two nearest neighbors has a probability p of being randomly rewired, and the resultant lattice has a topology between the regular and the random ones. It is important to note that the small-world topology creation process does not affect each site's original number of connections.

As reported by [48] and [61], for the OFC model to have a lattice with small-world-like features and self-organized critical behavior, the rewiring probability p must be in a range of values between $[10^{-3}, 10^{-2}]$, since for $p < 10^{-3}$, the behavior starts to be similar to the regular network, and for values of $p > 10^{-2}$ the criticality

of the model progressively decreases. In this work, we adopt $p = 0.001$.

Furthermore, in [48], the authors also show that, when adopting the small-world topology instead of the regular one, there is a minimization of the "border effects", which means the lattice borders considerably reduce their influence on the distribution of events throughout the lattice. One consequence is that it becomes unnecessary to use substantial lattice sizes to find earthquake characteristics, such as calm time distributions.

Thus, in our studies, we have used the OFC model with a small-world-like topology to create synthetic data catalogs to calculate spatial and temporal distributions and compare them to those produced by real data catalogs of earthquakes.

2.4 Data

In our analyses, we used real worldwide and synthetic earthquakes.

2.4.1 Worldwide earthquakes

From the World Catalog of Earthquakes of Advanced National Seismic System (ANSS)[1], we collected a dataset of global earthquakes covering the period between 2000 and 2019. Once shallow and deep earthquakes are mechanically different [72, 73], we divided our dataset into two to study them separately. We considered shallow earthquakes the events that occurred at depths up to 70 km, and the deep ones, those with hypocenter localized deeper than this value. For shallow events, magnitudes were considered greater than or equal to 4.5 on the Richter scale. It provides 107 118 shallow earthquakes. On the other hand, in the case of deep events, to ensure the uniformity of the catalog, we excluded all earthquakes with a magnitude less than 5.3, resulting in a total of 2 890 events. We considered magnitude types m_b (short-period body wave), m_{wc} (centroid), m_{ww} (moment magnitude) and excluded all non-earthquakes (e. g., mining explosion, quarry blast, and acoustic noise) available in the catalog.

2.4.2 Synthetic earthquakes

To generate the earthquake catalog with the modified OFC model, we considered four values of lattice size: $L = 200$, 300, 400, and 500. The different sizes allow us to analyze if the lattice size, L, influences the simulated seismic events' properties in space and time. In all cases, the probability of link rewiring was $p = 0.001$, and the dissipation coefficient, α, was equal to 0.20 (nonconservative case). Aiming to

[1] https://earthquake.usgs.gov/data/comcat/

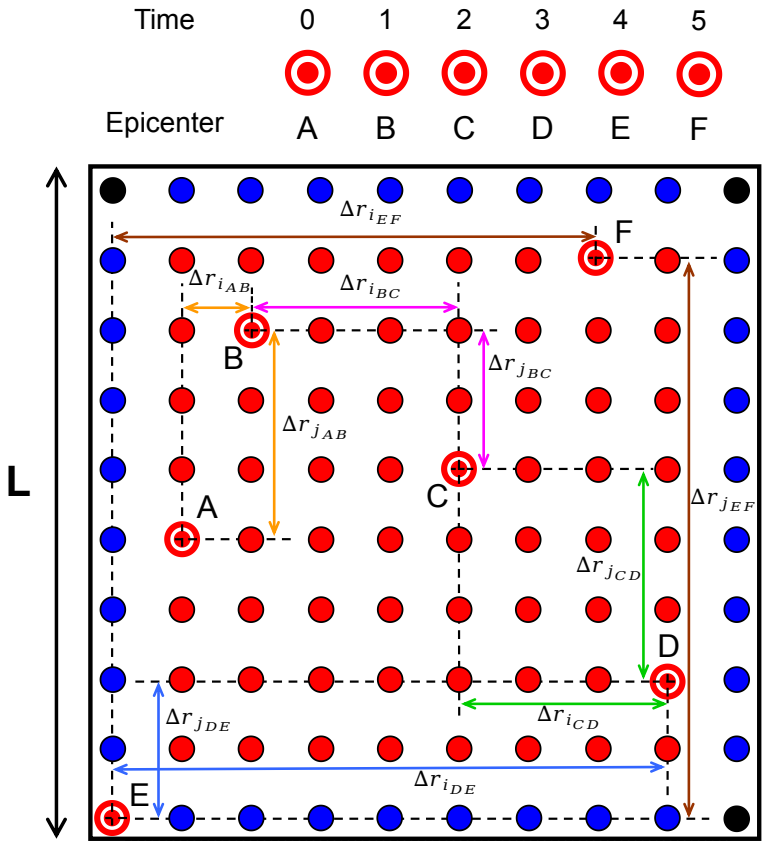

Fig. 2.1: Example of i and j projections for the distances between subsequent earthquakes in the OFC model for a lattice with $L = 10$. Vertical distances are given by Δr_j, and the horizontal ones are represented by Δr_i. At the top of the figure is shown the sequence of epicenters ordered by time. Calculations are explained in the body text.

reproduce the completeness feature of actual earthquake catalogs (where the catalogs are only complete above a particular value) and the influence of the magnitude threshold considered for each lattice size, we varied the lower threshold values of earthquake sizes in $s_{th} = 25$, 50, 75, and 100. We considered 5×10^5 events after the transient regime for all the calculations.

2.5 Results and discussion

As mentioned before, the OFC model is a SOC model that, despite its simplicity, is capable of reproducing several characteristics of actual earthquakes. Therefore, in order to help the improvement of the existing knowledge about the seismic events' dynamics, we have used data from the synthetic seismological catalog created with the modified OFC model to perform studies on probabilities distributions of spatiotemporal properties of earthquakes. Then, we compared the results from the

OFC model to those performed, using the same analysis, for actual data of shallow and deep earthquakes separately.

2.5.1 Spatial analysis

Due to the OFC model being formed by blocks in a squared topology, the distance between the hypocenters of two consecutive earthquakes generated with this model can be calculated by the geometrical distance between them. Adopting a similar procedure to that used to find the epicenters of actual earthquakes, we project on the "surface" of the lattice the point of occurrence of each synthetic earthquake (hypocenter) in our modeling. Each time an event occurs in block A, of coordinates (i_A, j_A), this point is projected on the lattice borders. As the lattice is squared, we will have two projections, in i and j. Thus, we will call *epicenters* the positions of the points referring to these projections. Therefore, the distance between the *epicenters* of two successive earthquakes in blocks A and B can be calculated by $\Delta r_{i_{AB}} = |i_A - i_B|$ or $\Delta r_{j_{AB}} = |j_A - j_B|$.

Fig. 2.1 depicts an example in which it is measured the distance between 5 pairs of consecutive earthquakes. In orange, we have the distances between the epicenters of the earthquakes A and B ($\Delta r_{i_{AB}} = 1$ and $\Delta r_{j_{AB}} = 3$); in purple, is represented the distances between the epicenters of B and C ($\Delta r_{i_{BC}} = 3$ and $\Delta r_{j_{BC}} = 2$); in green, we have the distances between C and D ($\Delta r_{i_{CD}} = 3$ and $\Delta r_{j_{CD}} = 3$); in blue, we have the distances between D and E ($\Delta r_{i_{DE}} = 8$ and $\Delta r_{j_{DE}} = 2$), and in brown, we have the distances between E and F ($\Delta r_{i_{EF}} = 7$ and $\Delta r_{j_{EF}} = 8$). All the distances in the modeling are adimensional.

Figs. 2.2(a) and 2.2(b) show, respectively, the cumulative probability distributions for the distances between successive epicenters projected in i (Δr_i) and j (Δr_j), for a lattice with $L = 500$ and $s_{th} = 100$. Both distributions are well-adjusted by q-exponential functions (Eq. 2.8) with $q < 1$, which is in agreement with the results for seismological data from California, Japan, and Iran [50, 51], showing the consistence of this method to calculate inter-event distances in the OFC model. For clarity, the insets in Fig. 2.2 represent the same plot but applying the q-logarithmic function (Eq. 2.5) to the data. When plotted in this form, the data follows straight lines, as should be for q-exponential distributions, where the β_s values correspond to the inclination of the q-logarithmic function fitted.

The cumulative distributions of Δr_i and Δr_j for the synthetic events present the same q-value, which shows that, regardless of the projection axes chosen to calculate the distance between epicenters in the modified OFC model, we have the same result. Therefore, we used the j-distance, Δr_j, between the epicenters for our spatial investigation in this work. For simplicity's sake, we use the notation

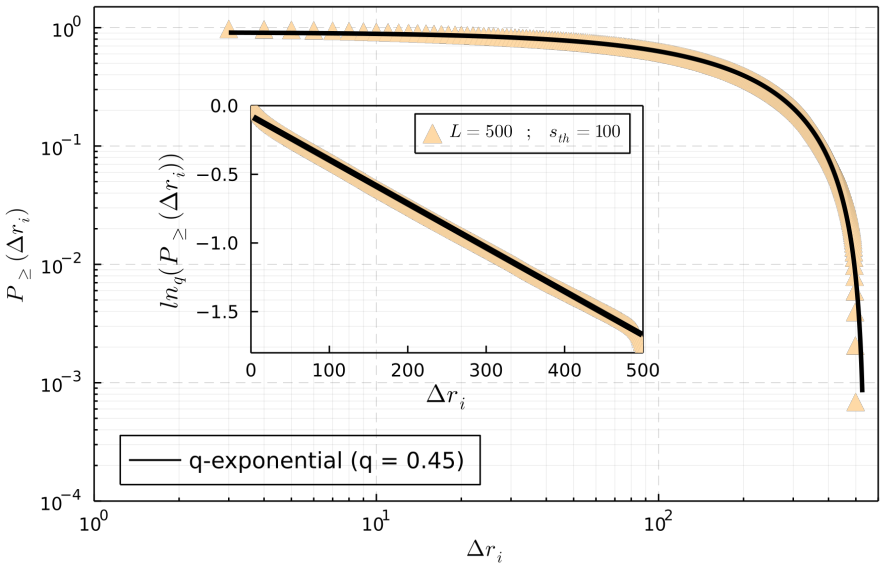

(a)

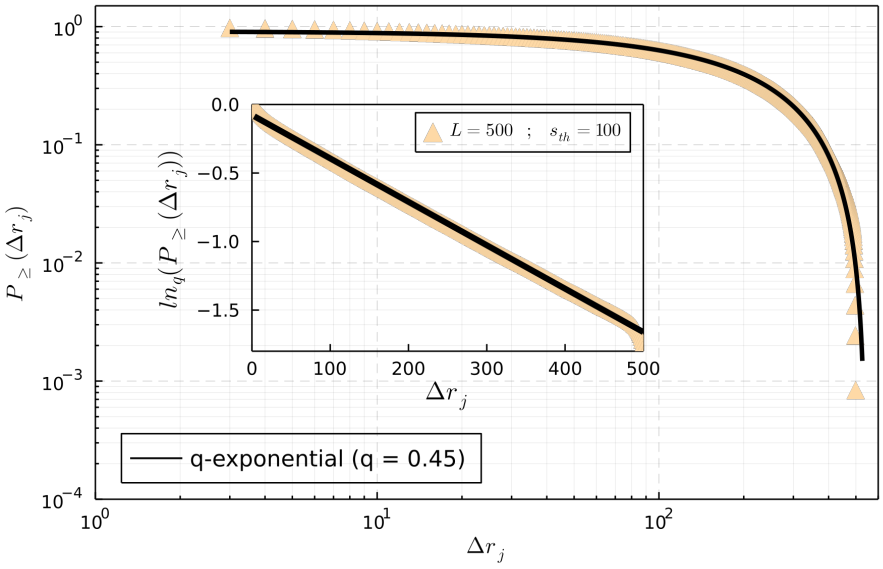

(b)

Fig. 2.2: Cumulative probability distribution of distances between consecutive earthquakes for the modified OFC model with $L = 500$ and $s_{th} = 100$. (a) Distance distribution for the i-projection. The solid black line represents an adjustment to a q-exponential function, with the best fit for $q = 0.45$ and $\beta_s = 3.377 \times 10^{-3}$. The correlation coefficient, R^2, between the synthetic data and the q-exponential model is 0.99898. (b) Distance distribution for the j-projection. The solid black line is a q-exponential with $q = 0.45$ and $\beta_s = 3.349 \times 10^{-3}$. The correlation coefficient is $R^2 = 0.99887$. *Insets*: semi-$q - log$ plots of the cumulative distributions for the (a) i and (b) j projections. In both cases, the black straight lines represent the q-logarithmic function, where the q and β_s values are the same found in the bigger plots.

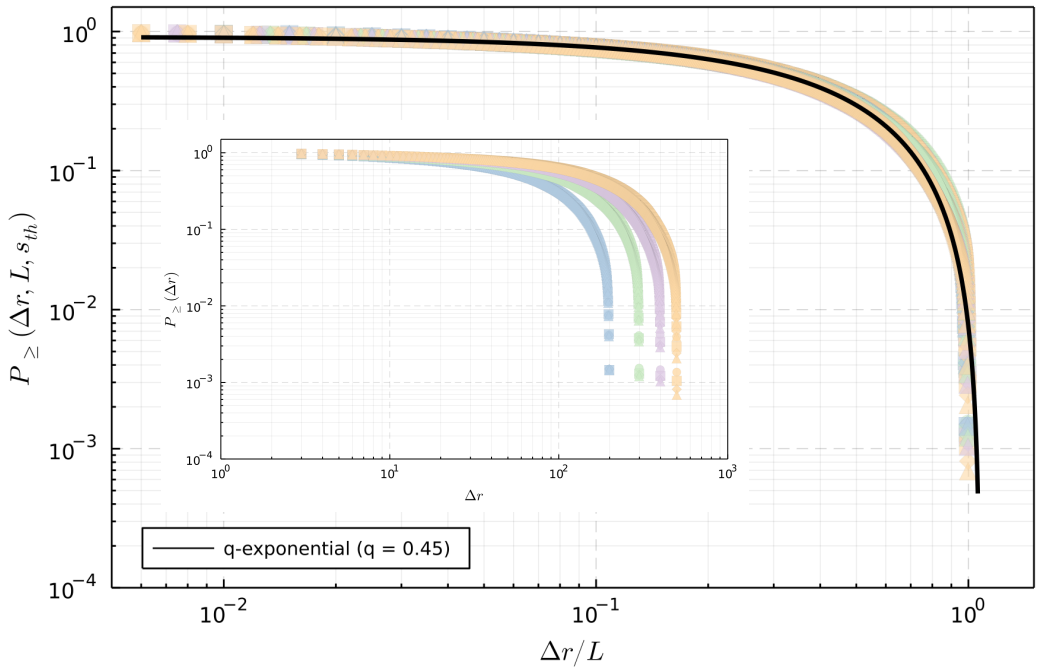

Fig. 2.3: Cumulative probability distributions for j-projections of the distance between successive earthquakes generated with the modified OFC model. The lattice sizes, L, are 200 (light blue), 300 (light green), 400 (light purple), and 500 (light yellow). Lower size thresholds, s_{th}, are 25 (circle), 50 (square), 75 (diamond), and 100 (triangle). The data collapse is obtained by applying the scaling law in Eq. 2.11. The distributions follow the q-exponential (solid black line) presented in Eq. 2.8, with $q = 0.45$ and $\beta_s = 1.688$. *Inset*: same distributions, but without data collapse.

$\Delta r_j \equiv \Delta r$.

Our analyses of the distributions Δr were conducted considering the different lower size thresholds, s_{th}, and different lattice sizes, L (previously mentioned in section 2.4.2). Hence, the probability distribution of Δr is a function of L and s_{th}. However, as shown in the inset of Fig. 2.3, the distribution is independent of the lower size threshold chosen. Besides that, it is possible to make this distribution invariant with respect to the values of L by using the scale relationship

$$P_{\geq}(\Delta r, L, s_{th}) = f(\Delta r/L), \tag{2.11}$$

where $f(x)$ decays as a q-exponential function, $e_q(-\beta_s x)$ (Eq. 2.8), with $\beta_s = 1.688$ and $q = 0.45$, as it can be seen in Fig. 2.3. For visual clarity and to independently show data collapse for different lattice sizes and earthquake size thresholds, the curves have been shifted along the x-axis for each L and s_{th}, as illustrated in Figs. 2.4(a) and 2.4(b), respectively. To explicit the nonextensive behavior in the spatial distribution and the finite-size effect imposed by the model, we also present the rescaled distribution in Fig. 2.5, where it is possible to better observe the agreement between the results from the simulated data and the q-exponential function. We also highlight that, for $q < 1$, the q-exponential probability distribution has a cutoff at $1/[\beta_s(1-q)]$. In that way, the β_s value found for our simulated data is consistent since it provides a cutoff similar to the lattice size (as shown in Figs. 2.3 and 2.5).

The scaling law for spatial distributions on the modified OFC model is similar to those found in previous works (using different approaches) for the distance between consecutive earthquakes from many world regions, such as, California, Canada, Central Asia, Greece, Japan and Iceland [74, 7, 22].

Here it is important to highlight some points from our results. First, we observe that regardless of the lattice size, the spatial distributions have the same form, similar to those obtained in [50, 51, 75] for earthquakes from Japan, California, Iran, and Greece. Furthermore, in [76], the author calculates the inter-event distances between successive events on a 2D spring-block (Burridge-Knopoff) original model. He also obtains the best-fitting for the probability distribution by a q-exponential function, with q-values similar to ours. However, although they have found the q-value does not change with the system's size, they have only used three different lattice sizes with no scaling function that allows the data to collapse into a single curve, as we did. It means that the OFC model with small-world topology provides spatial statistical properties similar to those found in actual seismological data, even for a small lattice size, as discussed in [48]. Moreover, the data collapse observed in our results is evidence of the critical state of the simulated earthquakes, in agreement

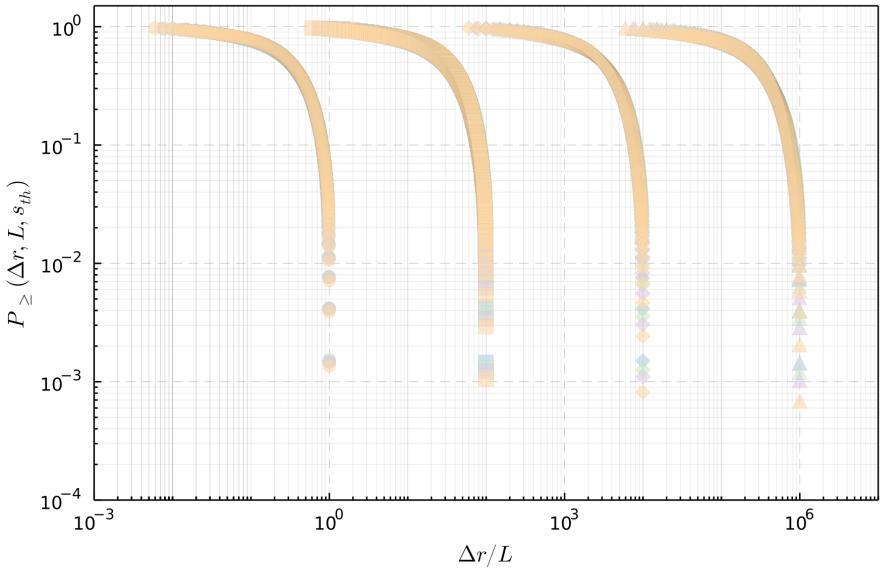

(a)

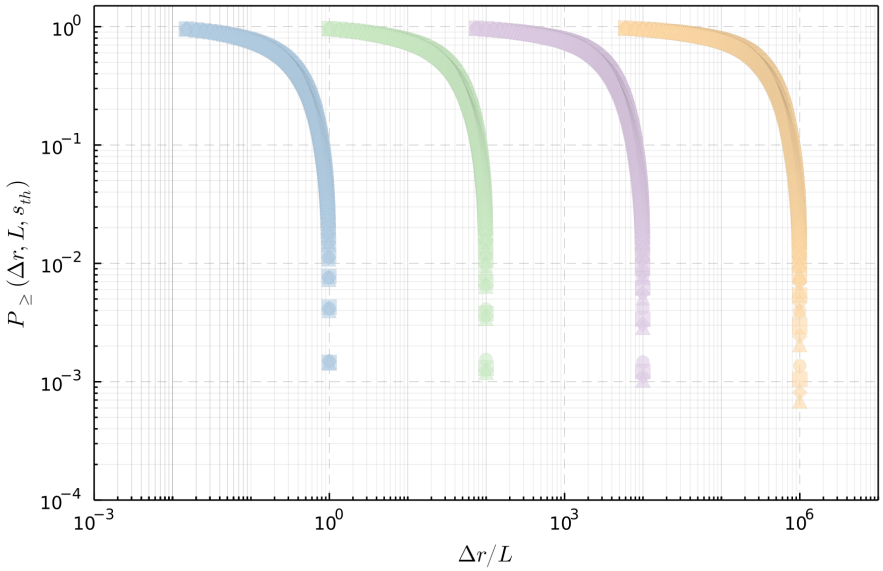

(b)

Fig. 2.4: Same plot as in Fig. 2.3, for the collapsed data, but shifted along the x-axis for each different (a) lower size threshold (s_{th}= 25, 50, 75, and 100, left to right), and (b) lattice size (L= 200, 300, 400, and 500, left to right).

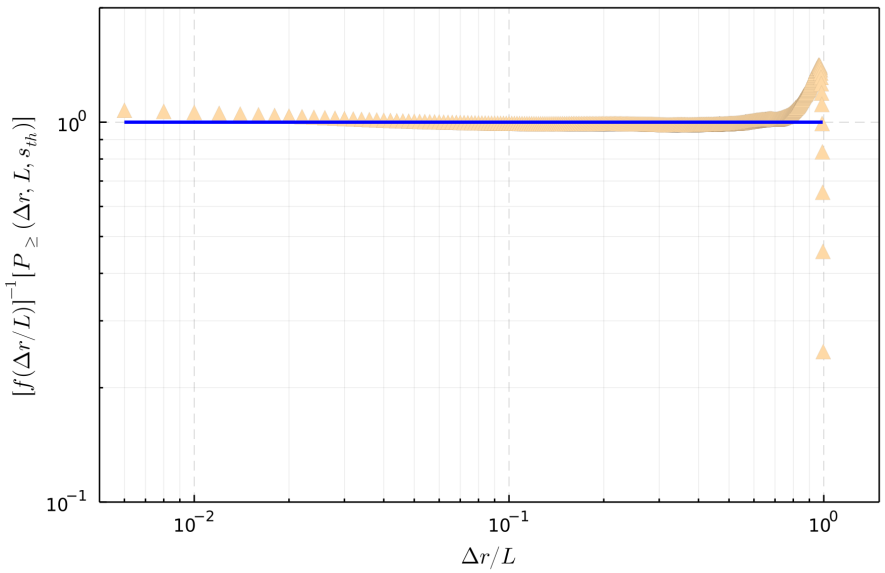

Fig. 2.5: Rescaled cumulative probability distribution for j-projection of the distance between consecutive earthquakes for the modified OFC model with $L = 500$ and $s_{th} = 100$. The parameters used in $f(\Delta r/L)$ (Eq. 2.11) were those obtained for the q-exponential function in Fig. 2.3. The solid blue line is a guide for the eyes, indicating the perfect theoretical match between the synthetic data and the q-exponential.

with the findings for actual seismological data. Given the results obtained for the modified OFC model, we compared them with the spatial analysis of the actual earthquakes, investigating the spatial behavior of worldwide earthquakes.

It is worth mentioning that there is not a vast amount of work in the literature dealing with spatiotemporal studies of earthquakes from a global perspective since most authors carry out analyses only for data from some specific areas of the world [50, 74, 7, 22]. Among the few authors who have conducted similar studies in worldwide earthquake catalogs, we can highlight Corral [32] and Vallianatos & Sammonds [77]. The former studied the use of the rate of earthquake occurrence in scaling relations for distributions of inter-event distances, considering only regions and periods with stationary seismic occurrence. Similar to the present work, the latter authors also consider the nonextensive statistics approach in their studies. However, they do not perform calculations on the influence of minimum magnitude thresholds and do not compare their results with critical models.

We have analyzed earthquakes from a global perspective, observed their properties, and compared the results with those found for the modified OFC model. From the latitude and longitude of each earthquake in our worldwide data, we have the geographical location of the earthquakes' epicenters, allowing us to calculate the distance, Δr, between subsequent epicenters. Those distances are determined by calculating the geometric distances over the Earth's surface, considering the spher-

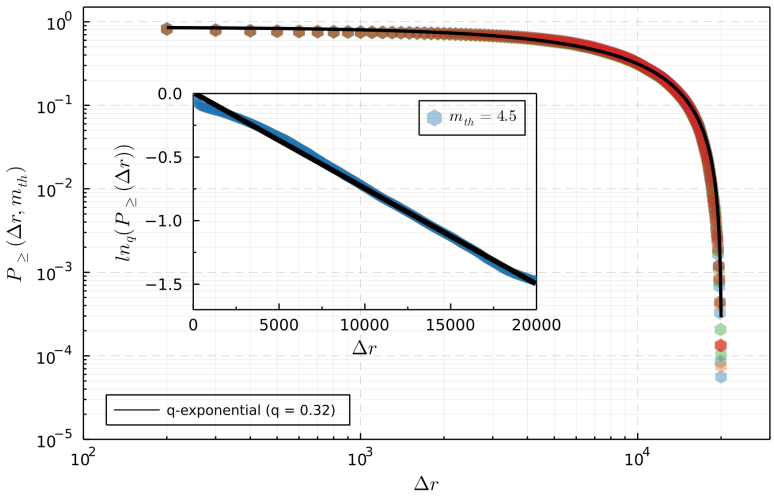

(a)

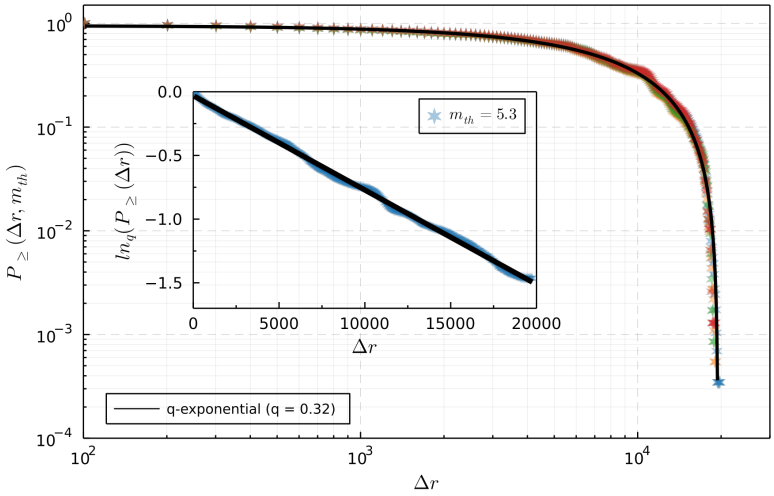

(b)

Fig. 2.6: Cumulative probability distributions of distances between subsequent earthquakes for worldwide seismological data from 2000 to 2019. All distances are in km. (a) Shallow earthquakes (hexagon). The magnitude thresholds, m_{th}, considered are 4.5 (blue), 4.7 (orange), 4.9 (green), and 5.1 (red). The best fit is given by a q-exponential (solid black line) with $q = 0.32$, $\beta_s = 7.581 \times 10^{-5}$, and correlation coefficient $R^2 = 0.99422$. (b) For deep earthquakes (star), the magnitude thresholds are 5.3 (blue), 5.5 (orange), 5.7 (green), and 5.9 (red). Best fit for a q-exponential (solid black line) with $q = 0.32$, $\beta_s = 7.544 \times 10^{-5}$, and $R^2 = 0.99773$. For both datasets, it is observed that the distribution of distances is independent of the m_{th} value considered. *Insets*: semi-$q - log$ plots of the cumulative distributions for (a) shallow (with $m_{th} = 4.5$) and (b) deep (with $m_{th} = 5.3$) earthquakes. The black straight lines represent the q-logarithmic function, where the q and β_s values are the same found un the bigger plots.

ical approximation, and using the well-known haversine formula.

Firstly, we have performed our calculations for shallow earthquakes only. We considered magnitude thresholds, m_{th}, equal to 4.5, 4.7, 4.9, and 5.1 to analyze whether the behavior of the distribution would change with this parameter. The result is shown in Fig. 2.6(a), where it is observed that the cumulative spatial distribution for shallow seismic events has no dependence on the magnitude threshold, m_{th}. Moreover, the probability distribution agrees with the q-exponential function (Eq. 2.8) for $q = 0.32$. This behavior is interesting since it was also found in studies for specific regions of the world (e.g., Japan, California, and Iran) [50, 51], as well as for worldwide shallow earthquakes with a magnitude larger than 5.5 [77]. These findings are in concordance with the q-exponential properties, such as the fractal behavior, characteristic of complex systems [36].

Secondly, we have calculated the cumulative probability distribution of distances for the worldwide data of deep earthquakes, taking into account magnitude thresholds, m_{th}, equal to 5.3, 5.5, 5.7, and 5.9. The resulting distribution can be seen in Fig. 2.6(b), where we can also note that this distribution is independent of m_{th} and follows a q-exponential function (Eq. 2.8) with $q = 0.32$. As done for synthetical data, in Fig. 2.6 *insets*, we also present the semi-$q - log$ plots, where the straight lines represent q-logarithmic functions with β_s being the inclination of the fitted line.

Our findings show that the nonextensive behavior is presented in the seismic phenomenon independently of its depth, magnitude, and geographical location and suggests no differentiation in the spatial occurrence of large and small earthquakes worldwide. We still note a strong agreement between the results of the modified OFC model and actual earthquakes, where the distance distributions follow q-exponential functions, as explicit in Fig. 2.5 for the simulated data and Fig. 2.7 for worldwide earthquakes. Fig. 2.7 also shows the effect caused by the finite size of the Earth since the maximum possible length to be covered on the surface from one point to another is approximately $2 \times 10^4 km$.

2.5.2 Temporal analysis

To perform the temporal analysis in the modified OFC model, we used the same method applied in [48]. As explained in Section 2.3.2, in the OFC model, there is a constant increase in the values of the forces in all system sites, and the earthquakes are considered instantaneous events. Also, as the model assumes that a constant strength variation occurs in all system sites, we can consider that the amount $F_{th} - F_{max}$ added to all sites in the lattice is proportional to the value of the time interval of consecutive events. Thus, we can calculate the cumulative waiting

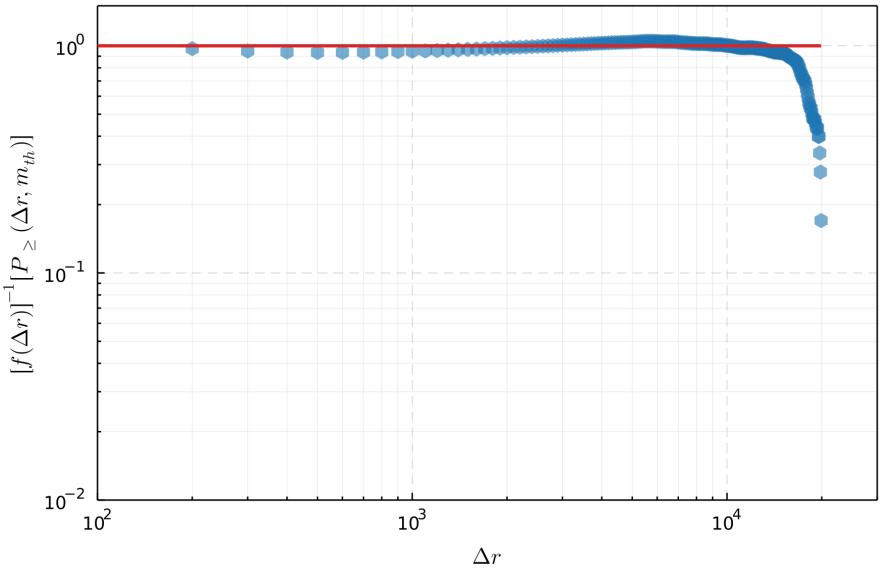

(a)

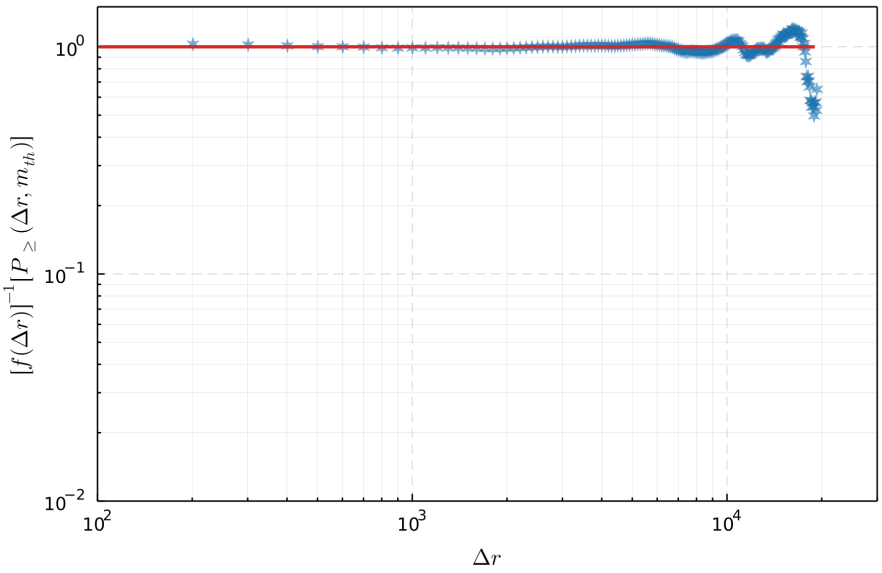

(b)

Fig. 2.7: Rescaled cumulative probability distribution of the distances between consecutive earthquakes for worldwide seismological data from 2000 to 2019. The distances are in km. The magnitude thresholds are (a) $m_{th} = 4.5$ for shallow earthquakes and (b) $m_{th} = 5.3$ for deep ones. The parameters used in $f(\Delta r)$ were those obtained for the q-exponential functions in Fig. 2.6. The solid red lines are guides for the eyes, which indicate the theoretical match between the data and the q-exponentials.

time distributions.

Following a similar procedure employed in the spatial analysis, we studied the cumulative probability distribution of time intervals between consecutive epicenters

for lattices of size $L = 200$, 300, 400, and 500, with $s_{th} = 25, 50, 75$, and 100, as shown in Fig. 2.8. In [6, 74, 78], the authors apply a scale relationship to collapse data of time interval distributions from California and Iceland. Using an analogous scaling rule applied by those authors, we observed that the waiting time distribution for data from the modified OFC model could be made invariant to the values of L and s_{th} by using the scaling

$$P_{\geq}(\Delta t, L, s_{th}) = f(L^{d_f}\Delta t/s_{th}^{b}), \tag{2.12}$$

where $d_f = 1.0$, $f(x)$ decays as a q-exponential function, $e_q(-\beta_t x)$ (Eq. 2.9), and the parameter $b = 0.88$ is the b-value (from the GR law) found for our data. The term $L^{d_f}\Delta t \,/\, s_{th}^{b}$ measures the average number of earthquakes with a size greater than or equal to s_{th}, occurring within a time interval Δt in a spatial range L.

Usually, d_f is considered the fractal dimension D_0 of the epicenter distribution (as shown in [6, 78], for example). This assumption is consistent with the results from our simulations, as we are making a one-dimensional projection from the 5×10^5 epicenters contained in our 2D-squared lattice, which has sides ranging from 200 to 500. It means that, on average, the epicenters fill the projected dimension, and consequently, the epicenter distribution has a fractal dimension equal to 1.0. However, we point out that the d_f value equal to 1.0 was also used in [74] for the waiting time distributions from California and Iceland earthquakes. In that work, the authors have made a complimentary observation showing that considering d_f always as the fractal dimension D_0 of the spatial distributions is not a closed question since the multifractal structure of the epicenters' spatial distribution cannot be entirely described by the capacity dimension D_0 alone.

Fig. 2.8 presents the cumulative probability distribution for the time intervals, with a data collapse accordingly with the scaling proposed in Eq. 2.12. As can be seen in Figs. 2.8 and 2.9, the lattice size and the earthquake lower size thresholds do not change the distributions' behavior of the temporal occurrence of earthquakes in the modified OFC model. However, it is possible to observe in Fig. 2.8 that the data collapse for time distributions is not perfect due to a limitation imposed by the modeling. As the maximum time interval between two events is related to the lattice's size, small lattices cannot reach time intervals as bigger as the larger ones, which is better noticed as the lower size thresholds increase, as shown in Fig. 2.9. Although, the data collapse found for the modified OFC, as a result of the rescaling of the time intervals, shows evidence of a critical phenomenon, following the previous studies for seismic data from actual earthquakes [6, 74, 78].

The temporal distributions for the earthquakes generated with the modified OFC model are well fitted by the q-exponential function (Eq. 2.9) with $q > 1$ (as shown

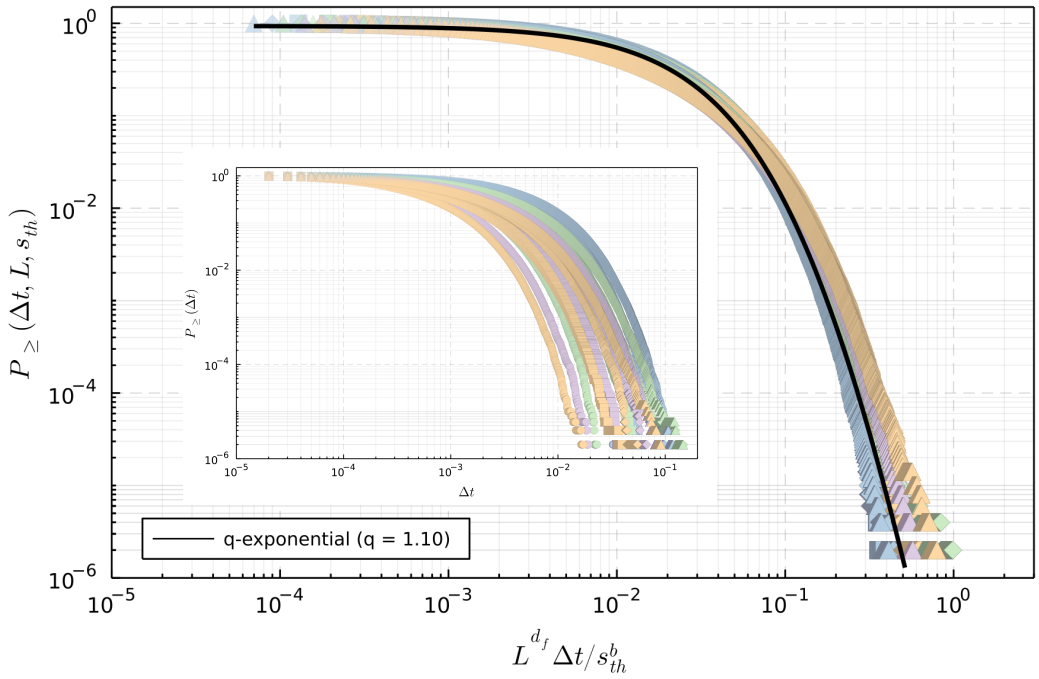

Fig. 2.8: Cumulative probability distributions of time intervals between consecutive earthquakes from the modified OFC model. The lattice sizes, L, are 200 (light blue), 300 (light green), 400 (light purple), and 500 (light yellow). Lower size thresholds, s_{th}, are 25 (circle), 50 (square), 75 (diamond), and 100 (triangle). The data collapse is obtained by applying the scaling law in Eq. 2.12. The solid black line represents the q-exponential function shown in Eq. 2.9, with $q = 1.10$ and $\beta_t = 55.506$. *Inset*: same distributions, but without data collapse.

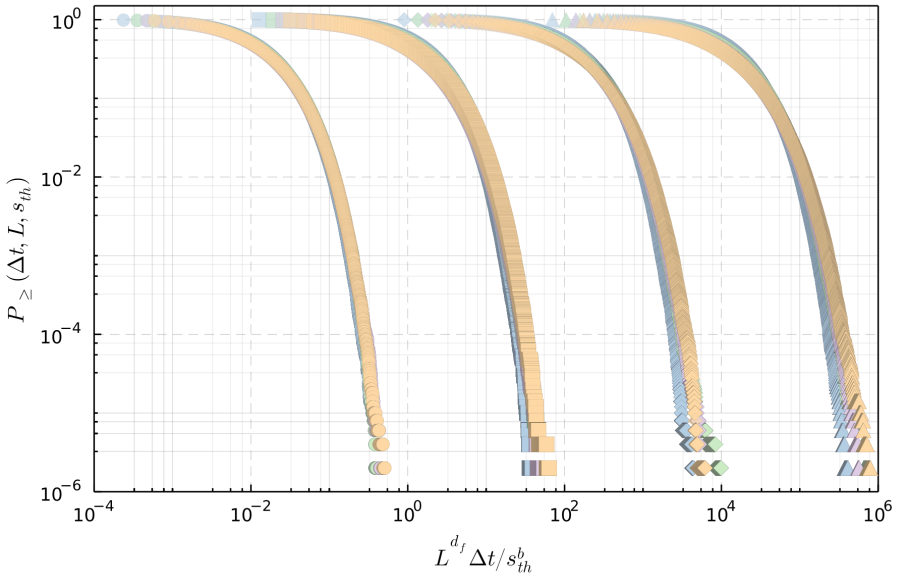

(a)

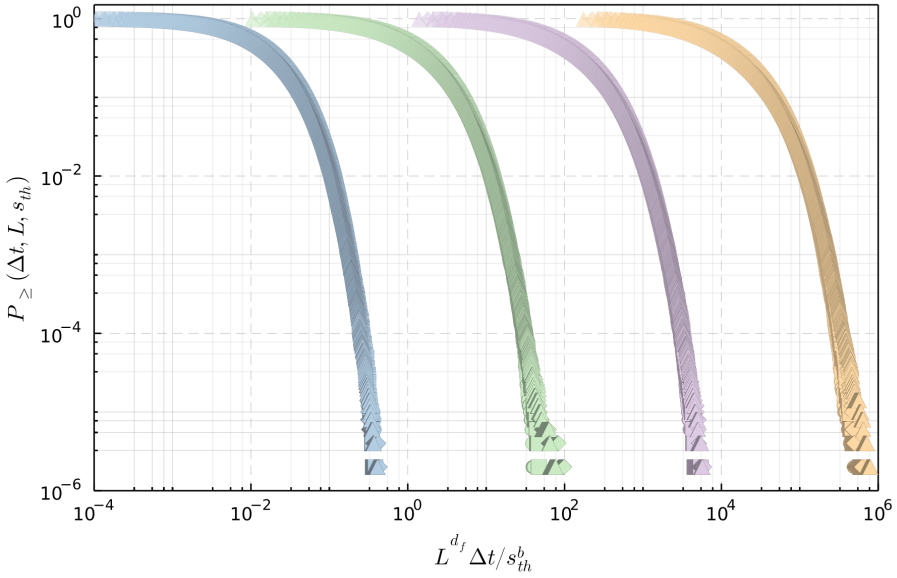

(b)

Fig. 2.9: Same plot as in Fig. 2.8, for the collapsed data, but shifted along the x-axis for each different (a) lower size threshold (s_{th}= 25, 50, 75, and 100, left to right), and (b) lattice size (L= 200, 300, 400, and 500, left to right).

in Figs. 2.8 and 2.10), agreeing with the results previously obtained for actual seismological data [64, 79, 51, 77]. Fig. 2.10 also evinces the finite-size effect and the q-exponential behavior for the time interval distribution.

We can further observe that the best-fitting is obtained for $q = 1.10$, similar to that found in [80], where the author analyzed interoccurrence time distributions on a two-dimensional spring-block model (Burridge-Knopoff) without the cellular

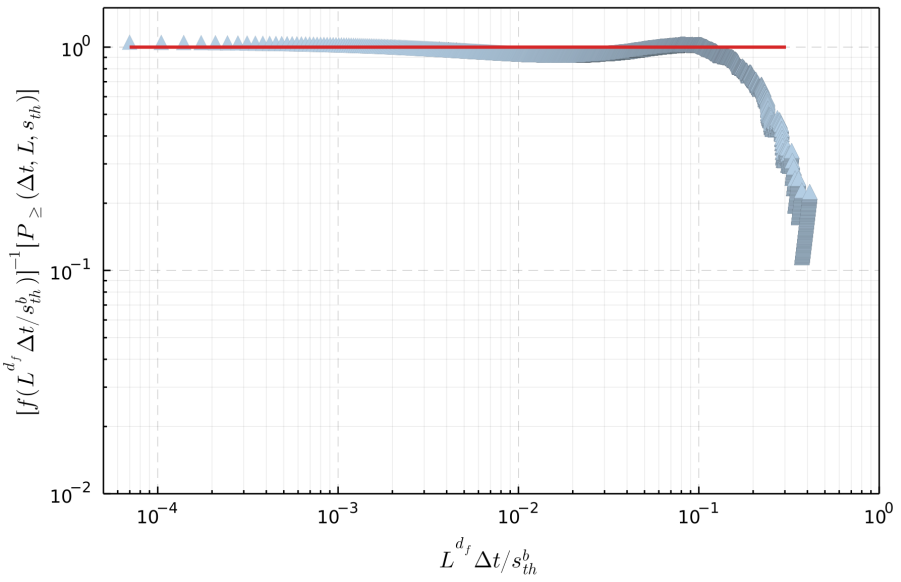

Fig. 2.10: Rescaled cumulative probability distribution of time intervals between consecutive earthquakes for the modified OFC model with $L = 200$ and $s_{th} = 100$. The parameters used in $f(L^{d_f}\Delta t/s_{th}^b)$ (Eq. 2.12) were those used for the q-exponential function in Fig. 2.8. The solid red line is a guide for the eyes, indicating the perfect theoretical match between the synthetic data and the q-exponential.

automata approach. However, the results found in the present work for the OFC model with small-world topology have waiting time distributions with considerably better fits for the q-exponential function than in [80]. Furthermore, we obtained scaling relationships for the system size and lower size threshold in this work, which had not been obtained previously.

Regarding the data of actual earthquakes, we considered the instant of occurrence of an earthquake and the next one to conduct the studies on temporal analysis. We have performed the calculations for shallow and deep earthquakes separately, for each pair of events, varying the magnitude threshold, m_{th}. The *Insets* in Figs. 2.11(a) and 2.11(b) show the results for cumulative probability distributions of time intervals between successive shallow and deep seismic events, respectively.

As the energy of an earthquake is proportional to 10^m, being m its magnitude, we can apply a similar scaling to the one used for the seismological data generated with the modified OFC model (Eq. 2.12). Nevertheless, for worldwide earthquakes, our data only have variations in the magnitude threshold. This way, the scaling relationship to be used is

$$P_{\geq}(\Delta t, m_{th}) = f(\Delta t \,/\, 10^{b.m_{th}}), \tag{2.13}$$

in which $f(x)$ decays as a q-exponential function (Eq. 2.9), and the b-values found for

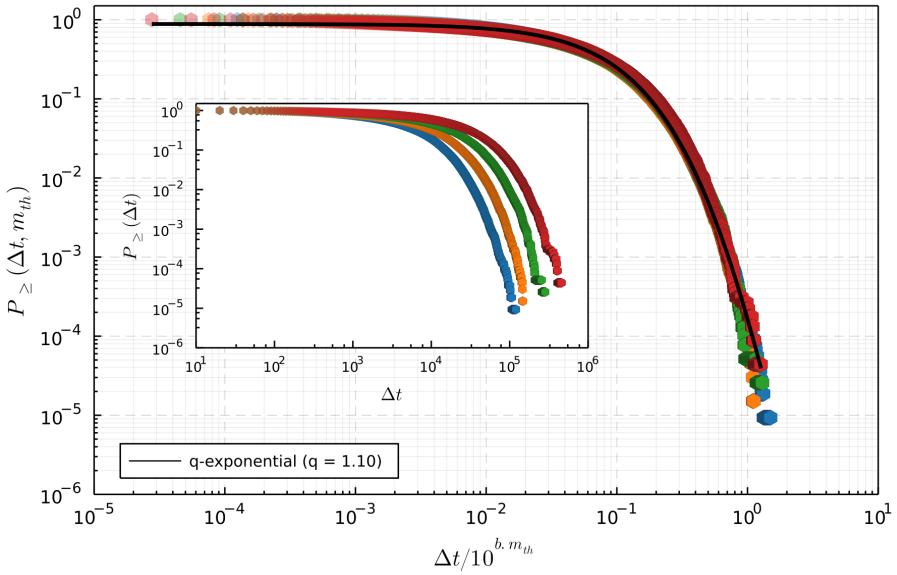

(a)

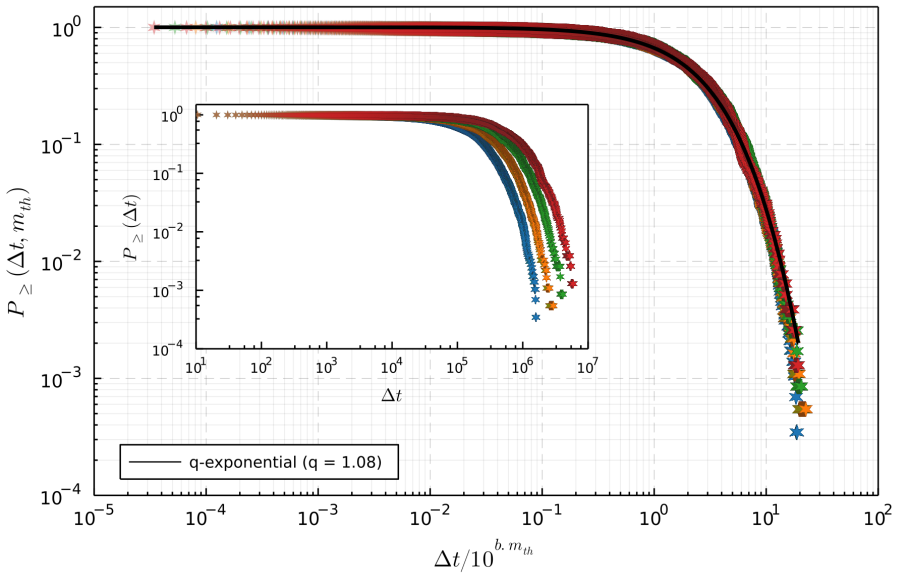

(b)

Fig. 2.11: Cumulative probability distributions of time intervals between consecutive earthquakes for worldwide seismological data from 2000 to 2019. All time intervals are in seconds (s). (a) For shallow earthquakes (hexagon), the magnitude thresholds, m_{th}, considered are 4.5 (blue), 4.7 (orange), 4.9 (green), and 5.1 (red). The best fit is given by a q-exponential (solid black line) with $q = 1.10$, $\beta_t = 13.607$, and correlation coefficient $R^2 = 0.99773$. *Inset:* distributions with no data collapse. (b) For deep earthquakes (star), $m_{th} = 5.3$ (blue), 5.5 (orange), 5.7 (green), and 5.9 (red). Best fit for a q-exponential (solid black line) with $q = 1.08$, $\beta_t = 4.158 \times 10^{-1}$, and $R^2 = 0.99944$. *Inset:* distributions with no data collapse.

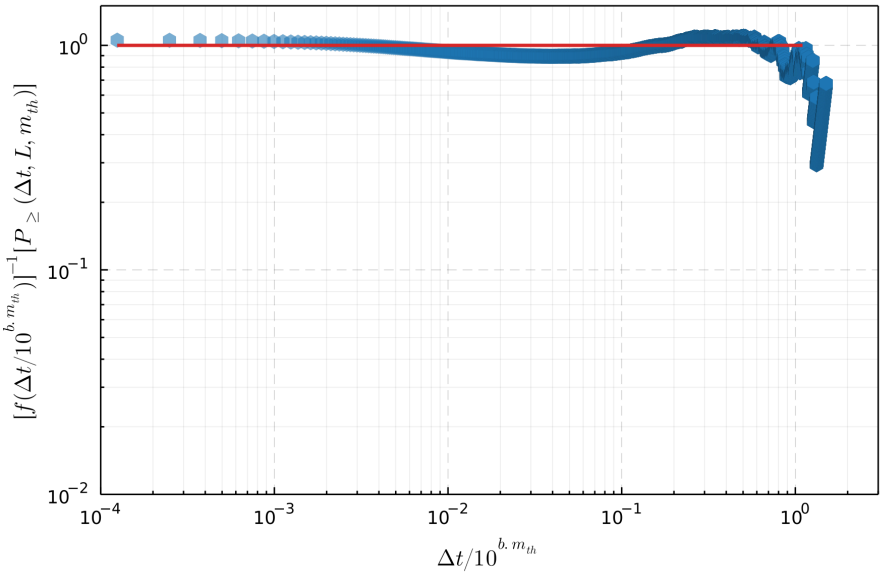

(a)

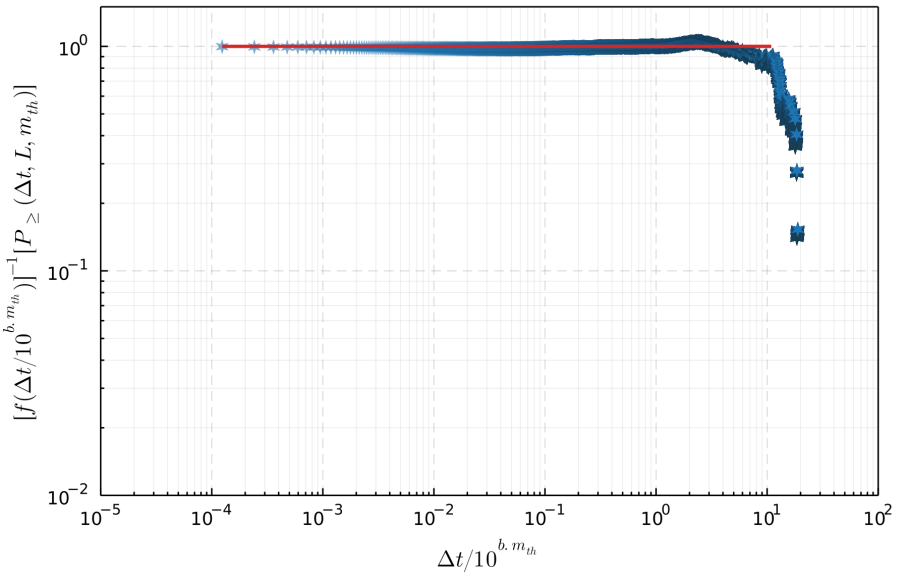

(b)

Fig. 2.12: Rescaled cumulative probability distribution of the time intervals between consecutive earthquakes for worldwide seismological data from 2000 to 2019. The time intervals are in seconds (s). The magnitude thresholds are (a) $m_{th} = 4.5$ for shallow earthquakes and (b) $m_{th} = 5.3$ for deep ones. The parameters used in $f(\Delta t \,/\, 10^{b.m_{th}})$ (Eq. 2.13) were those obtained for the q-exponential functions in Fig. 2.11. The solid red lines are guides for the eyes, which indicate the theoretical match between the data and the q-exponentials.

the shallow and deep data were 1.09 and 0.93, respectively. By applying this scaling relationship, the distributions for shallow and deep earthquakes become independent of m_{th}, as shown in Fig. 2.11.

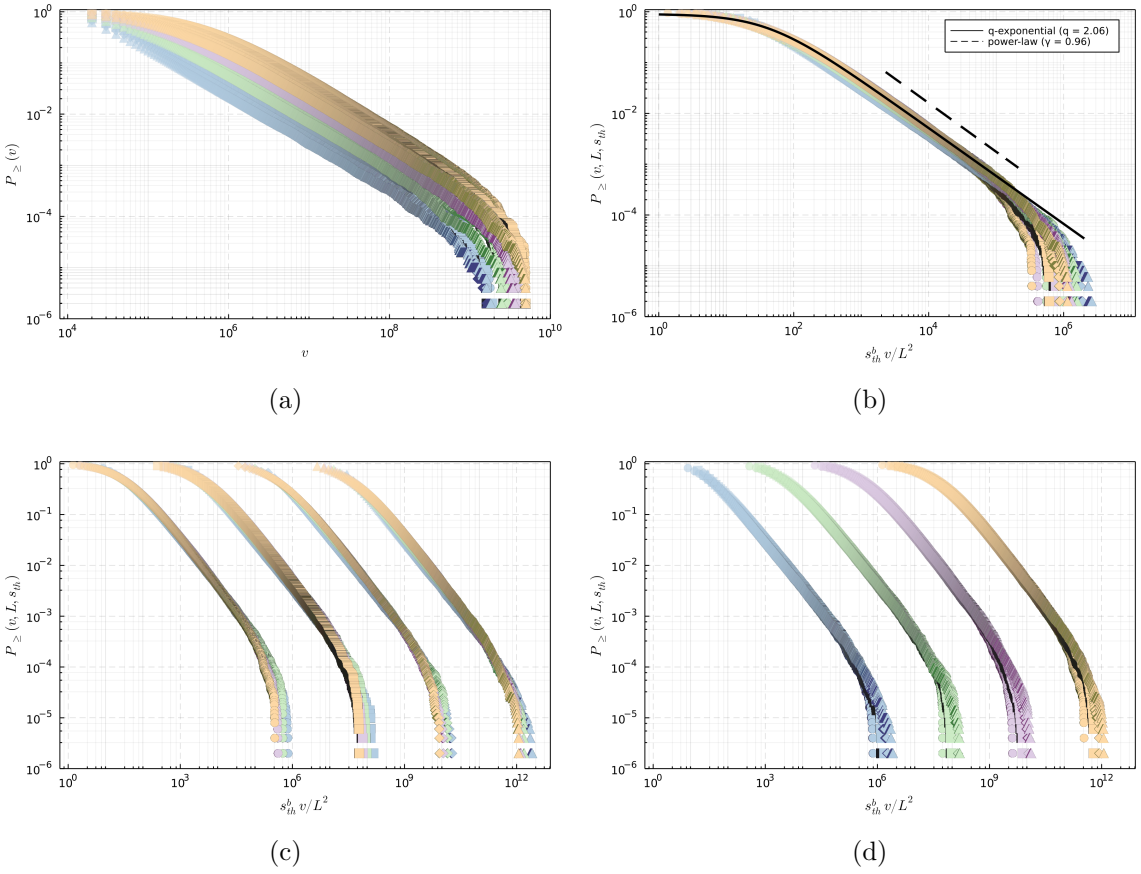

Fig. 2.13: Cumulative probability distributions of velocities for successive synthetic earthquakes from the modified OFC model. The lattice sizes considered are, L= 200 (light blue), 300 (light green), 400 (light purple), and 500 (light yellow). The lower size thresholds are, s_{th}= 25 (circle), 50 (square), 75 (diamond), and 100 (triangle). (a) Distributions for all sizes and lower size thresholds. (b) Data collapse by applying the scaling relationship presented in Eq. 2.14. The solid black line represents a q-exponential function with $q = 2.06$ and $\beta_v = 2.262 \times 10^{-2}$. The dashed black line shows the power-law behavior (given by Eq. 2.15), where the fitting was shifted for clarity. (c) and (d) represents the same plot as in (b), but data were shifted along the x-axis for each lower size threshold (s_{th}= 25, 50, 75, and 100, left to right) and lattice size (L= 200, 300, 400, and 500, left to right), respectively.

The best fitting for the collapsed curves gives the parameters $\beta_t = 13.607$, $q = 1.10$ for shallow earthquakes [Fig. 2.11(a)], and $\beta_t = 4.158 \times 10^{-1}$, $q = 1.08$ for the deep ones [Fig. 2.11(b)]. In Fig. 2.12, we have the rescaled time distribution with the same parameters as in Fig. 2.11, showing the q-exponential function agreement to the data and the Earth's finite size effect.

In addition, we highlight that some previous works have also studied the waiting time distributions for worldwide data, and, despite using different approaches, they also found data collapse for different region sizes and magnitude thresholds [81, 82, 8, 83, 84, 85]. Nevertheless, our work differs from these others since, besides comparing actual and simulated data, we also study the probability distributions

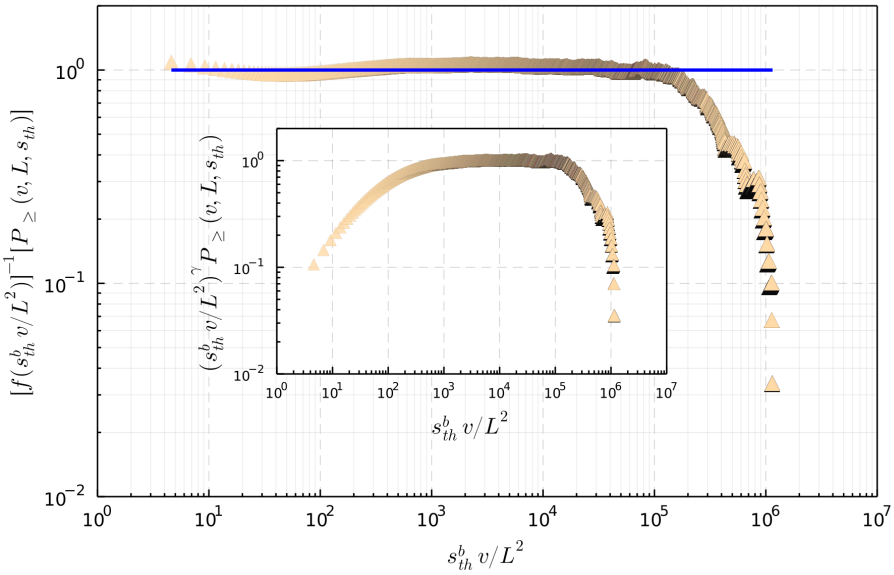

Fig. 2.14: Rescaled cumulative probability distribution of velocities for successive synthetic earthquakes from the modified OFC model with $L = 500$ and $s_{th} = 100$. The parameters in $f(s^b_{th}\,v/L^2)$ (Eq. 2.14) were those used for the q-exponential function in Fig. 2.13(b). The solid blue line is a guide for the eyes, indicating the perfect theoretical match between the synthetic data and the q-exponential. *Inset:* rescaled distribution for the power-law in Eq. 2.15, with $\gamma = 0.96$.

from the NESM viewpoint, which provides distributions that follow q-exponentials. Herein, we point out that the q-exponential function only appears in systems with long-range correlations in time and space. In that way, our results are also interesting since they reinforce the agreement between actual and simulated earthquakes, where the data collapse and the NESM behavior seem to indicate a single law for large and small earthquakes and regions.

2.5.3 Velocity analysis

From a spatial distance Δr_k and a time interval Δt_k between earthquakes k and $k+1$, we can define the "propagation" of the seismic activity, given by a quantity similar to *velocity*, $v_k = \Delta r_k/\Delta t_k$, as also proposed in [7]. It is important to highlight that this quantity does not have the physical meaning of *velocity*. Still, it is a measure of the "propagation" of subsequent events with a magnitude (or size) larger than a threshold m_{th} (or s_{th}). Thus, we studied the cumulative probability distribution of velocities for the synthetic earthquake catalog generated with the modified OFC model. Fig. 2.13 shows the results for lattice sizes from 200 to 500 and earthquake lower size thresholds equal to 25, 50, 75, and 100. It is possible to observe that, by dividing the scale relationships found for distance and time interval (Eqs. 2.11 and

2.12, respectively), for $d_f = 1.0$, the resulting scaling law,

$$P_{\geq}(v, L, s_{th}) = f(s_{th}^{b}\, v/L^2), \tag{2.14}$$

provides a data collapse for velocity. Similar to our previous analyses, the function $f(x)$ decays as a q-exponential, $e_q(-\beta_v x)$. As shown in Fig. 2.13(b), the best fitting is obtained for $q = 2.06$ and $\beta_v = 2.262 \times 10^{-2}$, where it was used the same previous b-value, $b = 0.88$.

For comparison purposes, Fig. 2.13(b) also displays the fitting for the data in the power-law range, i.e.,

$$P_{\geq}(v, L, s_{th}) \sim (s_{th}^{b}\, v/L^2)^{-\gamma}. \tag{2.15}$$

The exponent value found, $\gamma = 0.96$, agrees with the work mentioned earlier [7], where the authors found $\gamma = 1.0$ for actual earthquakes from southern California. We observe that our results agree with the stated in Eq. 2.4, i.e., $\gamma \approx 1/(1-q)$, for $[s_{th}^{b}\, v/L^2] \gg [-\beta_v(1-q)]^{-1}$, which implies that the velocity distributions for earthquakes in the modified OFC model are better fitted by q-exponentials than pure power-laws, as seen in Figs. 2.13(b) and 2.14. This way, we observed that the nonextensivity of the system of earthquakes is not only present in the spatial and temporal parameters but also in the "propagation" of the seismic activity.

It is important to note that the cutoff at large v, presented in Fig. 2.13(b), is due to the limitation imposed by the modeling. This limitation stems from the fact that, while the maximum distance between two events varies accordingly to the lattice size, L, the minimum time interval between two successive events does not have such variation, having the same value for all lattice sizes.

In Figs. 2.13(c) and 2.13(d), the rescaled distributions are shifted for different earthquake lower size thresholds and lattice lengths, respectively. Those separate plots aim to display the data collapse more clearly, presenting the scaling for L and s_{th} separately.

Finally, the distribution of velocities was analyzed for the worldwide data. The cumulative probability distribution of velocities for shallow and deep earthquakes, with different m_{th} values, are presented in Fig. 2.15. The scale relationship that allows the data to collapse is

$$P_{\geq}(v, m_{th}) = f(v/10^{-b.m_{th}}), \tag{2.16}$$

in which $f(x)$ decays as a q-exponential, $e_q(-\beta_v x)$, and the b-values were the same used for the temporal analysis, i.e., 1.09 and 0.93, for shallow and deep earthquakes, respectively. The fitting parameters obtained are $\beta_v = 9.087 \times 10^{-6}$, $q = 2.02$, for

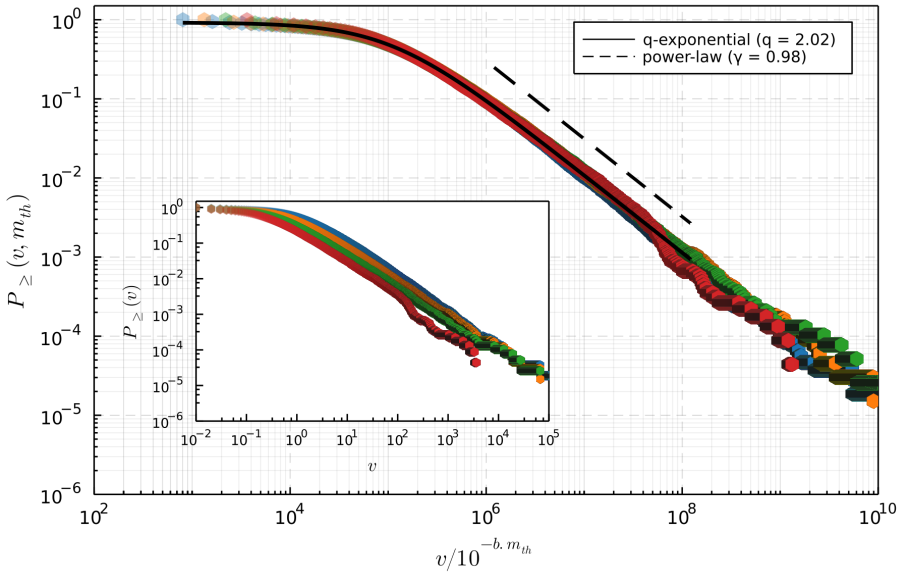

(a)

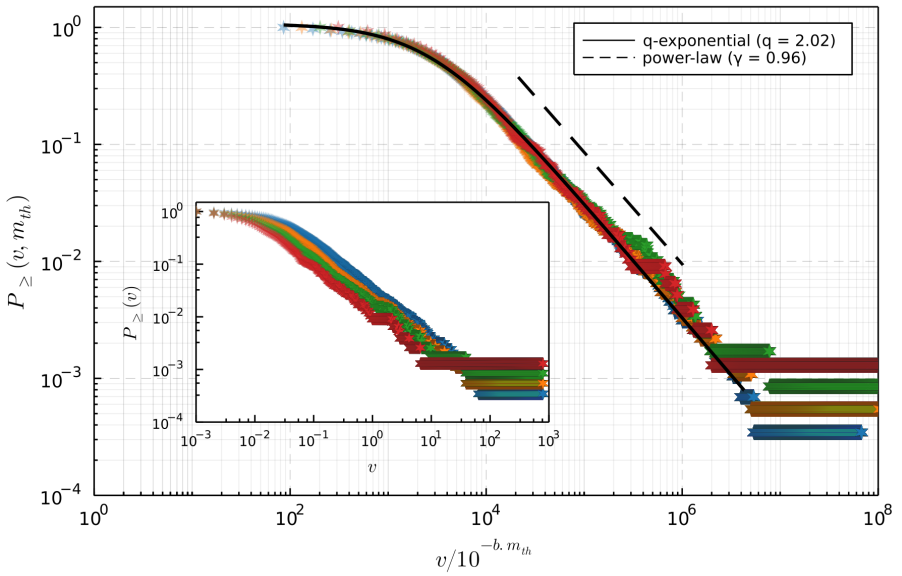

(b)

Fig. 2.15: Cumulative probability distributions of velocities for consecutive earthquakes from worldwide seismological data from 2000 to 2019. The velocities are in km/s. (a) For shallow earthquakes (hexagon), the magnitude thresholds, m_{th}, considered are 4.5 (blue), 4.7 (orange), 4.9 (green), and 5.1 (red). The solid black line is a q-exponential with $q = 2.02$ and $\beta_v = 9.087 \times 10^{-6}$. (b) For deep earthquakes (star), $m_{th} = 5.3$ (blue), 5.5 (orange), 5.7 (green), and 5.9 (red). The solid black line shows a q-exponential with $q = 2.02$ and $\beta_v = 3.612 \times 10^{-4}$. For both shallow and deep earthquakes, dashed black lines represent the power-law in Eq. 2.16, which were shifted for clarity. *Insets:* distributions with no data collapse.

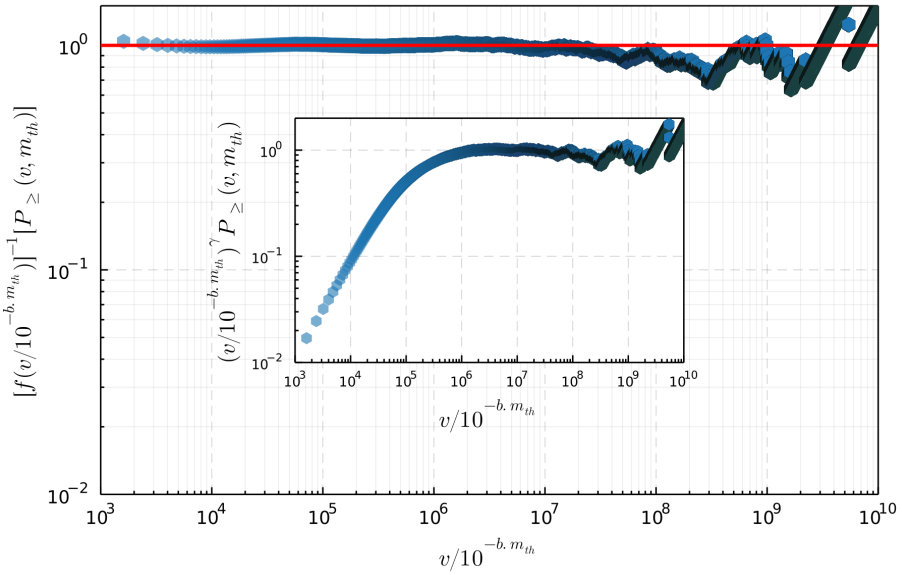

(a)

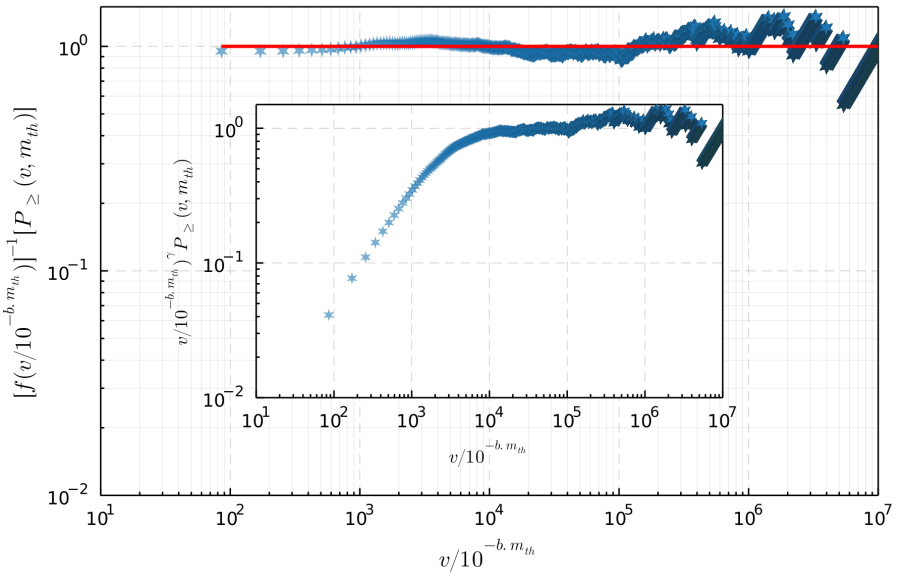

(b)

Fig. 2.16: Rescaled cumulative probability distribution of velocities for consecutive earthquakes from worldwide seismological data from 2000 to 2019. The velocities are in km/s. The parameters in $f(v/10^{-b.m_{th}})$ (Eq. 2.16) were those used for the q-exponential functions in (a) Fig. 2.15(a), for shallow earthquakes with $m_{th} = 4.5$, and (b) Fig. 2.15(b), for deep earthquakes with $m_{th} = 5.3$. In both shallow and deep earthquakes, the solid red line is a guide for the eyes, indicating the theoretical match between the data and the q-exponential. *Insets:* rescaled distributions for the power-law in Eq. 2.17.

the shallow events and $\beta_v = 3.612 \times 10^{-4}$, $q = 2.02$, for deep earthquakes.

Similar to what was done for the synthetic data, Fig. 2.15 shows the asymptotic

power-law behavior (described in Eq. 2.4) for the worldwide distributions,

$$P_{\geq}(v, m_{th}) \sim (v/10^{-b.m_{th}})^{-\gamma}, \tag{2.17}$$

where $\gamma \approx 1/(1-q)$, both for shallow and deep earthquakes. The exponent values for shallow and deep earthquakes were $\gamma = 0.98$ and $\gamma = 0.96$, respectively, which are close to unity, as found in [7] for California data. In Figs. 2.15 and 2.16, it is shown that the probability distributions of velocities for worldwide data have better agreements with q-exponentials than pure power-laws, being the power-law regime an asymptotic behavior for larger velocities. Figs. 2.14 and 2.16 show that, excluding the finite-size effects, the nonextensive approach fits the entire range of the distributions, differently from the power-law function, which produces two different behaviors, as found in [7].

Our findings show the robustness of seismicity behavior concerning the spatiotemporal scales and the "propagation" of the synthetic earthquakes produced by the modified OFC model, which is in good agreement with worldwide events. Moreover, the data collapse in all distributions presented in this work confirms the self-organized critical behavior of the seismological phenomenon.

2.6 Conclusions

In the present work, we have studied spatio-temporal features of synthetic earthquake data produced by a modified OFC model, using a *small-world-like* topology instead the original regular one. The results were compared with those found for actual worldwide earthquakes, where data from shallow and deep earthquakes were calculated separately, as in [59, 60].

Our analyses were performed by probability distributions of distances, time intervals, and "velocities", between successive events. The distributions were analyzed under the nonextensive statistical mechanics' viewpoint. We have found that all distributions, for both synthetic and actual earthquakes, follow the non-traditional q-exponential functions, which fits better the distributions than pure power-laws. Notably, the nonextensive behavior is only present in systems with strong correlation and long-range effects in space and time, indicating that these features are also present in earthquakes.

The agreement between the results produced by the model and those found for natural earthquakes, in all studied cases, is also remarkable. Since the OFC model with a *small-world-like* topology has self-organized criticality features and long-range interactions between the elements in the lattice, the concordance between synthetic and actual earthquake results indicates that the same two characteristics

are present in the seismic phenomenon. Therefore, our results strengthen the idea of self-organized criticality and long-range spatiotemporal correlations between earthquakes. We also note that the SOC perspective supports the view that the Earth's crust accumulates energy at a slow rate and that, at some point, this energy can no longer be maintained and is then released rapidly through faults.

The OFC model's synthetic data have been made using various lattice sizes and considering different lower threshold values of earthquake sizes. The worldwide shallow and deep earthquakes data were considered for different magnitude thresholds. For space, time, and velocity, in both synthetic and actual earthquakes, it was possible to produce data collapses using scaling laws, indicating the presence of criticality in the seismological phenomenon and spatiotemporal self-similarity, covering many types of tectonic environments and magnitude ranges. That result also implies no difference between the earthquake spatiotemporal statistics from small and large sizes or magnitudes, which also means that there is a no different mechanism for producing aftershocks. It means that, regardless of the physical mechanism of energy release and the consequent emergence of an earthquake, that mechanism operates similarly on all scales of space and time.

We also show that, for the spatiotemporal statistical studies provided in this work, the modified OFC model presents advances and consistencies that are not present in the original 2D spring-block (Burridge-Knopoff) model [80, 76]. The q-values found in our results are close to those in actual earthquakes, as well as the size and magnitude invariances evinced by the scaling relationships presented in all distributions.

Given our results, the present study complements previous works by strengthening the use of complex systems concepts to study seismological problems and the importance of nonextensive statistical physics for understanding the lithosphere dynamics.

Acknowledgements

D.S.R.F. and J.F.F.M acknowledges the FCT (Portuguese Funding Agency) Grants No. SFRH/BPD/123077/2016 and No. CEECIND/04697/2017. D.S.R.F., A.R.P., and R.P.F., thanks FAPERJ (Brazilian Funding Agency), for grant number 241029 and 262754. J.R. thanks CAPES (Brazilian Funding Agency), for the scholarship.

References

[1] Beno Gutenberg and Charles Francis Richter. Earthquake magnitude, intensity, energy, and acceleration. *Bulletin of the Seismological society of America*, 32 (3):163–191, 1942.

[2] Fusakichi Omori. Investigation of aftershocks, rep. earthq. inv. comm. 2, 103 (1894) and j. *Coll. Sci. Imper. Univ. Tokyo*, 7:111, 1894.

[3] Ole Peters, Christopher Hertlein, and Kim Christensen. A complexity view of rainfall. *Physical review letters*, 88(1):018701, 2001.

[4] Bruce D Malamud, Gleb Morein, and Donald L Turcotte. Forest fires: an example of self-organized critical behavior. *Science*, 281(5384):1840–1842, 1998.

[5] Andreas CW Baas. Chaos, fractals and self-organization in coastal geomorphology: simulating dune landscapes in vegetated environments. *Geomorphology*, 48(1-3):309–328, 2002.

[6] Per Bak, Kim Christensen, Leon Danon, and Tim Scanlon. Unified scaling law for earthquakes. *Physical Review Letters*, 88(17):178501, 2002.

[7] Jörn Davidsen and Maya Paczuski. Analysis of the spatial distribution between successive earthquakes. *Physical Review Letters*, 94(4):048501, 2005.

[8] Alvaro Corral. Mixing of rescaled data and bayesian inference for earthquake recurrence times. *Nonlinear processes in Geophysics*, 12(1):89–100, 2005.

[9] Jörn Davidsen, Peter Grassberger, and Maya Paczuski. Earthquake recurrence as a record breaking process. *Geophysical Research Letters*, 33(11), 2006.

[10] Yan Y Kagan and David D Jackson. Earthquake rate and magnitude distributions of great earthquakes for use in global forecasts. *Geophysical Journal International*, 206(1):630–643, 2016.

[11] Sangwon Chae, Suyoung Jang, Sangmok Lee, and Donghyun Lee. complex system analysis of korean peninsula earthquake data. *Scientific reports*, 10(1): 1–8, 2020.

[12] Per Bak, Chao Tang, and Kurt Wiesenfeld. Self-organized criticality: An explanation of the 1/f noise. *Physical review letters*, 59(4):381, 1987.

[13] Per Bak and Maya Paczuski. Complexity, contingency, and criticality. *Proceedings of the National Academy of Sciences*, 92(15):6689–6696, 1995.

[14] David C Roberts and Donald L Turcotte. Fractality and self-organized criticality of wars. *Fractals*, 6(04):351–357, 1998.

[15] Roman Frigg. Self-organised criticality—what it is and what it isn't. *Studies in History and Philosophy of Science Part A*, 34(3):613–632, 2003.

[16] Nicholas W Watkins, Gunnar Pruessner, Sandra C Chapman, Norma B Crosby, and Henrik J Jensen. 25 years of self-organized criticality: Concepts and controversies. *Space Science Reviews*, 198(1):3–44, 2016.

[17] Anne Sornette and Didier Sornette. Self-organized criticality and earthquakes. *EPL (Europhysics Letters)*, 9(3):197, 1989.

[18] Ian Main. Statistical physics, seismogenesis, and seismic hazard. *Reviews of Geophysics*, 34(4):433–462, 1996.

[19] Luciano Telesca, Vincenzo Cuomo, Vincenzo Lapenna, Filippos Vallianatos, and George Drakatos. Analysis of the temporal properties of greek aftershock sequences. *Tectonophysics*, 341(1-4):163–178, 2001.

[20] Donald L Turcotte. Self-organized criticality: Does it have anything to do with criticality and is it useful? *Nonlinear Processes in Geophysics*, 8(4/5):193–196, 2001.

[21] Didier Sornette. *Critical Phenomena in Natural Sciences*. Springer, Heidelberg, 2 edition, 2006.

[22] Elisaveta Marekova. Analysis of the spatial distribution between successive earthquakes occurred in various regions in the world. *Acta Geophysica*, 62(6): 1262–1282, 2014.

[23] Rene C Batac. Clustering regimes in a sandpile with targeted triggering. *EPL (Europhysics Letters)*, 135(1):19003, 2021.

[24] Deepak Dhar. Self-organized critical state of sandpile automaton models. *Physical Review Letters*, 64(14):1613, 1990.

[25] Barbara Drossel and Franz Schwabl. Self-organized critical forest-fire model. *Physical review letters*, 69(11):1629, 1992.

[26] Robert Burridge and Leon Knopoff. Model and theoretical seismicity. *Bulletin of the seismological society of america*, 57(3):341–371, 1967.

[27] Zeev Olami, Hans Jacob S Feder, and Kim Christensen. Self-organized criticality in a continuous, nonconservative cellular automaton modeling earthquakes. *Physical Review Letters*, 68(8):1244–1247, 1992.

[28] Kim Christensen and Zeev Olami. Scaling, phase transitions, and nonuniversality in a self-organized critical cellular-automaton model. *Physical Review A*, 46(4):1829, 1992.

[29] Zeev Olami and Kim Christensen. Temporal correlations, universality, and multifractality in a spring-block model of earthquakes. *Physical Review A*, 46 (4):R1720–R1723, 1992.

[30] Patrizia Tosi, Valerio De Rubeis, Vittorio Loreto, and Luciano Pietronero. Space-time combined correlation integral and earthquake interactions. *Annals of Geophysics*, 47(6):1849–1854, 2004.

[31] Luciano Telesca and Vincenzo Lapenna. Investigating the spatial variability of the time-scaling properties in italian seismicity. *Nonlinear Processes in Geophysics*, 11(5/6):545–552, 2004.

[32] Alvaro Corral. Universal earthquake-occurrence jumps, correlations with time, and anomalous diffusion. *Physical review letters*, 97(17):178501, 2006.

[33] Sabine Lennartz, Valerie N Livina, Armin Bunde, and Shlomo Havlin. Long-term memory in earthquakes and the distribution of interoccurrence times. *EPL (Europhysics Letters)*, 81(6):69001, 2008.

[34] Marco Baiesi. Correlated earthquakes in a self-organized model. *Nonlinear Processes in Geophysics*, 16(2):233–240, 2009.

[35] Maria C Mariani, Md Al Masum Bhuiyan, Osei K Tweneboah, and Hector Gonzalez-Huizar. Long memory effects and forecasting of earthquake and volcano seismic data. *Physica A: Statistical Mechanics and its Applications*, 559: 125049, 2020.

[36] Constantino Tsallis. Possible generalization of boltzmann-gibbs statistics. *Journal of statistical physics*, 52(1):479–487, 1988.

[37] Cleiton S Barbosa, Douglas SR Ferreira, Marco A do Espírito Santo, and Andrés RR Papa. Statistical analysis of geomagnetic field reversals and their consequences. *Physica A: Statistical Mechanics and its Applications*, 392(24): 6554–6560, 2013.

[38] Georgios Balasis, Ioannis A Daglis, Anastasios Anastasiadis, Constantinos Papadimitriou, Mioara Mandea, and Konstantinos Eftaxias. Universality in solar flare, magnetic storm and earthquake dynamics using tsallis statistical mechanics. *Physica A: Statistical Mechanics and its Applications*, 390(2):341–346, 2011.

[39] Filippos Vallianatos, Philip Benson, Philip Meredith, and Peter Sammonds. Experimental evidence of a non-extensive statistical physics behaviour of fracture in triaxially deformed etna basalt using acoustic emissions. *EPL (Europhysics Letters)*, 97(5):58002, 2012.

[40] Filippos Vallianatos. A non extensive view of electrical resistivity spatial distribution estimated using inverted transient electromagnetic responses in a karstified formation (keritis basin, crete, greece). *Physica A: Statistical Mechanics and its Applications*, 505:171–178, 2018.

[41] Kalliopi Chochlaki, Georgios Michas, and Filippos Vallianatos. Complexity of the yellowstone park volcanic field seismicity in terms of tsallis entropy. *Entropy*, 20(10):721, 2018.

[42] Carlos S Vilar, George S França, Raimundo Silva, and Jailson S Alcaniz. Nonextensivity in geological faults? *Physica A: Statistical Mechanics and its Applications*, 377(1):285–290, 2007.

[43] Thais M Scherrer, George S França, Raimundo Silva, Daniel B de Freitas, and Carlos S Vilar. Nonextensivity at the circum-pacific subduction zones—preliminary studies. *Physica A: Statistical Mechanics and its Applications*, 426:63–71, 2015.

[44] Amir H Darooneh and Ali Mehri. A nonextensive modification of the gutenberg–richter law:¡ i¿ q¡/i¿-stretched exponential form. *Physica A: Statistical Mechanics and its Applications*, 389(3):509–514, 2010.

[45] Thais M Scherrer, George S França, Raimundo Silva, Daniel B de Freitas, and Carlos S Vilar. Analysis of four brazilian seismic areas using a nonextensive approach. *Europhysics Letters*, 109(4):49001, 2015.

[46] Quetzalcoatl Rodríguez-Pérez, Víctor Hugo Márquez-Ramírez, and Francisco Ramón Zúñiga. Seismicity characterization of oceanic earthquakes in the mexican territory. *Solid Earth*, 11(3):791–806, 2020.

[47] VN Sychev and NA Sycheva. The earthquakes aftershock processes of the tien shan and its surrounding area. In *IOP Conference Series: Earth and Environmental Science*, volume 324, page 012003. IOP Publishing, 2019.

[48] Douglas SR Ferreira, Andrés RR Papa, and Ronaldo Menezes. On the agreement between small-world-like ofc model and real earthquakes. *Physics Letters A*, 379(7):669–675, 2015.

[49] Filippos Vallianatos and Kyriaki Pavlou. Scaling properties of the mw7. 0 samos (greece), 2020 aftershock sequence. *Acta Geophysica*, pages 1–18, 2021.

[50] Sumiyoshi Abe and Norikazu Suzuki. Law for the distance between successive earthquakes. *Journal of Geophysical Research: Solid Earth*, 108(B2), 2003.

[51] Amir H Darooneh and Cyruse Dadashinia. Analysis of the spatial and temporal distributions between successive earthquakes: Nonextensive statistical mechanics viewpoint. *Physica A: Statistical Mechanics and its Applications*, 387(14): 3647–3654, 2008.

[52] Vitor HA Dias, Andrés RR Papa, and Douglas SR Ferreira. Analysis of temporal and spatial distributions between earthquakes in the region of california through non-extensive statistical mechanics and its limits of validity. *Physica A: Statistical Mechanics and its Applications*, 529:121471, 2019.

[53] Luciano Telesca. Analysis of italian seismicity by using a nonextensive approach. *Tectonophysics*, 494(1-2):155–162, 2010.

[54] Luciano Telesca and Vincenzo Lapenna. Measuring multifractality in seismic sequences. *Tectonophysics*, 423(1-4):115–123, 2006.

[55] Filippo Caruso, Alessandro Pluchino, Vito Latora, Sergio Vinciguerra, and Andrea Rapisarda. Analysis of self-organized criticality in the olami-feder-christensen model and in real earthquakes. *Physical Review E*, 75(5):055101, 2007.

[56] Sumiyoshi Abe and Norikazu Suzuki. Small-world structure of earthquake network. *Physica A: Statistical Mechanics and its Applications*, 337(1-2):357–362, 2004.

[57] Sumiyoshi Abe and Norikazu Suzuki. Complex-network description of seismicity. *Nonlinear Processes in Geophysics*, 13(2):145–150, 2006.

[58] Douglas SR Ferreira, Andrés RR Papa, and Ronaldo Menezes. Small world picture of worldwide seismic events. *Physica A: Statistical Mechanics and its Applications*, 408:170–180, 2014.

[59] Douglas Ferreira, Jennifer Ribeiro, Andrés Papa, and Ronaldo Menezes. Towards evidence of long-range correlations in shallow seismic activities. *EPL (Europhysics Letters)*, 121(5):58003, 2018.

[60] Douglas SR Ferreira, Jennifer Ribeiro, Paulo SL Oliveira, André R Pimenta, Renato P Freitas, and Andrés RR Papa. Long-range correlation studies in deep

earthquakes global series. *Physica A: Statistical Mechanics and its Applications*, 560:125146, 2020.

[61] Filippo Caruso, Vito Latora, Alessandro Pluchino, Andrea Rapisarda, and Bosiljka Tadić. Olami-feder-christensen model on different networks. *The European Physical Journal B-Condensed Matter and Complex Systems*, 50(1):243–247, 2006.

[62] Marcelo L Lyra and Constantino Tsallis. Nonextensivity and multifractality in low-dimensional dissipative systems. *Physical review letters*, 80(1):53, 1998.

[63] Sumiyoshi Abe. Geometry of escort distributions. *Physical Review E*, 68(3): 031101, 2003.

[64] Sumiyoshi Abe and Norikazu Suzuki. Scale-free statistics of time interval between successive earthquakes. *Physica A: Statistical Mechanics and its Applications*, 350(2-4):588–596, 2005.

[65] Duncan J Watts and Steven H Strogatz. Collective dynamics of 'small-world'networks. *nature*, 393(6684):440–442, 1998.

[66] Yan Y Kagan and David D Jackson. Long-term earthquake clustering. *Geophysical Journal International*, 104(1):117–133, 1991.

[67] David P Hill, PA Reasenberg, A Michael, WJ Arabaz, G Beroza, D Brumbaugh, JN Brune, R Castro, S Davis, Diane dePolo, et al. Seismicity remotely triggered by the magnitude 7.3 landers, california, earthquake. *Science*, 260(5114):1617–1623, 1993.

[68] Ross S Stein. The role of stress transfer in earthquake occurrence. *Nature*, 402 (6762):605–609, 1999.

[69] Mirko S Mega, Paolo Allegrini, Paolo Grigolini, Vito Latora, Luigi Palatella, Andrea Rapisarda, and Sergio Vinciguerra. Power-law time distribution of large earthquakes. *Physical Review Letters*, 90(18):188501, 2003.

[70] Patrizia Tosi, Valerio De Rubeis, Vittorio Loreto, and Luciano Pietronero. Space–time correlation of earthquakes. *Geophysical Journal International*, 173 (3):932–941, 2008.

[71] Shinji Toda and Ross S Stein. Long-and short-term stress interaction of the 2019 ridgecrest sequence and coulomb-based earthquake forecasts. *Bulletin of the Seismological Society of America*, 110(4):1765–1780, 2020.

[72] Cliff Frohlich. The nature of deep-focus earthquakes. *Annual Review of Earth and Planetary Sciences*, 17:227, 1989.

[73] Cliff Frohlich. *Deep earthquakes*. Cambridge university press, UK, 1 edition, 2006.

[74] Jörn Davidsen and Christian Goltz. Are seismic waiting time distributions universal? *Geophysical Research Letters*, 31(21), 2004.

[75] Giorgos Papadakis, Filippos Vallianatos, and Peter Sammonds. Evidence of nonextensive statistical physics behavior of the hellenic subduction zone seismicity. *Tectonophysics*, 608:1037–1048, 2013.

[76] Tomohiro Hasumi. Hypocenter interval statistics between successive earthquakes in the two-dimensional burridge–knopoff model. *Physica A: Statistical Mechanics and its Applications*, 388(4):477–482, 2009.

[77] Filippos Vallianatos and Peter Sammonds. Evidence of non-extensive statistical physics of the lithospheric instability approaching the 2004 sumatran–andaman and 2011 honshu mega-earthquakes. *Tectonophysics*, 590:52–58, 2013.

[78] Alvaro Corral. Local distributions and rate fluctuations in a unified scaling law for earthquakes. *Physical Review E*, 68(3):035102, 2003.

[79] Chris G Antonopoulos, George Michas, Filippos Vallianatos, and Tassos Bountis. Evidence of q-exponential statistics in greek seismicity. *Physica A: Statistical Mechanics and its Applications*, 409:71–77, 2014.

[80] Tomohiro Hasumi. Interoccurrence time statistics in the two-dimensional burridge-knopoff earthquake model. *Physical Review E*, 76(2):026117, 2007.

[81] Alvaro Corral. Long-Term Clustering, Scaling, and Universality in the Temporal Occurrence of Earthquakes. *Physical Review Letters*, 92(10):108501, March 2004. ISSN 0031-9007, 1079-7114.

[82] Alvaro Corral. Universal local versus unified global scaling laws in the statistics of seismicity. *Physica A: Statistical Mechanics and its Applications*, 340(4):590–597, September 2004. ISSN 03784371.

[83] Alvaro Corral. Renormalization-Group Transformations and Correlations of Seismicity. *Physical Review Letters*, 95(2):028501, July 2005. ISSN 0031-9007, 1079-7114.

[84] Alvaro Corral. Time-decreasing hazard and increasing time until the next earthquake. *Physical Review E*, 71(1):017101, January 2005. ISSN 1539-3755, 1550-2376.

[85] Alvaro Corral. Dependence of earthquake recurrence times and independence of magnitudes on seismicity history. *Tectonophysics*, 424(3-4):177–193, October 2006. ISSN 00401951.

Chapter 3

Correlation Properties in Worldwide and Synthetic Earthquake Networks

Artigo publicado - *RIBEIRO, J., OLIVEIRA JR, P.S.O., PEREIRA, L.O., et al., 2022, "Correlation Properties in Worldwide and Synthetic Earthquake Networks", Brazilian Journal of Geophysics, v.40, n.1. DOI: 10.22564/brjg.v40i1.2134.*

Abstract

In this work, we studied the correlation properties of seismic networks by analyzing the assortativity of worldwide and synthetic earthquake networks. We used data from the World Earthquake Catalog for the period from 2002 to 2016, considering earthquakes with magnitude thresholds 4.5 and 5.0. Shallow earthquakes (a depth of up to 70 km) and deep earthquakes (a depth greater than 70 km) were analyzed separately. Synthetic data were produced from simulations using a modified version of the Olami-Feder-Christensen model, which can reproduce several statistical characteristics of actual earthquakes. The study was carried out for two methodologies of connections between the network elements, where the correlation measures were calculated for all networks. The results for shallow earthquakes and synthetic data indicate: assortative correlation (locations with similar seismic activities tend to have a greater number of connections between them); mainshocks induce other mainshocks in both close and further away regions; the structure found has a type of "attracting dynamics", where the places with a more intense seismic activity produce large numbers of connections in other locations around them. Deep earthquake networks are neutral and therefore do not have an explicit correlation type. Our findings agree with previous works for specific areas and contribute to better understand correlations between seismological regions.

3.1 Introduction

We are surrounded by several systems that contain a huge number of components in which their elements have many kinds of interactions with each other. These systems belong to the category of "complex systems", making it difficult to understand the dynamics of the entire system knowing only the behavior of the system elements, since the collective behavior is not trivial. In this framework, complex networks are in the heart of complex systems once they have the power to decode the interactions between the system elements, being a powerful tool to investigate the topological structure and statistical behavior of complex systems. The science of complex networks has been successfully applied in many real-world networked systems, such as the Internet, economic market, spread of diseases, solar flares, and social relationships [1, 2, 3, 4, 5, 6].

In the last thirty years, several works have implemented the concept of complexity in the study of earthquakes, aiming to better understand and characterize the seismological dynamics and properties [7, 8, 9, 10]. The complex network theories started to be used in the seismological study in [11, 12]. The authors constructed earthquake networks for seismic data from California and Japan, taking into account spatial and temporal information of successive earthquakes. After Abe's seminal paper, several authors have been applying similar complex network concepts to earthquake studies [13, 14, 15, 16, 17]. It is noteworthy that over the years, other authors have also studied the earthquake phenomenon under the viewpoint of complex networks, by using approaches different from Abe and Suzuki, such as the Baiesi-Packzuski model [18], the visibility graph model [19], and the space-time influence domain [20]. Despite the different network construction methods and analyses, the results found in the various models show that the earthquake networks have similar behavior to the ones of other networks found in nature for many different phenomena.

A handy tool in studying earthquakes is the use of computer simulations. These simulations can be of the type "simplified", where the models capture the main characteristics of the phenomenon, or of the type realistic and more comprehensive, trying to describe the phenomenon in a more detailed way. In statistical studies, it is common to use simplified models capable of generating large amounts of data without requiring substantial computational capacity. The use of complex networks for the statistical study of earthquakes can be done by using actual earthquake data or by using synthetic data generated through computer simulation models. One of the most used simplified models is the one created by Olami, Feder and Christensen (OFC model), which incorporates several characteristics of complex systems [21, 22, 23]. A more detailed explanation of this model will be presented in

the next section.

Previous works have analyzed seismological data (from actual and synthetic catalogs), performing some of the most common and fundamental features of complex networks, such as the degree distribution, the clustering coefficient, and the average shortest path. However, another interesting characteristic to be studied in earthquakes is the correlation property. Correlation properties can be analyzed in complex networks using a network measure named assortativity, which indicates a type of connection preference that elements tend to have when connecting to each other. For example, in social networks, it is observed that people tend to relate to other people belonging to the same group as themselves [5]. However, the protein-interaction network of yeast has the opposite property. The proteins with more significant connections interact much more with small-connected proteins [24]. In this way, the study of the assortativity correlation feature can help provide more complete information on the structure and dynamics of the system. The correlation property using the assortativity concept will be presented in the theoretical background section of this paper.

Therefore, in order to advance one more step towards greater knowledge about the earthquake phenomenon, we analyze in this paper the assortativity features for the networks created from worldwide seismic events using two different models of connections for two different datasets: one for shallow earthquakes and the other for deep earthquakes. We differentiate the seismic events concerning their depths since shallow and deep earthquakes are mechanically different from each other [25, 26]. Still, deep earthquakes occur, in general, in subduction zones of tectonic plates [25]. On the other hand, shallow earthquakes are not only related to these zones, but they also happen in faults and plate slippage, making their occurrence more distributed in geographic regions around the world than deep seismic events.

Therefore, we make the data division by depth to observe whether it would exist differences in the properties of the networks created with these two datasets. We adopted the division used in [26, 27]: shallow earthquakes are those with a depth of up to 70 km, and deep earthquakes are the ones located deeper than this value. Furthermore, a network of connections was also created using earthquake data simulated with a modified version of the Olami-Feder-Christensen model [28]. The results were compared with those of the actual seismic events. This paper is organized as follows. First, we have a brief theoretical background on complex networks and the OFC model. The following section is dedicated to presenting information about our worldwide and synthetic earthquake data catalogs. Then, the methods employed to construct our networks are described. Finally, we show and discuss the results obtained and present the conclusions.

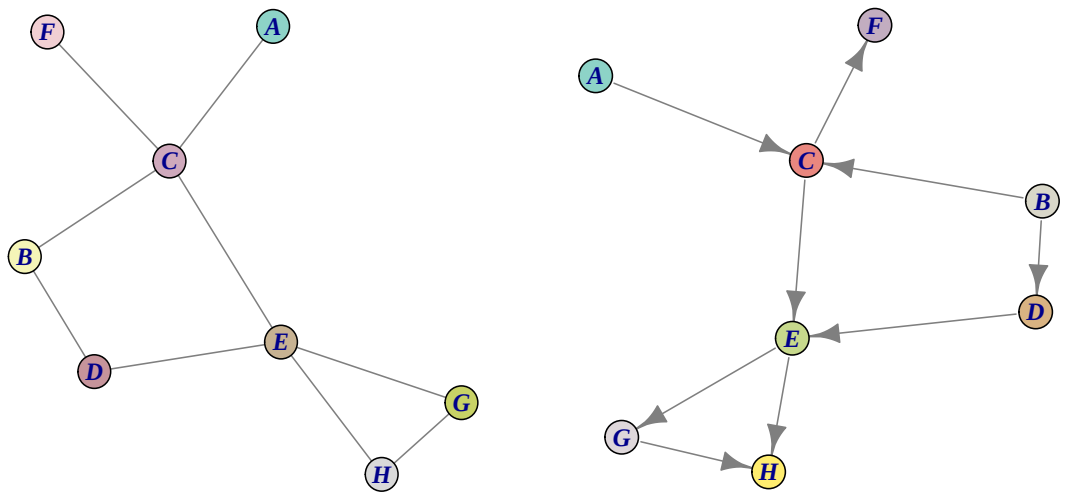

Fig. 3.1: Examples of (a) an undirected network and (b) a directed network. The networks have 8 nodes and 9 links each one.

3.2 Theoretical Background

Aiming to make this paper self-contained, we present a brief review of theoretical topics considered important to the development of this article.

3.2.1 Fundamental Concepts of Complex Networks

Networks are commonly represented by graphs, where the elements are nodes (or vertices), and the interactions are expressed by links (or edges) between the nodes. A fundamental property in networks is the degree, k_i, of each node, i, which gives the number of links between the node and other nodes. The links in a network can be directed (if the links have a specific direction, going from one node to another) or undirected (if there is no direction for the links between the nodes), as shown in Fig. 3.1. In a directed network, there is a distinction between the number of incoming links, expressed by the incoming degree, k_i^{in}, and the outgoing links, given by the outgoing degree, k_i^{out}.

In this way, the total degree in directed networks is provided by $k_i = k_i^{in} + k_i^{out}$. Examples of directed networks are the *World Wide Web (WWW)*, where the links point from one webpage to another, and an ecological web, where the directed links indicate which animal is a predator of the other. Undirected networks can be exemplified by a scientific collaboration, since if a scientist "A" collaborates with a scientist "B", the scientist "B" also collaborates with "A".

For a mathematical description, the networks are usually described by adjacency matrices. If an unweighted network (i.e., all links have the same weight) has N nodes, the links between them are represented by a $N \times N$ matrix, with elements:

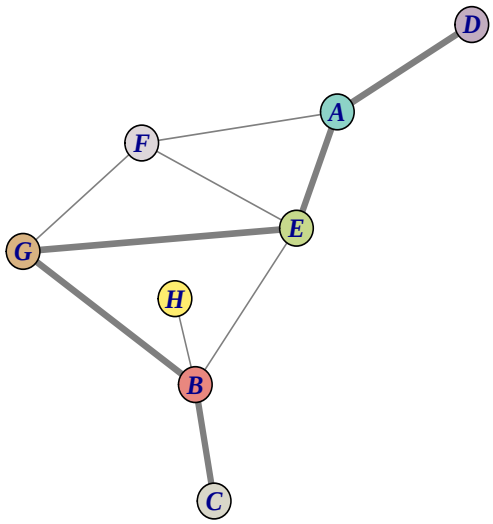

Fig. 3.2: The highlighted links exemplify one possible path between nodes C and D. However, the shortest path between these nodes is the one that follows the nodes sequence $C - B - E - A - D$.

$$A_{ij} = \begin{cases} 1, \text{ if there is a link from } i \text{ to } j \\ 0, \text{ if there is no link from } i \text{ to } j. \end{cases} \tag{3.1}$$

In an undirected network case, the adjacency matrix is symmetric, which means, $A_{ij} = A_{ji}$.

From the nodes' degrees, it is possible to calculate the network's degree distribution $P(k)$, which is the probability that a randomly selected node in the network has a degree k. Since the functional form of $P(k)$ is deeply related to many properties in the network, it assumes an essential role in network studies. One remarkable example is that if the degree distribution of nodes follows a power law, i.e., $P(k) \sim k^{-\gamma}$ (where γ is a positive constant), it represents a signature of an organizing principle, called *scale-free* property. The presence of a power-law for the degree distribution, instead of a Poisson distribution, implies that the nodes are not connected randomly; instead, they follow a preferential attachment rule to connect to each other. It means that a scale-free network has several small degree nodes and only a few with high degree values. These last ones are named *hubs*.

Another important feature of a complex network arises when every node is "close" to every other node, i.e., it is possible to go from one arbitrary node to another taking only a few "steps". When it happens, these networks are called small-world networks. As proposed by [1], two important metrics to classify a small-world network are the clustering coefficient and the average path length. The clustering coefficient measures how likely it is that two elements connected to a node are also connected to each other. The average path length is the average of the shortest

distances between all pairs of nodes in the network, where the distance between two nodes is the number of links between them, as exemplified in Fig. 3.2. Small-world networks have a high clustering coefficient value compared to a random network with the same characteristics and a small average path length compared to the number of nodes in the network.

Within this frame, the complex networks approach has been applied to seismological studies from many areas in the world, as Japan, California, Iran, Chile, Greece, and worldwide [11, 12, 13, 29, 30, 31]. The results found in the previous works show the scale-free and small-world features in the networks built from the seismological data, where the degree exponents γ for the networks are within the usual range $2 \leq \gamma \leq 3$, which is the range for several of the existing networks in nature [32, 33, 34]. As indicated by [35], the presence of scale-free properties in earthquake networks indicates that, geographically, aftershocks associated with a mainshock tend to return to the locus of the mainshock, creating *hubs* similarly to the preferential attachment rule. Furthermore, the small-world feature indicates that the earthquake network is significantly clustered, and the average distance between two arbitrary nodes (geographical regions where earthquakes have occurred) is very small.

3.2.2 Correlation Properties in Complex Networks

In the last twenty years, the study of correlation properties in networks using assortativity has been implemented in many real-world networks [36, 5, 37, 38, 39, 40, 6]. Assortativity (or assortative mixing) refers to the tendency of nodes in a network to connect to other nodes with similar properties, making the links not to be placed between nodes completely at random, but depending in some way on the property in question. Here, we focus on assortativity in terms of a node's degree. The analysis of this property allows us to investigate the relation between the connectivity degrees of the nodes that link to each other. A statistical measure that is commonly used to analyze this preference is the nearest-neighbors average connectivity of nodes, or also denominated degree correlation function [41, 42, 43], expressed as

$$k_{nn}(k) = \sum_{j} jP(j|k), \tag{3.2}$$

where $P(j|k)$ is the conditional probability that an arbitrary selected edge links a j-degree node with a k-degree node. This function considers the average degree of the neighbors of a node as a function of its degree k. If it is independent of k, the network has no obvious degree correlation and is called neutral. When, however,

$k_{nn}(k)$ increases with k, the network is assortative. It means that the hubs (nodes with high degrees) of the network tend to connect to other hubs and nodes with low degrees tend to be linked to other low degree nodes. On the other hand, if $k_{nn}(k)$ decreases with k, the network is disassortative, i.e., the hubs prefer to link to nodes with low degrees [43].

Thus, the degree correlation function can help detect the presence or absence of correlations in real networks. However, a helpful way to capture the magnitude of the correlations present in the networks is using a unique number. This number can be computed from the fitting of the $k_{nn}(k)$ plot or by calculating the degree correlation coefficient, defined as follows.

The degree correlation coefficient, which is the Pearson correlation coefficient between the degrees found at the two ends of the same link, is a complementation of the analysis of the degree correlation function and provides us with a quantitative characterization. We calculate this coefficient by

$$r = \sum_{jk} \frac{jk(e_{jk} - q_j q_k)}{\sigma^2}, \tag{3.3}$$

where e_{jk} is the probability of finding a node with degrees j and k at the two ends of a randomly selected link; q_k is the probability of existing a node with degree k at the end of a randomly selected link and

$$\sigma^2 = \sum_k k^2 q_k - \Big[\sum_k k q_k\Big]^2, \tag{3.4}$$

is the variance of q_k. The value of r varies from -1 (perfect disassortativity) to 1 (perfect assortativity). If $r = 0$, the network has no assortative (or disassortative) mixing and, therefore, is neutral.

Previous works have considered the assortative mixing approach to analyze the correlation properties in earthquake networks for some regions, such as California, Japan and Iran [35, 13, 15]. These studies found an assortative behavior for the earthquake networks.

3.2.3 The OFC Model

The model created in 1992 by Olami, Feder and Christensen (OFC model) can reproduce several statistical properties of earthquakes [21]. This model is widely used because, despite its apparent simplicity, it can reproduce several characteristics found in actual seismological data, such as the Gutenberg-Richter law.

Standard OFC model

The standard OFC model can be represented by a bi-dimensional square $\ell \times \ell$ lattice with $N = \ell^2$ blocks (sites) interconnected to its first neighbors by springs. Each block is connected through a spring to a single rigid driven plate and by friction to another rigid fixed plate on which they stay. This blocks arrangement represents a regular topology of the lattice. Due to the relative motion between the plates (imposed by the model), all the blocks will be subjected to an elastic force which tends to put them in motion, and to other frictional forces, opposite to the first. When the resulting force in one of the blocks is greater than the maximum static friction force, the block slides and relaxes to a position of zero force, and a fraction (α) of its tension is equally redistributed between its nearest neighbors. It produces a rearrangement of forces in its first neighbors, which can cause other slippages and the emergence of a chain reaction. The first block to move is the earthquake's epicenter, and the magnitude of this earthquake is measured by the number of blocks that skidded.

When an earthquake finishes, the continuous relative movement between the plates will cause a force accumulation in all blocks. In this way, the slip of a block will occur after some time, and a new earthquake process begins. The model assumes that the time interval between two earthquakes is considerably longer than the duration of an earthquake itself.

Small-world-like OFC model

As verified in [28], a better agreement with real data is obtained when the lattice's topology in the OFC model is not regular, but, instead of that, follows the rule of topology construction proposed by [44], based on the Watts–Strogatz mechanism to generate small-world networks [1]. Starting from the regular two-dimensional topology, the rule of construction consists of taking each edge of the lattice (the spring that connects the blocks) and randomly reconnecting it to other blocks with probability p (rewiring probability), keeping fixed each block's original number of connections. That mechanism generates a *small-world-like* lattice for the OFC model, in which the resultant lattice has a topology between the regular and the random ones.

The use of a small-world-like topology for the OFC topology makes the system more realistic since it allows more effective long-range interactions between the blocks, agreeing with several previous works which indicate spatial and temporal long-range interactions between earthquakes [45, 46, 47, 48, 49].

Thus, in our studies, we used the OFC model with a small-world-like topology to create synthetical data catalogs to calculate spatial and temporal distributions and compare them to those produced by real data catalogs of earthquakes.

3.3 Data

In this study, we used natural and synthetic earthquake data catalogs.

3.3.1 Worldwide Earthquakes

The dataset was obtained from the World Catalog of Earthquakes of the Advanced National Seismic System (ANSS)[1], and it covers earthquakes from the entire world between 2002 and 2016. We considered the magnitude types M_b (body-wave magnitude), M_L (local magnitude) and M_w (moment magnitude). For the record, we only considered earthquakes with magnitude (m) larger or equal to 4.5 because, in that catalog, the events with magnitudes less than 4.5 are not completely registered for the whole world. The total of events is 101746, of which 80520 are shallow earthquakes (earthquakes with a depth of up to 70 km), and 21226 are deep earthquakes (events occurred at depths greater than 70 km).

These data had a good agreement with the Gutenberg-Richter law (GR)[50], with a b-value exponent equal to 1.080 $\pm$ 0.003 for the shallow seismic events, and 1.080 $\pm$ 0.010 for the deep ones. In concordance with many previous works [51, 52, 53, 54], given that in our data we consider only earthquakes with magnitude greater than or equal to 4.5, the b-value close to 1.0 is a consistent result for earthquakes worldwide.

We have not distinguished mainshocks from aftershocks in our data in this work. [55] and [56] discuss in their studies the relevance of small earthquakes and aftershocks in triggering other earthquakes, where it is observed that these seismic events appear to be of major importance in the earthquakes interactions. Therefore, as we aim to study how earthquakes worldwide are correlated, it makes sense that we do not eliminate aftershocks from our datasets. Moreover, this approach was also adopted in [9, 57, 58].

3.3.2 Synthetic Earthquakes

For the process of earthquake nucleation (i.e., how the earthquakes are generated) we have used the small-world-like OFC model, which generates a synthetic seismological catalog. In our simulations, we have used non-periodic open boundary conditions. This condition imposes that all blocks in the OFC lattice have the same parameter α, independently of their location on the lattice. With that condition, the blocks located at the lattice boundary will have a more dissipative behavior than those in bulk since the elements in bulk are connected to 4 neighbors, and the elements in the borders are connected to only 3 or 2.

[1] https://earthquake.usgs.gov/data/comcat

Previous studies showed that for the OFC model to have a lattice with small-world-like features and critical behavior, the rewiring probability must be in a range of values $[10^{-3}, 10^{-2}]$ [44, 28]. Thus, our analysis was conducted using $p = 0,001$ for a lattice of size $L = 400$, a dissipation coefficient $\alpha = 0,20$, and the number of events generated was 2×10^7 after the transient regime. It is relevant to highlight that we have excluded the earthquakes with magnitude $s = 1$ from the construction of the network because these events seem to obey their own statistics [59].

3.4 Method

The earthquake prediction is one of the goals of a seismological research. However, before that, it is necessary to better understand the earthquake dynamics and possible correlations between different earthquake events and locations. Accordingly, it makes sense to look for interactions due to long-range correlations since, as mentioned earlier, several authors have pointed out in previous works the existence of this kind of interaction, meaning that this characteristic cannot be neglected when studying seismological data.

Therefore, intending to study and search for possible correlations in global earthquakes, [14] constructed a network of worldwide epicenters. Similar to the studies for specific regions, they found that the global network is also scale-free and small-world, showing evidence of long-range correlations across the planet.

To construct the network of global epicenters, following the definition used in [14], we divided the planet in this work into equal square cells (sites) of size $L \times L$, with $L = 20\,km$. A cell becomes a node of the network every time the epicenter of an earthquake is located therein. Besides that, we used the two methods described below to create the links between the nodes.

3.4.1 Successive Model

This methodology was created by [11, 12] and employed in [14]. It consists of connecting a node to its successive one in the temporal order by a directed link. Thus, in this model, the construction of the network considers that each earthquake is related to the one that happens right after it in the temporal series, regardless of the time difference between them.

3.4.2 Time Window Model

In [29], a refined model, called the "time window" model, was created to construct networks of epicenters from all around the globe, which improves the previous

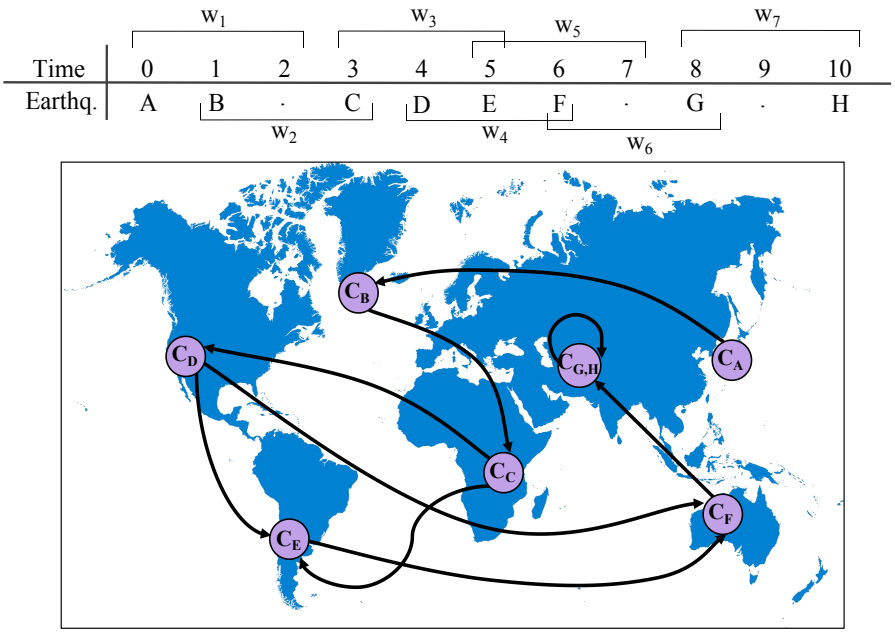

Fig. 3.3: Example of the network's construction for the time window model. The time windows are represented by w_i, where i is the window number, and all the time windows must have the same value (in this example, $T = 2$, in arbitrary units). Events in the same window are connected, as explained in the text. We can see that there are 8 earthquakes (A, B, C, D, E, F, G, H), but the epicenters network has only 7 nodes $(C_A, C_B, C_C, C_D, C_E, C_F, C_G)$, because $C_G = C_H$. It can also be observed that the link between C_G and C_H is a self-link.

successive methodology, and showed evidence of being a better approach to building networks of earthquakes than the successive one. It consists of defining a time window, with size T, placed on the chronologically ordered data to create the links between the nodes, where the nodes correspond to the cells where the epicenter of an earthquake has occurred. In this way, the first node inside the window is connected to all other nodes within that window by directed links. After that, the window is moved forward to the next event, and the connections procedure is repeated. Fig. 3.3 illustrates an example of this process. As it can be seen, the time window T works as a temporal filter to connect the nodes.

We built networks using both the successive and the time window models for the shallow and deep earthquakes collected. The time window values were $T = 3800\,s$ for shallow seismic events and $T = 16500\,s$ for deep earthquakes. These values are the same calculated and used in [29, 60], respectively.

Regarding the data generated with the OFC model, each epicenter was defined as a node. We constructed a network using the successive model of connections, as it was done in [28].

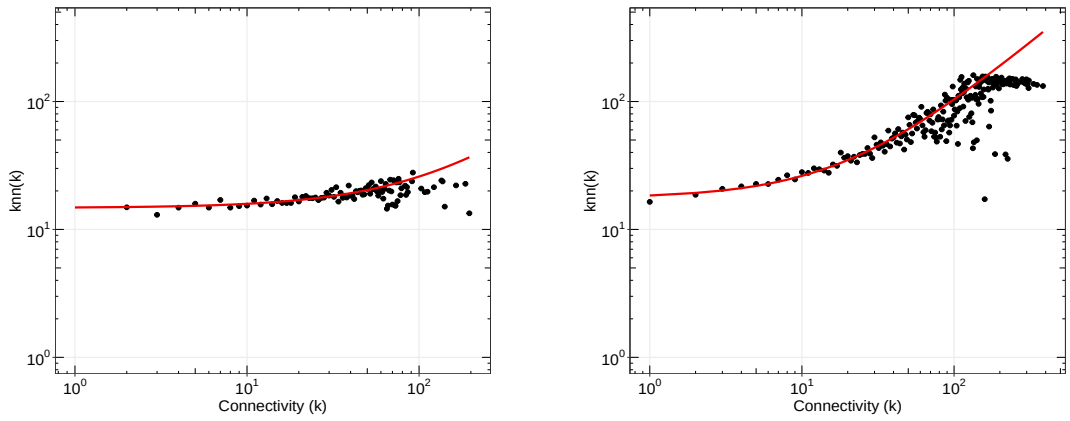

(a) (b)

Fig. 3.4: Nearest-neighbors average connectivity of nodes $k_{nn}(k)$ for the network of shallow earthquakes, for $m_{th} = 4, 5$, using (a) the successive model and (b) the time window model. It can be observed that both distributions follow a crescent linear fit (red line). These plots show that both networks have assortative mixing, being the network constructed with the time window model much more assortative.

3.5 Results

3.5.1 Degree Correlation Function

From Eq. 3.2, we calculated the degree correlation function of our networks, using the degree of the nodes. Fig. 3.4 shows a comparison between the network of shallow earthquakes ($m_{th} = 4, 5$) built using the successive model and the time window model. It is observed that in both distributions the nearest-neighbors average connectivity of nodes, $k_{nn}(k)$, increases linearly with k, which means that these networks are assortative. Therefore, the nodes with a high degree connect on average to nodes with a high degree. This result was the same found in networks of earthquakes from California and Japan [35], which makes sense since most earthquakes that occur in these areas have depths of up to 70 km (shallow earthquakes).

However, the network constructed with the time window model is more assortative than the one built with the successive model. It is interesting because [29, 60] showed that the time window model gives results that make more sense than the successive model (e. g., it naturally identifies the world's places with more occurrence of seismic events). The high assortative value found implies that areas of the world with intense shallow seismic activity are not only correlated but strongly correlated.

It is also interesting to note that in Fig. 3.4 the linear growth does not hold for high degree-nodes. This behavior is expected in scale-free networks, like ours, since the system is unable to sustain assortativity for high-degree because there are only a few nodes with large values of degree (hubs). The same happens for other real networks, as citation networks.

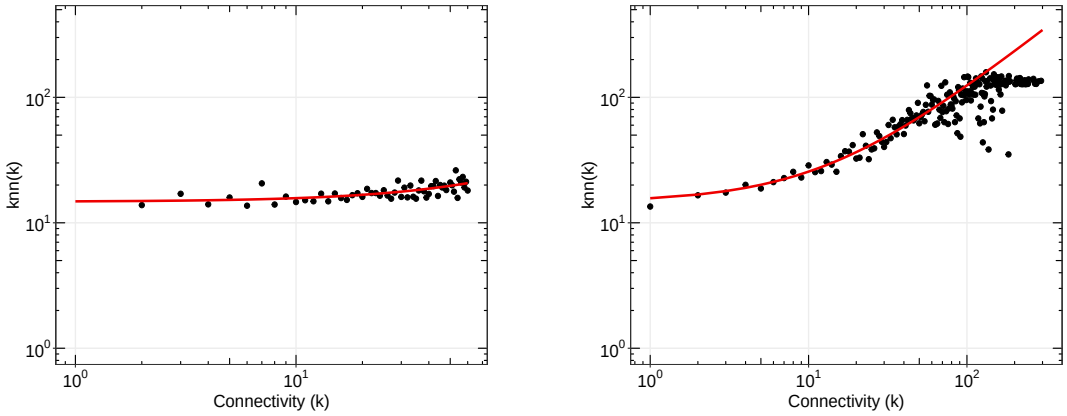

(a) (b)

Fig. 3.5: Nearest-neighbors average connectivity of nodes $k_{nn}(k)$ for the network of shallow earthquakes, for $m_{th} = 4,5$ and without depth equal to $10\,km$. The networks were constructed with (a) the successive model and (b) the time window model. Both distributions follow an increasing linear fit (red line), which means that these networks are assortative. Again, the network constructed with the time window model is much more assortative.

Moreover, in the global catalog from which we collected our data, there are several events with a "fixed depth" equal to 10 km [2], when there is no certainty about the actual focus depth. Thus, to analyze if this value of depth is biasing our results for the shallow earthquakes, we removed them and plotted the nearest-neighbors average connectivity of nodes for the successive and time window models for the remaining data. As we can see in Fig. 3.5, both distributions have a behavior very similar to those considering all depths (Fig. 3.4), which means that the assortative behavior of the networks of epicenters for shallow earthquakes is not dependent of this value of depth, being, in fact, a property of shallow earthquakes.

We have also analyzed the shallow seismological data in respect to its magnitude threshold m_{th} to check if the consideration $m_{th} = 4,5$ is satisfactory and if this value influences our results. Figs. 3.6(a) and 3.6(b) show the nearest-neighbors average connectivity of nodes, $k_{nn}(k)$, for the successive and time window models, respectively, using $m_{th} = 5,0$. The distributions show a linear growth between $k_{nn}(k)$ and k, similarly to what we have found when considering $m_{th} = 4,5$. Therefore, these networks are assortative, independently of the minimum magnitude value adopted.

The results for the networks of deep earthquakes with $m_{th} = 4,5$ are shown in Fig. 3.7. In both cases, successive and time window models, the networks are neutral, i.e., $k_{nn}(k)$ is independent of k. It means that the world's geographical regions with greater deep seismic activity are correlated both with each other and with areas of less occurrence of deep earthquakes, without preference.

[2]https://www.usgs.gov/faqs/why-do-so-many-earthquakes- ocorrer-profundidade-10km

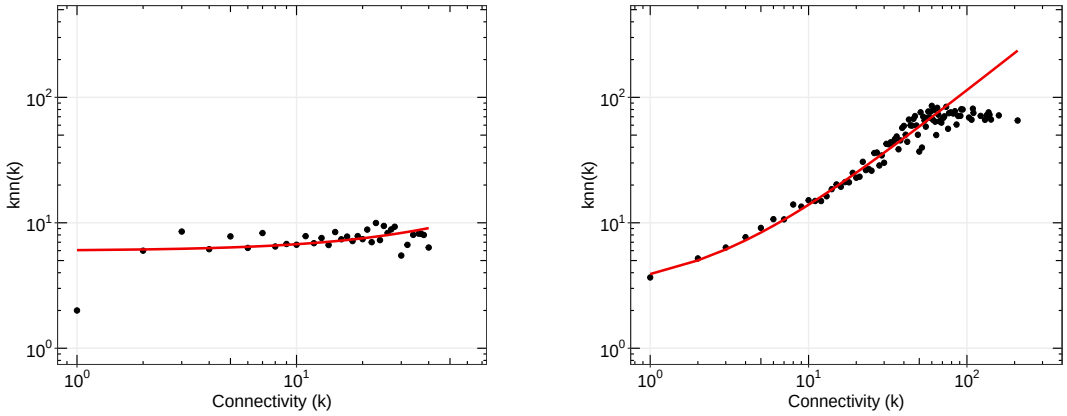

(a) (b)

Fig. 3.6: Nearest-neighbors average connectivity of nodes $k_{nn}(k)$ for the network of shallow earthquakes, for $m_{th} = 5,0$, created with (a) the successive model and (b) the time window model. By the crescent linear relation between $k_{nn}(k)$ and k (red line), these networks have assortative mixing, being the time window network much more assortative.

Following the same analysis for the shallow seismological data, we analyzed the epicenter networks' assortativity of deep earthquakes using $m_{th} = 5,0$. For the network created using the successive model of connections, no correlation was observed between $k_{nn}(k)$ and k; thus, this network is neutral (Fig. 3.8(a)), as it was found when considering (Fig. 3.7(a)). On the other hand, in the case of the network constructed with the time window model, $k_{nn}(k)$ increases linearly with k, indicating that this network has assortative mixing (Fig. 3.8(b)), which differs from the result obtained for (Fig. 3.7(b)). However, when comparing the distributions presented in Figs. 3.7 e 3.8, we note a significant reduction in the number of nodes for the network built using $m_{th} = 5,0$ (this decrease in the number of nodes can also be seen in Table 3.1). Then, in this case, the results found for deep earthquakes with cannot be considered very consistent since the low number of nodes does not allow us to perform good statistics.

Finally, as shown in Fig. 3.9, we found that the nearest-neighbors average connectivity of nodes $k_{nn}(k)$ for the network of earthquakes simulated with the modified OFC model has an increasing behavior with k, in agreement with the results found for shallow earthquakes. Similar results were also found in a previous work conducted for networks built using the standard OFC model [61].

3.5.2 Degree Correlation Coefficient

In addition, to obtain a quantitative result from Eq. 3.3, we have calculated the degree correlation coefficient (r) for each of our networks, and the values are shown in Table 3.1. As seen by the positive values obtained, the networks of shallow

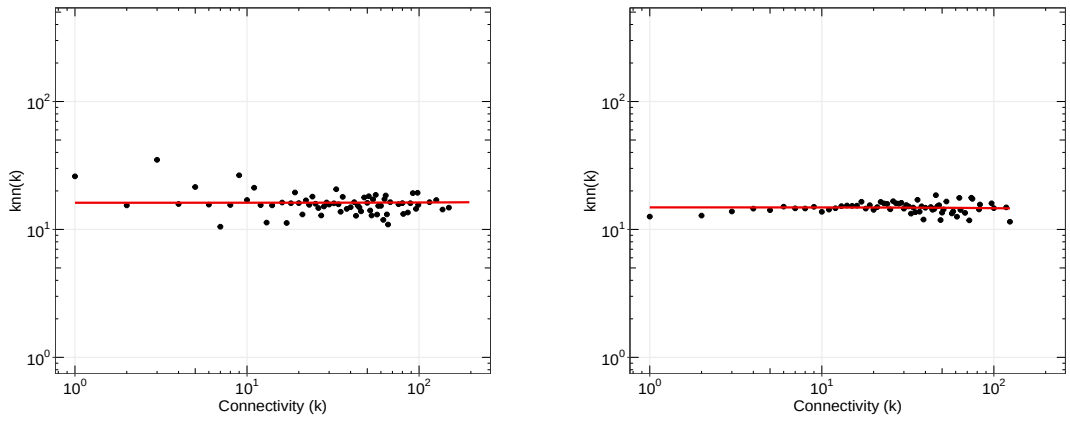

(a) (b)

Fig. 3.7: Nearest-neighbors average connectivity of nodes $k_{nn}(k)$ for the network of deep earthquakes, $m_{th} = 4,5$, constructed with (a) the successive model and (b) the time window model. No correlation between $k_{nn}(k)$ and k is presented in the distributions, which means that both networks are neutral.

events (for both successive and time window models) are assortative in all cases, i.e., considering data for $m_{th} = 4,5$ with all depths; for $m_{th} = 4,5$ excluding the fixed depth of 10 km; and for $m_{th} = 5,0$ with all depths. For these three cases, considering each model separately, the values of r are very close. Moreover, once again, we have noticed that the network of shallow earthquakes constructed with the time window model is much more assortative. It is noteworthy that the values found for this network are consistent with a similar finding for Japan data, using a different technique from ours [62]. As the Japan region has a predominance of shallow earthquakes, our results make sense.

The networks of deep earthquakes with $m_{th} = 4,5$ for both models, successive and time window, present $r \approx 0$, indicating that they are neutral, as found in the nearest-neighbors average connectivity of nodes ($k_{nn}(k)$) analyses. Additionally, as we observed in the $k_{nn}(k)$ study, a difference was found when looking for the degree correlation coefficient r for deep earthquakes with $m_{th} = 5,0$. While the network constructed with the successive model presents $r \approx 0$, the one created with the time window model has $r > 0$. However, as shown in Fig. 3.8 and Table 3.1, when we consider only magnitudes greater than or equal to 5.0, the number of nodes in the networks of deep earthquakes is much smaller than for $m_{th} = 4,5$ (Fig. 3.7 e Table 3.1). Consequently, the results indicated by the value of r for deep earthquakes with $m_{th} = 5,0$ are inconsistent due to the low number of nodes.

The positive degree correlation coefficient found for the network of earthquakes built from the modified OFC model shows assortativity, as seen in Table 3.1. This result is in concordance with our findings for the nearest-neighbors average connectivity of nodes $k_{nn}(k)$.

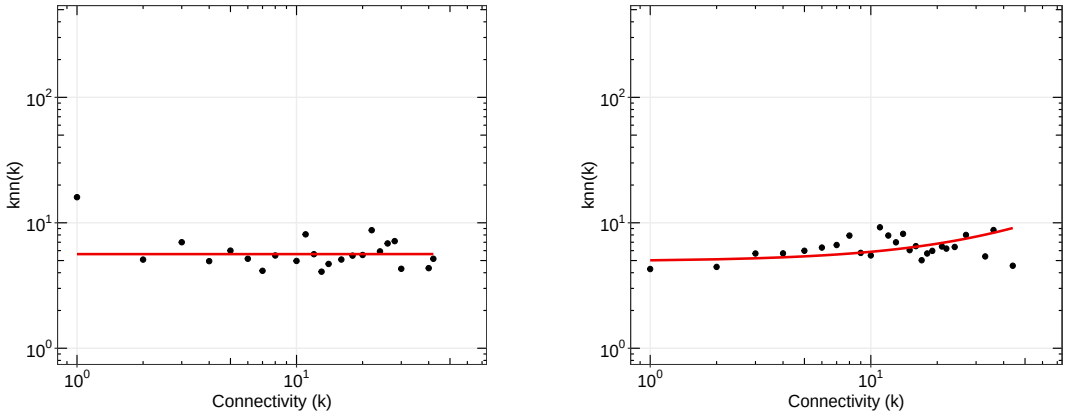

(a) (b)

Fig. 3.8: Nearest-neighbors average connectivity of nodes $k_{nn}(k)$ for the network of deep earthquakes, $m_{th} = 5,0$. In (a) the network was constructed with the successive model. No correlation between $k_{nn}(k)$ and k is presented, showing that this network is neutral. (b) presents the $k_{nn}(k)$ distribution of the network created using the time window model. The distribution shows an increasing behavior, indicating that this network is assortative. The explanation of this difference is in the body of the text.

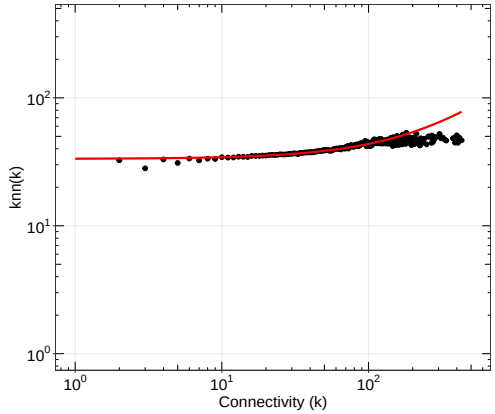

Fig. 3.9: Nearest-neighbors average connectivity of nodes $k_{nn}(k)$ for the network of earthquakes generated with the modified OFC model using the successive model. This network has $k_{nn}(k)$ linearly increasing with k (red line); therefore, it is assortative.

3.6 Discussion

To better understand the triggering of earthquakes and their dynamics, it is of great relevance to study how they correlate to each other worldwide. As the authors show in [56], knowing how the temporal and spatial domain link together is important to understand the diffusion processes in the earthquake system.

The assortative correlation exhibited in shallow and synthetic earthquake networks is an exciting result. As the hubs are connected to other hubs in earthquake networks, the regions of the world where large earthquakes occurred (e. g. Japan, Sumatra, and Chile) tend to, on average, be linked to each other. It means that the

Table 3.1: The number of nodes (N) and the degree correlation coefficient (r) values of the worldwide and synthetic earthquake networks used in this study.

Network	**N**	**r**
Shallow earthquakes, $m_{th} = 4,5$ (successive)	28471	0.0711
Shallow earthquakes, $m_{th} = 4,5$ and depth equal to 10 km excluded (successive)	20222	0.0809
Shallow earthquakes, $m_{th} = 5,0$ (successive)	12323	0.0774
Shallow earthquakes, $m_{th} = 4,5$ (time window)	23380	0.508
Shallow earthquakes, $m_{th} = 4,5$ and depth equal to 10 km excluded (time window)	14737	0.510
Shallow earthquakes, $m_{th} = 5,0$ (time window)	6184	0.582
Deep earthquakes, $m_{th} = 4,5$ (successive)	8958	0.000763
Deep earthquakes, $m_{th} = 5,0$ (successive)	3086	0.0163
Deep earthquakes, $m_{th} = 4,5$ (time window)	7675	0.0152
Deep earthquakes, $m_{th} = 5,0$ (time window)	2478	0.0944
OFC model earthquakes	115510	0.0750

regions where mainshocks occurred are connected to other regions where other mainshocks also appeared, suggesting that mainshocks may induce other mainshocks. Fig. 3.10(a) presents the geospatial image of the network of shallow earthquakes ($m_{th} = 4,5$) created with the time window model. Despite Fig. 3.10(a) displaying only the 2% of nodes with the highest degree of the network, they hold 16% of the links of the entire network. It is also possible to observe that hubs are not connected only to other close hubs (as in the case of Japan, which holds more than one hub), but they are also linked across the planet.

Another point is that removing high-degree nodes in assortative networks is a relatively inefficient strategy for destroying the network connectivity, since removing a hub does not cause significant damage to the network because the hubs form a core group [43]. Consequently, being the earthquake network assortative, even if a seismically active region does not have earthquakes for some time, this will not influence the global seismic dynamics since the network structure will not undergo significant changes.

Besides that, the assortative earthquake networks also reveal a kind of "attracting dynamics", where many hubs tend to be located near each other, i.e., large events tend to produce many hubs in a relatively small region. However, as depicted in Fig. 3.10(a), these regions are not isolated from the rest of the network; instead, they are also connected to hubs in other regions.

Furthermore, analyzing the networks themselves, the assortative property makes the giant component of the networks unable to reach large values. Once the giant component is the largest subset of nodes in the network (where each of its nodes must be connected to at least one other node), the assortative result means that, in earthquake networks, the regions with higher degrees are forced to connect much

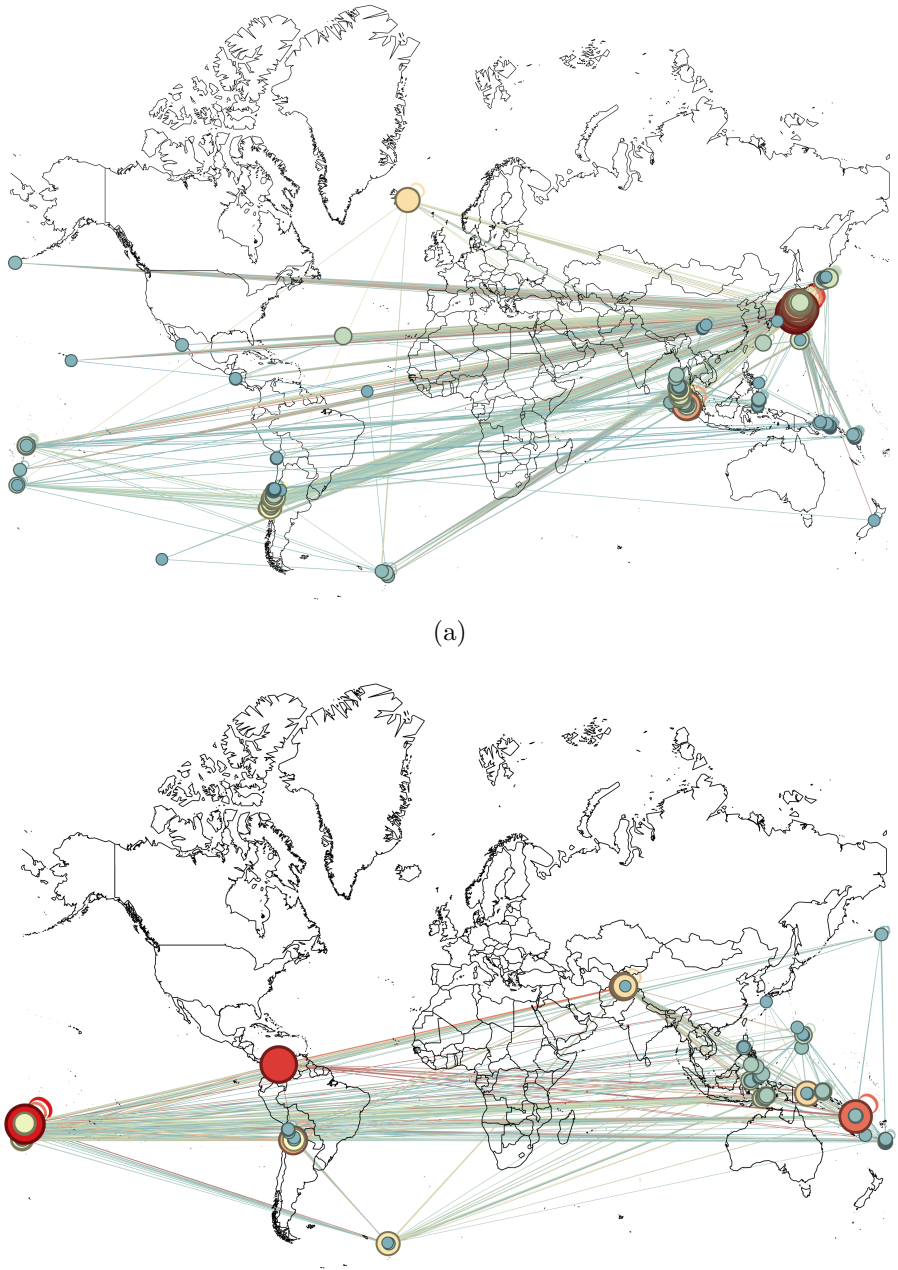

(a)

(b)

Fig. 3.10: Geospatial images of the networks constructed with the time window model between 2002 and 2016, for (a) shallow earthquakes and (b) deep earthquakes, considering $m_{th} = 4,5$. The 2% of nodes with the highest degrees (hubs) in each network are shown, as well as the links between them. Larger and reddish cells have a higher number of connections.

more to each other, than to the ones with small degree, making the hubs have more probability of belonging to the giant component than to the disconnected parts of the network.

A further interesting point is an agreement between the results for the small-world-like OFC model and for shallow earthquakes, which strengthens the credibility of the OFC model for the study and statistical description of earthquakes. Given the importance of using theoretical-computational models in earthquake research, the validation of a model such as the OFC, which does not need large computational requirements, is an interesting result once it allows inferring characteristics of actual earthquakes from those found using the model.

In the case of deep earthquakes, the neutral behavior found in the networks indicates that the earthquakes correlate at random since, in neutral networks, the nodes are linked arbitrarily [43]. The geospatial image of the network of deep earthquakes, with magnitude threshold $m_{th} = 4,5$, constructed with the time window model, is presented in Fig. 3.10(b). This figure depicts 2% of the most connected nodes of the network and 3% of the network links, showing that for deep earthquakes networks the hubs do not concentrate a large number of connections between each other. This result implies that deep seismic events worldwide have no obvious correlation, making the understanding of their correlations more difficult than for the shallow ones.

3.7 Conclusions

In this work, the assortativity of networks of worldwide and synthetic earthquakes was studied in order to better characterize correlation properties and understand the spread of information in the system of earthquakes. Concerning the global events, we analyzed shallow and deep earthquakes separately. From these datasets, we built networks of epicenters by using two methodologies: the successive model and the time window model of connections. For the shallow earthquakes, the networks of both models of linking nodes (sites) presented assortative mixing, with the difference that the network constructed with the time window model was found to be much more assortative. These results were similar to those obtained for seismic event networks from California and Japan (regions with a predominance of shallow earthquakes).

The assortative mixing was also found for the network created using a catalog produced by an improved version of the computational model proposed by Olami, Feder and Christensen, which shows agreement between real data for shallow events and synthetic data catalogs. On the other hand, the deep earthquake networks, for both successive and time window models, presented no correlation between the

degree of the nodes.

We have also tested our networks under two different constraints, taking only earthquakes with magnitude larger than or equal to 5.0 and excluding the events with "fixed depths" of 10 km from our data. The results found were consistent with those without the constraints. These tests had the objective to check if our results (using the entire data) were biased by the magnitude threshold 4.5 or by the "fixed depths".

Our results suggest that shallow and deep earthquakes have different temporal and spatial correlation properties. While we have positive degree correlations for shallow earthquakes, these correlations seem not to exist for deep earthquakes. Because of this, the shallow earthquake networks tend to link high-degree regions (regions with large earthquakes) with other high-degree areas, making it more difficult to change the seismological behavior of the earthquake networks even if a specific region stops having earthquakes for a period of time. Moreover, the results seem to indicate that, for shallow earthquakes, mainshocks may induce mainshocks in other areas, even if these areas are not close to each other. Another interesting feature revealed by our results from shallow earthquakes is a kind of "attracting dynamics". This feature causes the hubs to create several other hubs close to them; however, it does not prevent them from being connected to others further away. On the other hand, for deep earthquakes, our network analysis indicates that they connect randomly, i.e., with no specific preference.

An additional consequence of our findings is the validation of the OFC model to describe the degree correlation of shallow earthquake networks. It implies one more verification of the applicability of the OFC model. This step forward may help to study statistical correlations in actual earthquakes, given that the model presented similar results to those for natural earthquakes.

The correlation properties found in our analyses concern both temporal and spatial relations since we use time sequences to establish links between different spatial regions of the globe. It is known that earthquakes can induce others thousands of kilometers away from their epicenters [63], and our findings reinforce these long-range interactions in the worldwide seismicity. Here, these properties appear naturally using only complex network theory, showing how powerful this theory is to study correlated systems, such as earthquakes.

The present study shows that more than just degree distributions must be investigated when analyzing an earthquake network. Still, it is also necessary to observe how the network nodes are related. In this way, we have shown that the presence of mixing patterns in earthquake networks has a profound effect on the network's topological properties as it affects the detailed wiring of links among nodes.

For future works, we intend to study the earthquake clusters and communities

performed from deep and shallow earthquakes.

Acknowledgements

The authors would like to thank the Brazilian agencies FAPERJ and CNPq, for funding and scholarships.

Conflicts of Interest

The authors declare that they have no known competing financial interests or personal relationships that could have appeared to influence the work reported in this paper.

References

[1] Duncan J Watts and Steven H Strogatz. Collective dynamics of 'small-world'networks. *nature*, 393(6684):440–442, 1998.

[2] Albert-László Barabási and Réka Albert. Emergence of scaling in random networks. *science*, 286(5439):509–512, 1999.

[3] Réka Albert and Albert-László Barabási. Topology of evolving networks: local events and universality. *Physical review letters*, 85(24):5234, 2000.

[4] Sergei N Dorogovtsev and José FF Mendes. *Evolution of networks: From biological nets to the Internet and WWW*. Oxford university press, 2003.

[5] Mark EJ Newman. Mixing patterns in networks. *Physical review E*, 67(2): 026126, 2003.

[6] Akbar Gheibi, Hossein Safari, and Mohsen Javaherian. The solar flare complex network. *The Astrophysical Journal*, 847(2):115, 2017.

[7] Per Bak and Maya Paczuski. Complexity, contingency, and criticality. *Proceedings of the National Academy of Sciences*, 92(15):6689–6696, 1995.

[8] David C Roberts and Donald L Turcotte. Fractality and self-organized criticality of wars. *Fractals*, 6(04):351–357, 1998.

[9] Per Bak, Kim Christensen, Leon Danon, and Tim Scanlon. Unified scaling law for earthquakes. *Physical Review Letters*, 88(17):178501, 2002.

[10] Nicholas W Watkins, Gunnar Pruessner, Sandra C Chapman, Norma B Crosby, and Henrik J Jensen. 25 years of self-organized criticality: Concepts and controversies. *Space Science Reviews*, 198(1):3–44, 2016.

[11] Sumiyoshi Abe and Norikazu Suzuki. Scale-free network of earthquakes. *EPL (Europhysics Letters)*, 65(4):581, 2004.

[12] Sumiyoshi Abe and Norikazu Suzuki. Small-world structure of earthquake network. *Physica A: Statistical Mechanics and its Applications*, 337(1-2):357–362, 2004.

[13] Nastaran Lotfi and Amir Hossein Darooneh. The earthquakes network: the role of cell size. *The European Physical Journal B*, 85:1–4, 2012.

[14] Douglas SR Ferreira, Andrés RR Papa, and Ronaldo Menezes. Small world picture of worldwide seismic events. *Physica A: Statistical Mechanics and its Applications*, 408:170–180, 2014.

[15] Xuan He, Syed Bilal Hussain Shah, Bo Wei, and Zheng Liu. Comparison and analysis of network construction methods for seismicity based on complex networks. *Complexity*, 2021:1–11, 2021.

[16] Denisse Pastén, Felipe Torres, Benjamín Toledo, Victor Munoz, José Rogan, and Juan Alejandro Valdivia. Time-based network analysis before and after the m w 8.3 illapel earthquake 2015 chile. *The Chile-2015 (Illapel) Earthquake and Tsunami*, pages 123–131, 2017.

[17] Daniel Leon, Juan Valdivia, and Victor Bucheli. A revision of seismicity models based on complex systems and earthquake networks. *Journal of Seismology*, pages 1–9, 2022.

[18] Marco Baiesi and Maya Paczuski. Scale-free networks of earthquakes and aftershocks. *Physical review E*, 69(6):066106, 2004.

[19] Luciano Telesca and Michele Lovallo. Analysis of seismic sequences by using the method of visibility graph. *Europhysics Letters*, 97(5):50002, 2012.

[20] Xuan He, Hai Zhao, Wei Cai, Zheng Liu, and Shuai-Zong Si. Earthquake networks based on space–time influence domain. *Physica A: Statistical Mechanics and its Applications*, 407:175–184, 2014.

[21] Zeev Olami, Hans Jacob S Feder, and Kim Christensen. Self-organized criticality in a continuous, nonconservative cellular automaton modeling earthquakes. *Physical Review Letters*, 68(8):1244–1247, 1992.

[22] Kim Christensen and Zeev Olami. Scaling, phase transitions, and nonuniversality in a self-organized critical cellular-automaton model. *Physical Review A*, 46(4):1829, 1992.

[23] Kim Christensen and Zeev Olami. Variation of the gutenberg-richter b values and nontrivial temporal correlations in a spring-block model for earthquakes. *Journal of Geophysical Research: Solid Earth*, 97(B6):8729–8735, 1992.

[24] Hawoong Jeong, Sean P Mason, A-L Barabási, and Zoltan N Oltvai. Lethality and centrality in protein networks. *Nature*, 411(6833):41–42, 2001.

[25] Cliff Frohlich. *Deep earthquakes*. Cambridge university press, UK, 1 edition, 2006.

[26] Cliff Frohlich. The nature of deep-focus earthquakes. *Annual Review of Earth and Planetary Sciences*, 17:227, 1989.

[27] William Spence, Stuart A Sipkin, and George L Choy. Measuring the size of an earthquake. *Earthquake Information Bulletin (USGS)*, 21(1):58–63, 1989.

[28] Douglas SR Ferreira, Andrés RR Papa, and Ronaldo Menezes. On the agreement between small-world-like ofc model and real earthquakes. *Physics Letters A*, 379(7):669–675, 2015.

[29] Douglas Ferreira, Jennifer Ribeiro, Andrés Papa, and Ronaldo Menezes. Towards evidence of long-range correlations in shallow seismic activities. *EPL (Europhysics Letters)*, 121(5):58003, 2018.

[30] Denisse Pastén, Felipe Torres, Benjamín A Toledo, Víctor Muñoz, José Rogan, and Juan Alejandro Valdivia. Non-universal critical exponents in earthquake complex networks. *Physica A: Statistical Mechanics and its Applications*, 491: 445–452, 2018.

[31] D Chorozoglou, Eleftheria Papadimitriou, and Dimitris Kugiumtzis. Investigating small-world and scale-free structure of earthquake networks in greece. *Chaos, Solitons & Fractals*, 122:143–152, 2019.

[32] Réka Albert, Hawoong Jeong, and Albert-László Barabási. Diameter of the world-wide web. *nature*, 401(6749):130–131, 1999.

[33] Albert-László Barabási. The new science of networks. *Cambridge: Perseus*, 2002.

[34] Holger Ebel, Lutz-Ingo Mielsch, and Stefan Bornholdt. Scale-free topology of e-mail networks. *Physical review E*, 66(3):035103, 2002.

[35] Sumiyoshi Abe and Norikazu Suzuki. Complex earthquake networks: Hierarchical organization and assortative mixing. *Physical Review E*, 74(2):026113, 2006.

[36] Mark EJ Newman. Assortative mixing in networks. *Physical review letters*, 89 (20):208701, 2002.

[37] Michele Catanzaro, Guido Caldarelli, and Luciano Pietronero. Assortative model for social networks. *Physical review e*, 70(3):037101, 2004.

[38] Jacob G Foster, David V Foster, Peter Grassberger, and Maya Paczuski. Edge direction and the structure of networks. *Proceedings of the National Academy of Sciences*, 107(24):10815–10820, 2010.

[39] Samuel Johnson, Joaquín J Torres, J Marro, and Miguel A Munoz. Entropic origin of disassortativity in complex networks. *Physical review letters*, 104(10): 108702, 2010.

[40] Mahendra Piraveenan, Mikhail Prokopenko, and Albert Zomaya. Assortative mixing in directed biological networks. *IEEE/ACM Transactions on computational biology and bioinformatics*, 9(1):66–78, 2010.

[41] Romualdo Pastor-Satorras, Alexei Vázquez, and Alessandro Vespignani. Dynamical and correlation properties of the internet. *Physical review letters*, 87 (25):258701, 2001.

[42] Alexei Vázquez, Romualdo Pastor-Satorras, and Alessandro Vespignani. Large-scale topological and dynamical properties of the internet. *Physical Review E*, 65(6):066130, 2002.

[43] Marton Posfai and Albert-Laszlo Barabasi. *Network science*. Cambridge University Press, 2016.

[44] Filippo Caruso, Vito Latora, Alessandro Pluchino, Andrea Rapisarda, and Bosiljka Tadić. Olami-feder-christensen model on different networks. *The European Physical Journal B-Condensed Matter and Complex Systems*, 50(1):243–247, 2006.

[45] Yan Y Kagan and David D Jackson. Long-term earthquake clustering. *Geophysical Journal International*, 104(1):117–133, 1991.

[46] Ross S Stein. The role of stress transfer in earthquake occurrence. *Nature*, 402 (6762):605–609, 1999.

[47] Mirko S Mega, Paolo Allegrini, Paolo Grigolini, Vito Latora, Luigi Palatella, Andrea Rapisarda, and Sergio Vinciguerra. Power-law time distribution of large earthquakes. *Physical Review Letters*, 90(18):188501, 2003.

[48] Patrizia Tosi, Valerio De Rubeis, Vittorio Loreto, and Luciano Pietronero. Space–time correlation of earthquakes. *Geophysical Journal International*, 173 (3):932–941, 2008.

[49] Shinji Toda and Ross S Stein. Long-and short-term stress interaction of the 2019 ridgecrest sequence and coulomb-based earthquake forecasts. *Bulletin of the Seismological Society of America*, 110(4):1765–1780, 2020.

[50] Beno Gutenberg and Charles Francis Richter. Earthquake magnitude, intensity, energy, and acceleration. *Bulletin of the Seismological society of America*, 32 (3):163–191, 1942.

[51] Rachel E Abercrombie. The magnitude-frequency distribution of earthquakes recorded with deep seismometers at cajon pass, southern california. *Tectonophysics*, 261(1-3):1–7, 1996.

[52] Hiroo Kanamori and Emily E Brodsky. The physics of earthquakes. *Reports on progress in physics*, 67(8):1429, 2004.

[53] Naseer Ahmed, Shahid Ghazi, and Perveiz Khalid. On the variation of b-value for karachi region, pakistan through gumbel's extreme distribution method. *Acta Geodaetica et Geophysica*, 51:227–235, 2016.

[54] Bernhard Fiedler, Sebastian Hainzl, Gert Zöller, and Matthias Holschneider. Detection of gutenberg–richter b-value changes in earthquake time seriesdetection of gutenberg–richter b-value changes in earthquake time series. *Bulletin of the Seismological Society of America*, 108(5A):2778–2787, 2018.

[55] Agnes Helmstetter, Yan Y Kagan, and David D Jackson. Importance of small earthquakes for stress transfers and earthquake triggering. *Journal of Geophysical Research: Solid Earth*, 110(B5), 2005.

[56] David Marsan and Olivier Lengline. Extending earthquakes' reach through cascading. *Science*, 319(5866):1076–1079, 2008.

[57] Jörn Davidsen and Maya Paczuski. Analysis of the spatial distribution between successive earthquakes. *Physical Review Letters*, 94(4):048501, 2005.

[58] Sumiyoshi Abe and Norikazu Suzuki. Complex-network description of seismicity. *Nonlinear Processes in Geophysics*, 13(2):145–150, 2006.

[59] Peter Grassberger. Efficient large-scale simulations of a uniformly driven system. *Physical Review E*, 49(3):2436, 1994.

[60] Douglas SR Ferreira, Jennifer Ribeiro, Paulo SL Oliveira, André R Pimenta, Renato P Freitas, and Andrés RR Papa. Long-range correlation studies in deep earthquakes global series. *Physica A: Statistical Mechanics and its Applications*, 560:125146, 2020.

[61] Tiago P Peixoto and Carmen PC Prado. Network of epicenters of the olami-feder-christensen model of earthquakes. *Physical Review E*, 74(1):016126, 2006.

[62] Joel N Tenenbaum, Shlomo Havlin, and H Eugene Stanley. Earthquake networks based on similar activity patterns. *Physical Review E*, 86(4):046107, 2012.

[63] Robert T O'Malley, Debashis Mondal, Chris Goldfinger, and Michael J Behrenfeld. Evidence of systematic triggering at teleseismic distances following large earthquakes. *Scientific reports*, 8(1):11611, 2018.

Capítulo 4

Caracterizações Topológicas de Redes Multicamadas de Terremotos

4.1 Fundamentação Teórica

Como foi observado no capítulo anterior, a aplicação da teoria de redes complexas na sismologia permite um conhecimento amplo do sistema de terremotos, como a identificação dos locais e eventos mais importantes do sistema, tipos de interação entre eles, difusão de informação, entre outros. Dentro da teoria de redes complexas, um novo conceito tem sido utilizado para estudar sistemas com grande número de elementos que interagem entre si por diferentes tipos de relacionamentos, são as chamadas redes multicamadas [1, 2]. Esses relacionamentos podem representar diferentes "aspectos" do mesmo sistema, como, por exemplo, múltiplos níveis de organização em um sistema biológico, ou relações sociais em diferentes esferas. Na Fig. 4.1 é apresentado um exemplo esquemático de aplicação de redes multicamadas.

Um exemplo de área em que as redes multicamadas têm sido particularmente úteis é nos sistemas de transporte. Por exemplo, em [4] os autores usaram uma abordagem de rede multicamadas para analisar a interdependência dos sistemas de metrô e ônibus em Chongqing, uma famosa cidade montanhosa do interior da China. Eles descobriram que os dois modos de transporte eram altamente interdependentes e que as interrupções em um sistema poderiam ter impactos significativos no outro.

Assim, no presente trabalho aplicamos a abordagem de estudo de redes por multicamadas, a fim de contribuir para uma melhor compreensão das interações ao longo do tempo entre terremotos de diferentes locais do planeta. Nas próximas seções, apresentamos o formalismo matemático e as definições desses tipos de redes.

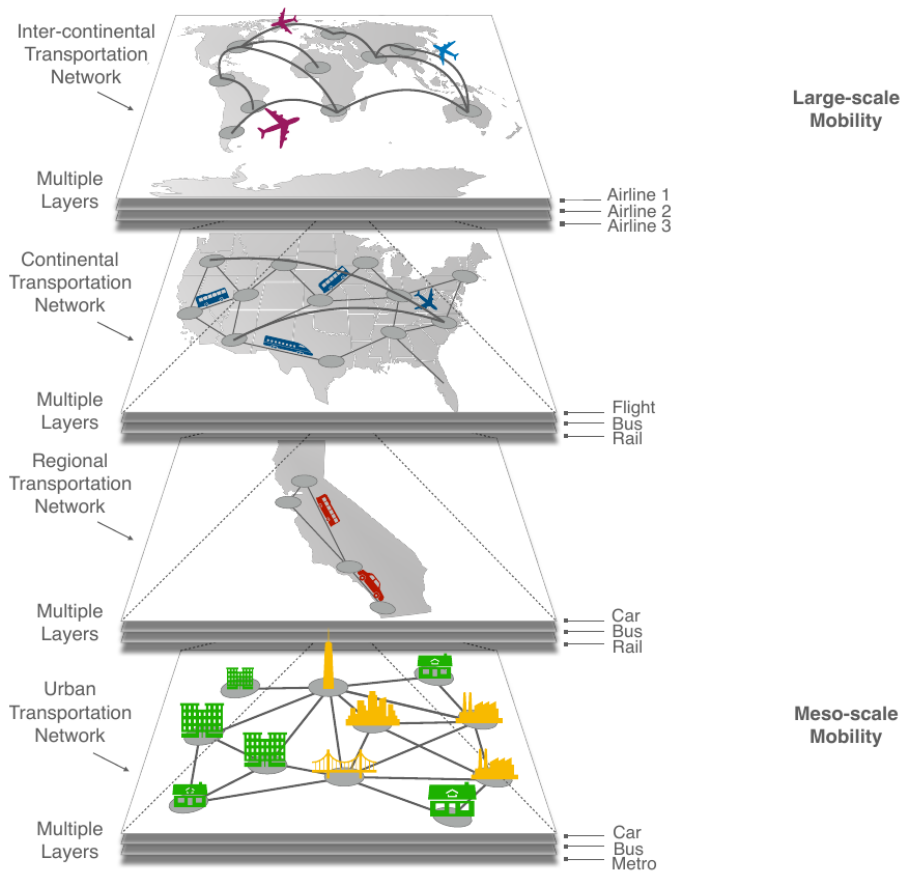

Fig. 4.1: Representação esquemática de redes multicamadas de transportes em diferentes escalas geográficas. De cima para baixo: rede de transportes intercontinentais, em que cada camada representa uma linha aérea diferente; rede de transportes continentais nos EUA, com três camadas: voos, rodovias e trilhos; rede de transportes regionais na Califórnia, com três tipos de mobilidade: por carro, ônibus e trem; por fim, a rede de transportes urbanos, sendo cada camada referente ao transporte por carro, ônibus e metrô. Figura retirada de [3].

4.1.1 Definições e Notações

Em uma rede multicamadas, cada camada é uma rede complexa para um determinado tipo de interação entre os elementos. Como definido em [1, 2], uma rede multicamadas é um par $\mathcal{M} = (\mathcal{G}, \mathcal{C})$, onde $\mathcal{G}$ denota o conjunto de grafos (direcionados ou não direcionados, ponderados ou não ponderados) que representam as camadas de $\mathcal{M}$, isto é, $\mathcal{G} = \{G_\alpha;\, \alpha \in \{1, \ldots, M\}\}$. Dessa forma, cada camada α é expressa como um grafo $G_\alpha = (V_\alpha, E_\alpha)$, em que $V_\alpha = \{{v_1}^\alpha, \ldots, {v_{N_\alpha}}^\alpha\}$ é o conjunto de vértices de G_α, e E_α são as conexões intracamadas de $\mathcal{M}$, referentes a G_α. Ademais, temos que

$$\mathcal{C} = \{E_{\alpha\,\beta} \subseteq V_\alpha \times V_\beta;\, \alpha, \beta \in \{1, \ldots, M\}, \alpha \neq \beta\} \tag{4.1}$$

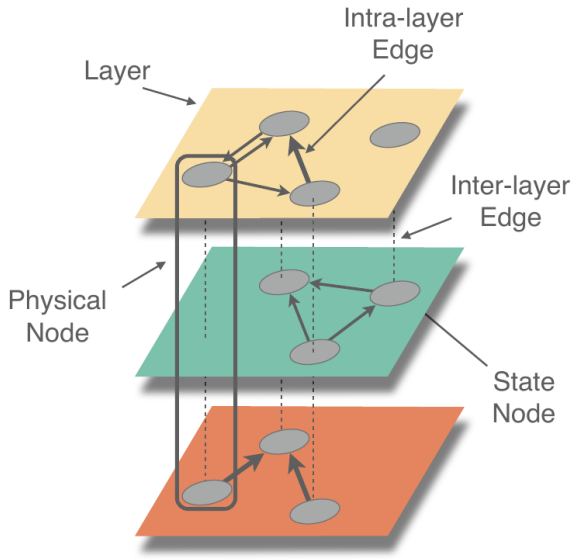

Fig. 4.2: Ilustração esquemática de uma rede multicamadas com 3 camadas, onde cada camada constitui uma rede. Vértices (círculos cinzas) podem existir em várias camadas, sem a necessidade de estar em todas elas. Vértices de estado são aqueles relacionados a uma camada específica, enquanto vértices físicos não dependem de uma camada exclusiva. Ligações dentro das camadas (arestas intracamadas) são representadas por setas, que apontam o sentido da ligação. Vértices físicos são conectados por linhas tracejadas (arestas intercamadas). Figura retirada de [3].

é o conjunto de conexões intercamadas de $\mathcal{M}$ entre vértices de camadas diferentes G_α e G_β com $\alpha \neq \beta$. Ao longo do texto, usaremos letras gregas $(\alpha, \beta, \dots)$ para nos referenciar aos índices das camadas e letras latinas $(i, j, \dots)$ para os índices de um elemento da rede.

Em redes multicamadas, um mesmo vértice pode estar presente em várias camadas, apresentando ligações com outros vértices a depender do tipo de rede representada. Assim, usamos o par vértice-camada (v_i, α) para representar o vértice i da camada α. Tais vértices relacionados a uma camada específica são chamados de vértices de estado. Por outro lado, quando eles não apresentam essa dependência, são chamados de vértices físicos (ver Fig. 4.2). Na Seção 3.2.1, apresentamos o conceito de matriz adjacência para redes simples (monocamadas). No caso de redes multicamadas, considerando a rede não ponderada (ou seja, todas as arestas têm o mesmo peso), temos que a matriz adjacência de cada camada G_α é denotada por $A^{[\alpha]} = ({a_{ij}}^{\alpha}) \in \mathbb{R}^{N_\alpha \times N_\alpha}$, onde

$$ {a_{ij}}^{\alpha} = \begin{cases} 1, \text{ se } ({v_i}^{\alpha}, {v_j}^{\alpha}) \in E_\alpha, \\ 0, \text{ caso contrário.} \end{cases} \tag{4.2} $$

para $1 \leq i, j \leq N_\alpha$ e $1 \leq \alpha \leq M$. Já a matriz adjacência das ligações intercamadas correspondente a $E_{\alpha\,\beta}$ é igual a $A^{[\alpha,\beta]} = ({a_{ij}}^{\alpha\,\beta}) \in \mathbb{R}^{N_\alpha \times N_\beta}$, dada por

$$a_{ij}{}^{\alpha\,\beta} = \begin{cases} 1, \text{ se } (v_i{}^{\alpha}, v_j{}^{\beta}) \in E_{\alpha\,\beta}, \\ 0, \text{ caso contrário.} \end{cases} \tag{4.3}$$

A classificação básica de modelos de redes multicamadas identifica duas categorias baseadas na presença ou não de conexões intercamadas: redes não-interconectadas e redes interconectadas. Redes não-interconectadas consistem de múltiplas camadas, cada uma representando um relacionamento específico entre os vértices. Vértices de estado existem em pelo menos uma camada e não apresentam ligações entre as camadas. Já as redes interconectadas possuem as mesmas características das redes anteriores, porém, podem existir ligações entre os estados de diferentes camadas. Elas possuem três tipos: (i) redes *multiplex*: são aquelas que apresentam apenas ligações entre estados do mesmo vértice físico. (ii) redes interdependentes: apresentam apenas conexões entre estados de diferentes vértices físicos. (iii) redes interconectadas gerais: não possuem restrições para os tipos de ligação intercamadas.

Neste trabalho, focamos no estudo de redes *multiplex* para analisar dados sismológicos. A seguir, detalharemos melhor sobre essas redes.

4.1.2 Redes *Multiplex*

Um dos casos especiais de redes multicamadas mais comuns são as chamadas redes *multiplex*. Na literatura, existem duas maneiras de se definir redes *multiplex*: em uma delas é necessário que todas as camadas compartilhem o mesmo conjunto de vértices [1], e na outra, mais geral, não é exigido que todos os vértices existam em todas as camadas [2]. Em nossas análises, seguimos a última definição. Dessa forma, as ligações intercamadas são dadas por $E_{\alpha\,\beta} = \left\{(v_i{}^{\alpha}, v_i{}^{\beta});\, v_i{}^{\alpha}, v_i{}^{\beta} \in V_{\alpha}, V_{\beta}\right\}$ para todo $1 \leq \alpha \neq \beta \leq M$. Assim, podemos associar uma rede *multiplex* $\mathcal{M}$ a uma rede monocamada $\tilde{\mathcal{M}} = (\tilde{V}, \tilde{E})$, em que $\tilde{V}$ é a união disjunta de todos os vértices de $G_1, \ldots, G_M$, ou seja,

$$\tilde{V} = \bigsqcup_{1 \leq \alpha \leq M} V_{\alpha} = \{v^{\alpha}\,;\, v \in V_{\alpha}\}\,, \tag{4.4}$$

e $\tilde{E}$ é dado pela união de E_{α} e $E_{\alpha\,\beta}$, isto é,

$$\left(\bigcup_{\alpha=1}^{M} \{(v_i{}^{\alpha}, v_j{}^{\alpha})\,;(v_i{}^{\alpha}, v_j{}^{\alpha}) \in E_{\alpha}\}\right) \bigcup \left(\bigcup_{\substack{\alpha,\beta=1 \\ \alpha\neq\beta}}^{M} \left\{(v_i{}^{\alpha}, v_i{}^{\beta});\, (v_i{}^{\alpha}, v_i{}^{\beta}) \in E_{\alpha\,\beta}\right\}\right) \tag{4.5}$$

Com isso, podemos notar que $\tilde{\mathcal{M}}$ é um grafo monocamada com $N \times M$ vértices, que pode ser representado por uma matriz supra-adjacência, $\tilde{A}$, a qual pode ser

escrita como uma matriz de blocos:

$$\tilde{A} = \left(\begin{array}{c|c|c|c} A_1 & I_N & \dots & I_N \\ \hline I_N & A_2 & \dots & I_N \\ \hline \vdots & \vdots & \ddots & \vdots \\ \hline I_N & I_N & \dots & A_M \end{array}\right) \in \mathbb{R}^{NM \times NM},$$

onde A_α é a matriz adjacência referente a cada grafo G_α, com $1 \leq \alpha \leq M$, e I_N é a matriz identidade de dimensão N. Esse processo de atribuir uma matriz a uma rede multicamadas é chamado de matriciação [2].

Podemos pensar no conceito de redes *multiplex* no contexto das redes sociais, por exemplo, uma vez que um mesmo usuário pode optar por se cadastrar em uma, duas ou mais redes sociais *online* e criar diferentes tipos de relacionamento (como profissional, familiar e de amizade) com os mesmos usuários em cada plataforma social [5].

Além disso, podemos representar redes temporais [6] como redes *multiplex*, em que cada camada representa a interação entre os elementos em determinado período de tempo. Essas redes permitem uma análise da evolução temporal das relações. Nesse caso, vértices de estado são conectados apenas entre camadas subsequentes, de forma que a matriz supra-adjacência se torna:

$$\tilde{A} = \left(\begin{array}{c|c|c|c|c|c} A_1 & I_N & 0 & 0 & \dots & 0 \\ \hline I_N & A_2 & I_N & 0 & \dots & 0 \\ \hline 0 & I_N & A_3 & I_N & \dots & 0 \\ \hline \vdots & \vdots & \vdots & \vdots & \ddots & \vdots \\ \hline 0 & 0 & 0 & 0 & \dots & A_M \end{array}\right) \in \mathbb{R}^{NM \times NM}.$$

Na Fig. 4.3, apresentamos: um exemplo de rede *multiplex* temporal, a matriz adjacência referente ao grafo de cada camada e a matriz supra-adjacência correspondente.

No caso dos terremotos, apesar da ampla quantidade de estudos realizados para redes monocamadas, até o momento, no melhor de nosso conhecimento, apenas um trabalho foi publicado para redes multicamadas [7]. Nesse estudo, os autores aplicaram redes temporais *multiplex* em dados de terremotos da Califórnia e do Irã, com o intuito de avaliar com maior detalhe a atividade sísmica nessas regiões, obtendo informações que seriam "mascaradas" ao considerar uma única rede englobando todos os anos de dados sismológicos.

Seguindo essa linha, na presente dissertação também realizamos estudos de redes temporais *multiplex* em catálogos de terremotos globais reais. Apresentaremos a seguir as métricas e metodologias utilizadas, bem como os resultados obtidos.

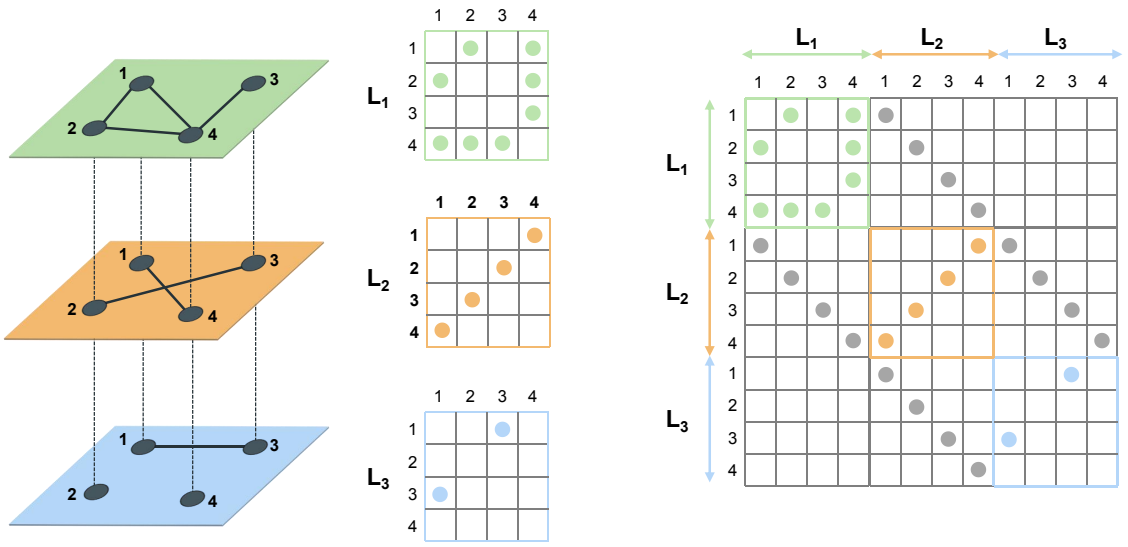

Fig. 4.3: Exemplo de uma rede *multiplex* temporal de três camadas. São apresentadas a representação esquemática da rede, as matrizes adjacência correspondentes a cada camada e a matriz supra-adjacência.

4.1.3 Métricas de Redes

Abaixo, são apresentados conceitos originais criados para redes monocamadas, e em seguida, serão expandidas suas formulações para os casos multicamadas. Tais conceitos serão usados em nossas redes *multiplex* de terremotos.

Conectividade

Uma das métricas de redes complexas mais importantes é a chamada conectividade (ou grau), k, dada pelo número de ligações que um vértice possui com outros vértices da rede (como comentado na Seção 3.2.1), ou seja, a conectividade de um vértice i é dada por $k_i = \sum_j a_{ij}$, em que a_{ij} são os elementos da matriz adjacência. Ao trabalhar com redes multicamadas, a maneira mais simples de generalizar esse conceito é adotar que para cada camada α um vértice físico i terá um valor de conectividade $k_i^{[\alpha]} = \sum_j a_{ij}{}^{[\alpha]}$. Assim, a conectividade total do vértice i é a soma dos valores de conectividade $k_i^{[\alpha]}$, isto é, $k_i = \sum_\alpha k_i^{[\alpha]}$ [2].

Ademais, caso as ligações entre pares de vértices tenham pesos diferentes (rede ponderada), podemos calcular a chamada *strength* ("força"), s_i, que fornece a soma dos pesos das arestas de cada vértice i, isto é, $s_i = \sum_j w_{ij}$, sendo w_{ij} o peso das ligações entre os vértices i e j. Expandindo para redes multicamadas, semelhantemente à conectividade, a *strength* total de um vértice físico i é dada pela soma de seu valor em cada camada α, isto é,

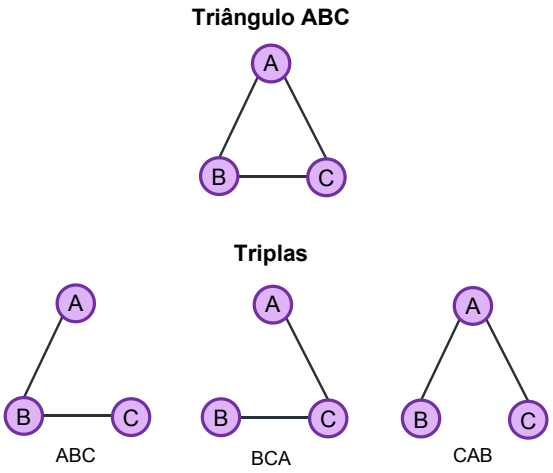

Fig. 4.4: Exemplo de um triângulo formado pelas ligações entre os vértices A, B e C e suas respectivas triplas.

$$s_i = \sum_{\alpha} s_i^{[\alpha]}. \tag{4.6}$$

Coeficiente de Aglomeração

O coeficiente de aglomeração é uma medida que captura o grau com que os vizinhos de um vértice estão conectados entre si. Para um vértice i com conectividade igual a k_i, o coeficiente de aglomeração local é definido como

$$C_i = \frac{2\mathcal{E}_i}{k_i(k_i - 1)} \tag{4.7}$$

onde $\mathcal{E}_i$ representa o número de ligações entre os k_i vizinhos do vértice i. O valor de C_i varia de 0 a 1, uma vez que $k_i(k_i - 1)$ é o número máximo de ligações entre os vizinhos de i. Assim, C_i pode ser interpretado como a probabilidade de existir uma ligação entre dois vizinhos de um vértice i.

Para a rede como um todo, o grau de aglomeração é dado através do coeficiente de aglomeração médio, $\langle C \rangle$, representando a média dos C_i sobre todos os vértices $i = 1, \cdots, N$ [8],

$$\langle C \rangle = \frac{1}{N} \sum_{1}^{N} C_i. \tag{4.8}$$

Essa medida pode ser entendida como a probabilidade de que dois vizinhos de um vértice selecionado aleatoriamente estejam conectados.

Outra forma de medir a aglomeração na rede é através da transitividade do sistema, utilizando-se o coeficiente de aglomeração global [9], C, que é medido a

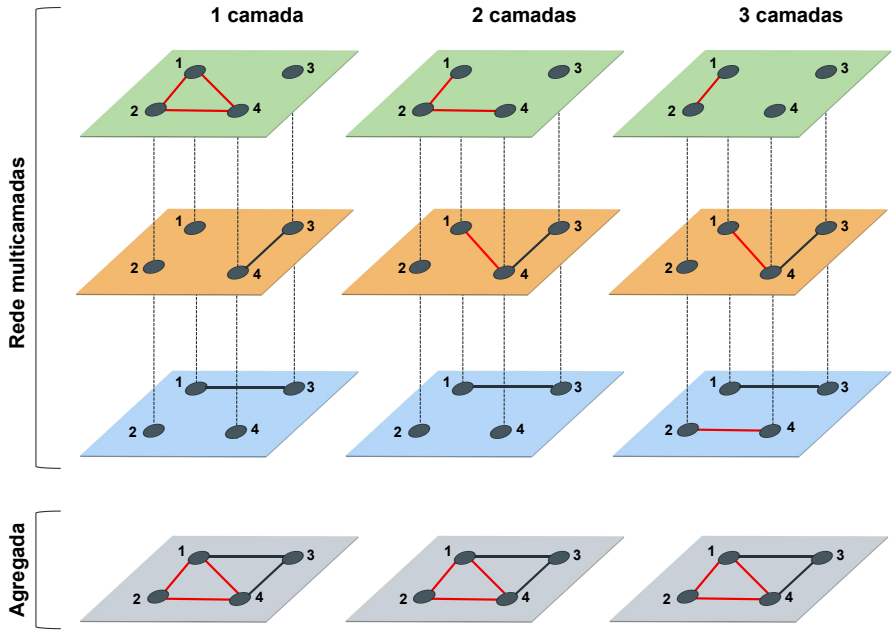

Fig. 4.5: Exemplos de triângulos formados em uma, duas e três camadas em uma rede *multiplex* de três camadas. Estão destacados em vermelho os triângulos formados entre os vértices físicos v_1, v_2 e v_4 em cada um desses casos. As redes agregadas não são capazes de distinguir os tipos de triângulos formados.

partir dos triângulos formados na rede. Ele é definido por

$$C = \frac{3 \times \text{Número de Triângulos}}{\text{Número de Triplas}}, \tag{4.9}$$

em que uma tripla é um conjunto ordenado de três vértices ABC, de forma que A está conectado a B e B está conectado a C. Por exemplo, um triângulo ABC é formado por três triplas: ABC, BCA e CAB (Fig. 4.4). O fator 3 no numerador é devido ao fato de cada triângulo contar como três triplas.

É possível calcular o coeficiente de aglomeração global em termos de passos em uma rede [10]. Para tanto, dada uma matriz adjacência A e um número inteiro m, tem-se que cada elemento $(A^m)_{ij}$ é o número de passos distintos para sair de um vértice i para um vértice j. Portanto, para $i = j$ e $m = 3$, fica $(A^3)_{ii}$, que é justamente o número de triângulos fechados distintos com centro no vértice i. Já para o cálculo do número de triplas, o segundo passo deve ser dado em uma matriz totalmente conectada (ou seja, todos os vértices se conectam entre si), $F = U - I$, sendo U uma matriz de "uns" e I a matriz identidade de mesma dimensão. Com isso, o coeficiente de aglomeração global de uma rede pode ser calculado usando

$$C = \frac{[A^3]}{[A\,F\,A]}. \tag{4.10}$$

No caso de redes multicamadas, diferentes abordagens foram utilizadas em trabalhos prévios [2, 10, 11]. Ao trabalhar com redes *multiplex*, há um maior número de possibilidades para a transitividade ocorrer ao longo da rede. Desta forma, para processos dinâmicos, além dos triângulos formados em cada camada, é importante levar em consideração aqueles que cruzam diferentes camadas. Existem três maneiras de formar triângulos em redes *multiplex*: (*i*) considerando ligações dentro de uma mesma camada; (*ii*) considerando duas ligações em uma determinada camada e a outra ligação em uma camada distinta; (*iii*) considerando cada ligação para uma camada diferente. Para exemplificar, a Fig. 4.5 apresenta uma esquematização para triângulos fechados em uma, duas e três camadas.

O exemplo apresentado na Fig. 4.5 também permite observar a diferença entre uma rede multicamadas e uma rede agregada. Enquanto a primeira mapeia os diferentes "aspectos" do sistema em camadas distintas, a segunda é a representação do sistema multicamadas em uma única camada que engloba todos os múltiplos tipos de relacionamentos, sem diferenciação. Como pode ser visto no exemplo, a rede agregada não é capaz de distinguir se o triângulo é formado em apenas uma camada ou devido às ligações através de múltiplas camadas, sendo perdida essa informação.

Em nossas análises, utilizamos o cálculo do coeficiente de aglomeração global, considerando tanto triângulos quanto triplas formados em uma, duas e três camadas.

Comprimento de Menor Caminho Médio

Além da conectividade e do coeficiente de aglomeração, outra medida topológica fundamental em redes é o comprimento de menor caminho médio (ℓ). Em uma rede, o conceito de distância física (como a distância entre dois átomos em um cristal, por exemplo) é substituído pelo chamado comprimento de caminho [9]. Um caminho é definido como uma rota entre vértices percorrida através de arestas. Dessa forma, o comprimento de um caminho corresponde ao número de arestas que foram percorridas entre os dois vértices de interesse, e o menor caminho é aquele em que é necessário passar por menos arestas.

Uma maneira de calcular os menores caminhos é a partir da matriz adjecência, A. Quando existe uma ligação direta entre dois vértices i e j, tem-se que $A_{ij} = 1$ e a distância entre esses vértices é $d_{ij} = 1$. A distância será $d_{ij} = 2$, se existir um caminho de tamanho 2 entre i e j, ou seja, $A_{ik}\,A_{kj} = 1$. O número de caminhos $d_{ij} = 2$ entre os vértices i e j é

$$\mathcal{N}_{ij}^{(2)} = \sum_{k=1}^{N} A_{ik}\,A_{kj} = A_{ij}^{(2)}, \tag{4.11}$$

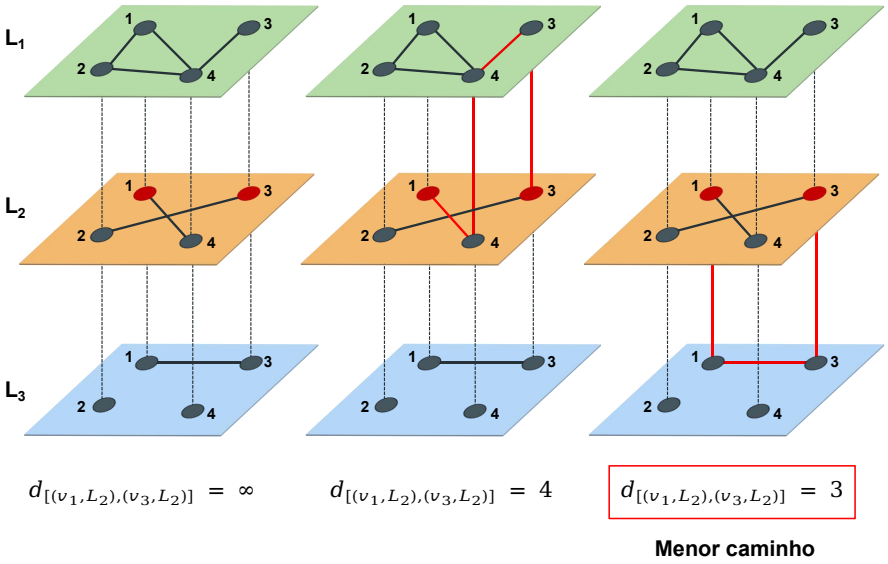

Fig. 4.6: Esquematização do cálculo do comprimento de menor caminho entre dois vértices em uma rede *multiplex*. A distância entre o vértice 1 da camada 2 (v_1, L_2) e o vértice 3 da camada 2 (v_3, L_2) é considerada infinita, pois não existe ligação entre eles nesta camada. Contudo, isso é contornável devido às ligações intercamadas estabelecidas pela abordagem *multiplex*. Dois caminhos possíveis entre esses dois vértices estão representados (arestas destacadas em vermelho): (i) (v_1, L_2) - (v_4, L_2) - (v_4, L_1) - (v_3, L_1) - (v_3, L_2), com tamanho igual a 4; (ii) (v_1, L_2) - (v_1, L_3) - (v_3, L_3) - (v_3, L_2), com tamanho igual a 3. Logo, a menor distância entre os vértices (v_1, L_2) e (v_3, L_2) é igual a 3.

onde $[\cdots]_{ij}$ denota o elemento (ij)-ésimo elemento de uma matriz e N é o número de vértices. Dessa forma, o número de caminhos com tamanho d entre i e j é $\mathcal{N}_{ij}^{(d)} = A_{ij}^{(d)}$, e a distância considerada entre esses vértices é dada pelo caminho com menor valor d para a qual $\mathcal{N}_{ij}^{(d)} > 0$.

O comprimento de menor caminho médio (ℓ), que informa o menor número de passos que, em média, é preciso dar na rede para sair de um vértice até outro, é definido por

$$\ell = \frac{1}{N(N-1)} \sum_{i,j=1,N;i\neq j} d_{ij}, \tag{4.12}$$

sendo d_{ij} a menor distância entre os vértices i e j.

No caso de redes multicamadas, os menores caminhos podem variar significativamente entre diferentes camadas, e também entre as camadas e a rede agregada. Ademais, pode haver casos em que não exista um caminho entre dois vértices em uma camada, mas, como consequência da abordagem *multiplex*, eles sejam alcançáveis entre si através de caminhos que percorram mais de uma camada. Na Fig. 4.6 apresentamos uma esquematização para exemplificar um caso desse tipo. Assim, para capturar a contribuição *multiplex*, consideramos para o cálculo das distâncias entre

os vértices das redes os menores caminhos percorridos em uma ou mais camadas.

4.2 Dados

Os dados utilizados neste estudo foram obtidos do catálogo mundial pertencente ao *Advanced National Seismic System (ANSS)*[1], sendo considerados dados sismológicos de todo o planeta para o período de 2000 a 2019 (20 anos), e com magnitude mínima igual a 4,5. Seguindo nossas análises anteriores apresentadas nos Capítulos 2 e 3, dividimos o conjunto de dados obtido em terremotos rasos (profundidade de até 70 km) e terromotos profundos (profundiade maior que 70 km) [12, 13]. O total de dados é 107 118 e 28 507 eventos sísmicos rasos e profundos, respectivamente. Os tipos de magnitude considerados foram m_b (onda de corpo de curto período), m_{wc} (centroide), m_{ww} (magnitude do momento).

Para cada conjunto de dados, aplicamos a metodologia de construção de redes multicamadas comentada na próxima seção.

4.3 Construção das Redes *Multiplex* de Terremotos

Na seção 4.1.2 foi apresentada a definição de redes *multiplex* e abordado o conceito de redes temporais. Para criar as redes temporais de terremotos, construímos cada camada considerando o período de um ano de dados. Dessa forma, dado um número M de camadas, consideramos que cada conjunto de M anos consecutivos está conectado formando uma rede *multiplex*, isto é, para o conjunto de anos t_0 a t_{M-1}, construímos uma rede *multiplex* de M camadas. A seguir considera-se o ano seguinte como o inicial e cria-se uma rede para o conjunto t_1 a t_M. Esse processo é repetido até cobrirmos os 20 anos de dados sismológicos.

Seguindo trabalhos prévios [14, 15, 16] e o estudo realizado no Capítulo 3, os vértices foram definidos como sendo células quadradas (sítios) de tamanho $20\,km \times 20\,km$ recortadas sobre a superfície do globo, onde ao menos um terremoto tenha ocorrido. Em cada camada, as ligações entre os vértices foram estabelecidas seguindo o modelo sucessivo proposto por [17]. Ou seja, dado um terremoto A, ocorrido na célula C_A, e um evento subsequente B, ocorrido na célula C_B, criamos uma aresta entre os vértices C_A e C_B. Essas são as ligações *intracamadas*. Para estabelecer uma rede *multiplex*, cada vértice foi conectado a si mesmo na camada seguinte, configurando as ligações *intercamadas*.

[1] https://earthquake.usgs.gov/data/comcat/

Com o objetivo de investigar o comportamento das propriedades topológicas das redes de acordo com o número de camadas consideradas, variamos o número de camadas das redes temporais *multiplex* construídas. Além disso, analisamos a possibilidade da existência de um valor para o número de camadas que apresente melhores resultados, de acordo com os obtidos em trabalhos prévios de redes monocamadas de terremotos. Em todos os casos, consideramos redes não-direcionadas.

4.4 Resultados

No método de construção de redes de terremotos utilizado neste trabalho, é possível saber a localização geográfica de cada célula, bem como as ligações existentes entre todos os vértices da rede. Dessa forma, foram geradas imagens geoespaciais das redes temporais *multiplex* para um melhor entendimento sobre elas e também para a visualização da evolução da ocorrência de terremotos ao longo do planeta nos 20 anos de dados sismológicos usados nas análises. Na Fig. 4.7 é apresentada uma rede *multiplex* de terremotos rasos com 3 camadas, abrangendo os anos de 2000 a 2002, assim como a respectiva rede agregada (uma única rede contendo os dados de todas as camadas consideradas). Cada camada da rede *multiplex* é constituída por uma rede criada com o modelo sucessivo, considerando dados sismológicos de 1 ano, onde cada vértice é conectado a si mesmo na camada consecutiva de forma a estabelecer uma rede *multiplex* (as ligações intercamadas não estão representadas na Fig. 4.7).

Os vértices com maiores número de ligações (*hubs*) variam a cada ano, porém se encontram sempre em torno de lugares localizados nos limites das placas tectônicas, podendo ser destacados o Japão (e seus arredores), as Ilhas Sumatra, o Chile e a região ao redor da fossa oceânica de Tonga. Tais resultados fazem sentido, visto que esses locais possuem intensa atividade sísmica. Além disso, é interessante notar que as ligações, em cada camada, ocorrem não apenas entre células espacialmente próximas, mas também entre regiões distantes umas das outras, evidenciando correlações de longo alcance entre terremotos de todo o mundo, como foi encontrado em trabalhos prévios. Destaca-se ainda o fato de que ao se considerar a rede monocamada agregada dos 3 anos, 2000 - 2002, (Fig. 4.7) a informação de quais locais apresentam mais conexões com outras regiões (e assim, apresentando um papel mais fundamental na rede de terremotos) a cada ano é "mascarada", sendo mais difícil de se analisar a influência de ocorrência de terremotos entre diferentes locais em todo o planeta.

Para exemplificar, a Fig. 4.8 apresenta 4 redes temporais *multiplex*, com 3 camadas cada, de forma a cobrir os anos entre 2001 e 2006. Assim, o terremoto de magnitude 9,1 (M_W) ocorrido em 26 de dezembro de 2004, em Sumatra, Indonésia,

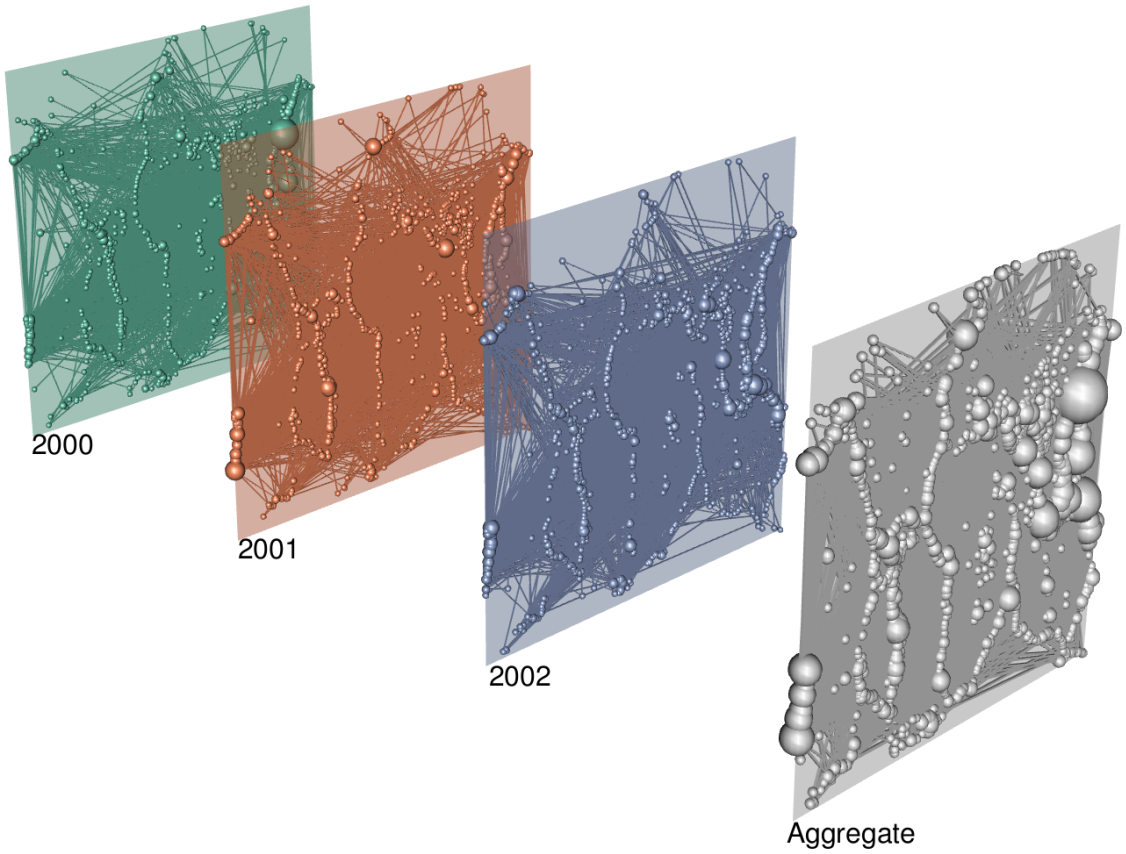

Fig. 4.7: Rede temporal *multiplex* de terremotos rasos com 3 camadas. Os anos considerados para a criação dessa rede são 2000, 2001 e 2002. Os vértices são representados por esferas e as arestas intracamadas são dadas por retas que as conectam. Os vértices delimitam perfeitamente os limites das placas tectônicas. Quanto maior o tamanho do vértice, maior é o número de ligações que ele possui (são os *hubs* da rede). Também é apresentada a rede agregada dos 3 anos. As arestas intercamadas não são mostradas para facilitar a visualização.

está contido nesses dados, bem como dados de anos anteriores e posteriores a ele. Nota-se que no ano de 2002, a maioria dos *hubs* se encontram localizados em regiões próximas de Sumatra, evidenciando uma atividade sísmica maior nesses locais nesse ano do que em outras regiões do planeta. Nos anos seguintes, de 2003 e 2004, tal comportamento permanece, culminando com o terremoto de elevada magnitude. Os reflexos desse evento sísmico são especialmente notáveis no ano seguinte, 2005, onde pode-se verificar enormes *hubs* dessa rede localizados em Sumatra e seus arredores. Isto se deve ao fato de que terremotos de grande magnitude costumam ocasionar muitas réplicas em localidades próximas do terremoto principal, fazendo com que surjam mais conexões entre esses vértices.

Outro ponto interessante é o fato de que o aumento na ocorrência de terremotos após o evento de 2004 não se deu apenas em regiões próximas, mas também na China e na Islândia, que são locais onde outros *hubs* da rede estão localizados no ano de

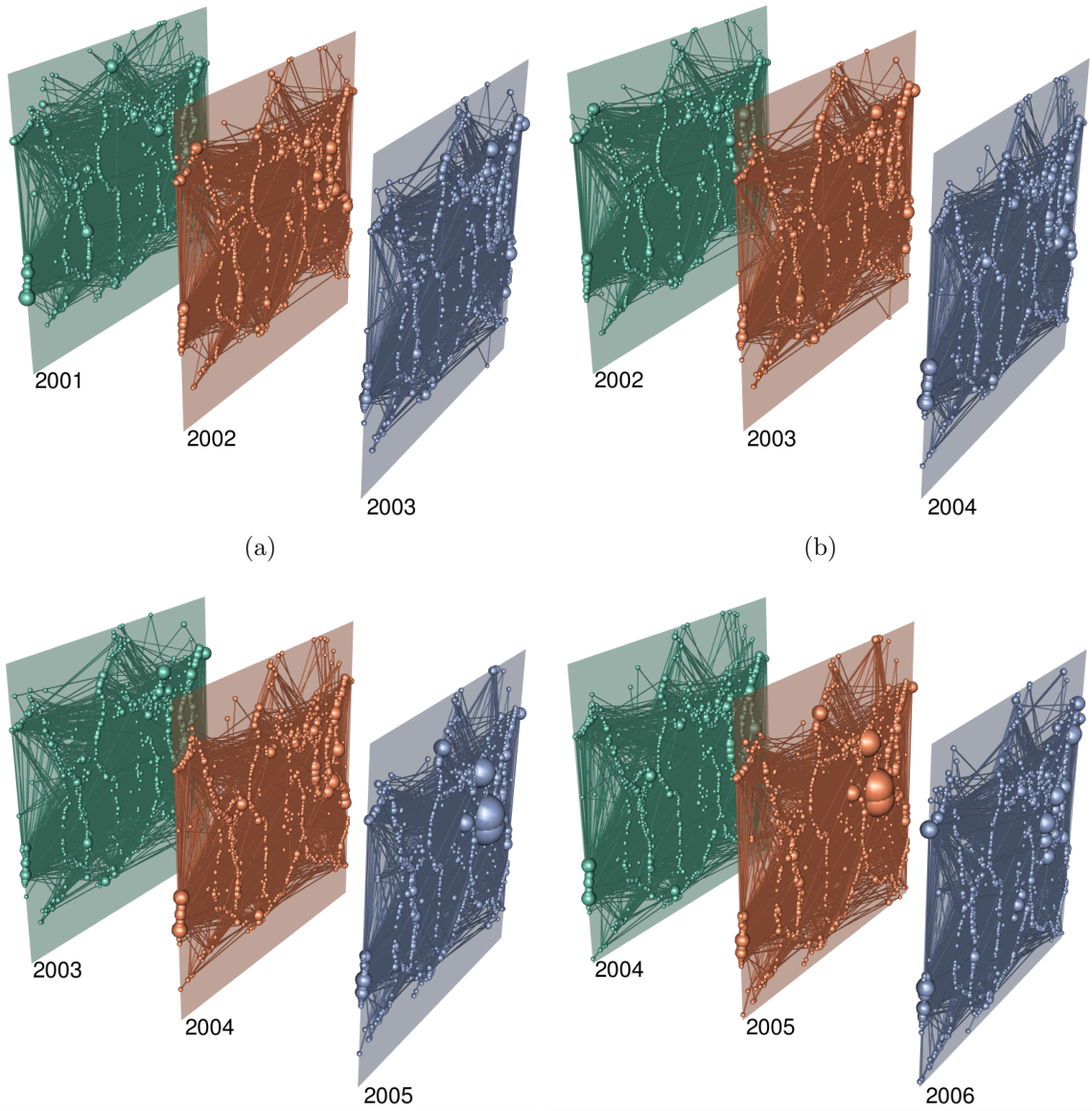

Fig. 4.8: Redes *multiplex* com 3 camadas de terremotos rasos para os anos (a) 2001 a 2003, (b) 2002 a 2004, (c) 2003 a 2005 e (d) 2004 a 2006. Maiores vértices representam aqueles com maior número de ligações. As arestas intercamadas não são mostradas.

2005. Isso corrobora com a ideia de que a influência desses grandes terremotos não se dá somente em curtas distâncias, mas também a milhares de quilômetros, sendo mais um indicativo de possíveis correlações de longo alcance espacial e temporal no fenômenos sismológico. Finalmente, em 2006, observa-se que a atividade sísmica mundial permanece maior do que nos anos anteriores ao terremoto de 2004 em Sumatra, no entanto, os *hubs* se encontram mais diluídos em várias células. Novos locais também passam a ser *hubs* da rede, como as Ilhas Curilas, ao Norte do Japão, local onde ocorreu um tremor de magnitude 8,3 (M_W) em novembro de 2006 [18].

Análise semelhante foi realizada para as redes temporais *multiplex* de terremotos

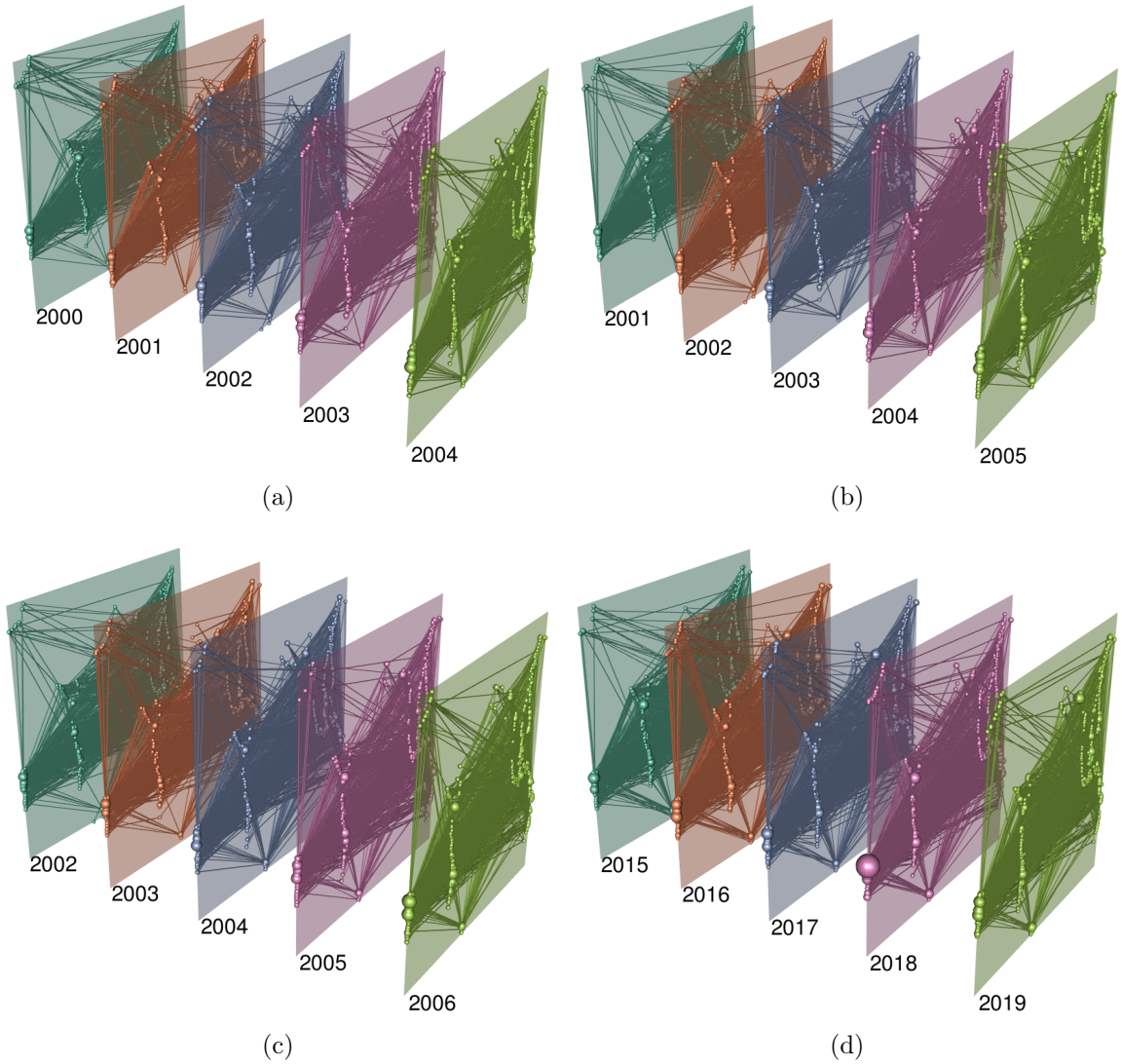

Fig. 4.9: Redes *multiplex* com 5 camadas de terremotos profundos para os anos (a) 2000 a 2004, (b) 2001 a 2005, (c) 2002 a 2006 e (d) 2015 a 2019. Vértices maiores são os que apresentam mais ligações (*hubs*). As arestas intercamadas não são mostradas para facilitar a visualização.

profundos, considerando 5 camadas. O resultado é apresentado na Fig. 4.9, para o período de 2000 a 2006, e também para o conjunto de 2015 a 2019. Os vértices são localizados em regiões onde, em geral, ocorrem terremotos profundos (majoritariamente em zonas de subducção nos limites de placas convergentes [19]), como era esperado. No entanto, diferentemente dos terremotos rasos, que apresentaram variações consideráveis nas redes das atividades sísmicas global ao longo dos anos, no caso dos eventos sísmicos profundos não houve mudanças significativas na aparência das redes de um ano para outro. Os *hubs* se localizam, frequentemente, nas Ilhas Fiji, na Argentina e na Colômbia, o que faz sentido, visto que a maioria dos terremotos profundos ocorrem nesses locais. Apesar disso, eles não possuem muito mais ligações que outras regiões do planeta. Tal fato é evidenciado pelo tamanho dos

vértices, que são muito parecidos.

Seguindo a apresentação das análises realizadas no presente estudo, os outros resultados obtidos dizem respeito às propriedades topológicas das redes temporais *multiplex* investigadas, como será comentado a seguir.

Em trabalhos prévios considerando redes monocamadas de ligações sucessivas para terremotos de regiões pequenas do mundo (como Califórnia, Japão e Chile [20, 21]), foi observado que as distribuições de *strength* (s) dessas redes são caracterizadas por leis de potência, $P_{\geq}(s) \sim s^{-\gamma}$ (sendo γ uma constante positiva), evidenciando o comportamento livre de escala das redes de terremotos. No entanto, conforme apontado em [14], quando realizada essa investigação em redes de terremotos globais, é observado que essas distribuições apresentam um corte exponencial para grandes valores de *strength*, ou seja, elas são melhor ajustadas por leis de potência com um corte exponencial,

$$P_{\geq}(s) \sim s^{-\delta}\, e^{-s/s_c}, \tag{4.13}$$

em que δ e s_c são constantes positivas.

Com relação aos dados sismológicos globais do período de 2000 a 2019 utilizados no presente estudo (conjunto de dados rasos e profundos), quando analisadas as distribuições acumuladas de *strength* das redes agregadas de 20 anos, nota-se que elas também seguem leis de potência com corte exponencial. Como pode ser visto na Fig. 4.10, o regime em lei de potência desses gráficos é obedecido apenas para os primeiros pontos.

Ao ser utilizado o método de redes temporais *multiplex* para construir as redes de terremotos, alguns pontos interessantes são observados. Para cada conjunto de redes *multiplex* com M camadas, os valores de *strength* dos vértices foram calculados a partir da Eq. 4.6, e esses valores foram utilizados na construção das distribuições de probabilidade acumulada de *strengths*. O número de camadas foi variado entre 1 (que produz 20 redes monocamadas, com cada rede considerando o período de 1 ano), e 15 (produzindo 6 redes multicamadas, iniciando no intervalo entre 2000 e 2014, depois de 2001 a 2015, e assim sucessivamente, até serem englobados os 20 anos de dados). Nas Figs. 4.11 e 4.12 são apresentados os resultados para redes *multiplex* com 1, 3, 5 e 15 camadas, considerando terremotos rasos e profundos, respectivamente.

No caso das redes criadas para dados de terremotos rasos, é possível notar que conforme o número de camadas aumenta as distribuições passam a ser cada vez mais bem ajustadas por funções em lei de potência com corte exponencial (Fig. 4.11), como era de se esperar, uma vez a distribuição da rede agregada também possui este comportamento (Fig. 4.10(a)). Contudo, vale destacar que quando o número de ca-

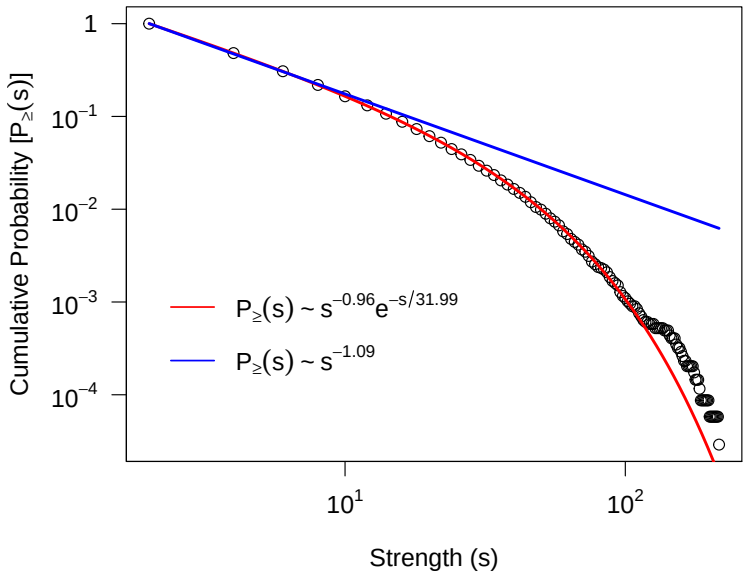

(a)

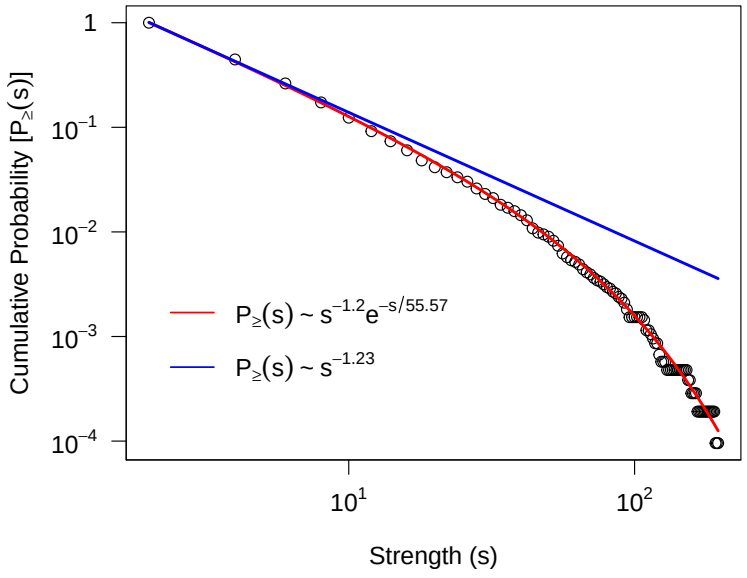

(b)

Fig. 4.10: Distribuição log-log de probabilidade acumulada de *strength* das redes agregadas de dados de terremotos globais ocorridos no período de 2000 a 2019. Em ambos os casos, o melhor ajuste é dado para uma lei de potência com corte exponencial, dada por $P_{\geq}(s) \sim s^{-\delta}\, e^{-s/s_c}$. (a) Terremotos rasos, com parâmetros de ajuste igual a $\delta = 0,96$ e $s_c = 31,99$ (ajuste em vermelho). (b) Terremotos profundos. Os parâmetros do ajuste obtido foram $\delta = 1,20$ e $s_c = 55,57$ (ajuste em vermelho). Foram também ajustadas leis de potência ($P_{\geq}(s) \sim s^{-\gamma}$) para comparação (ajuste em azul). Os valores dos parâmetros são (a) $\gamma = 1,09$, e (b) $\gamma = 1,23$.

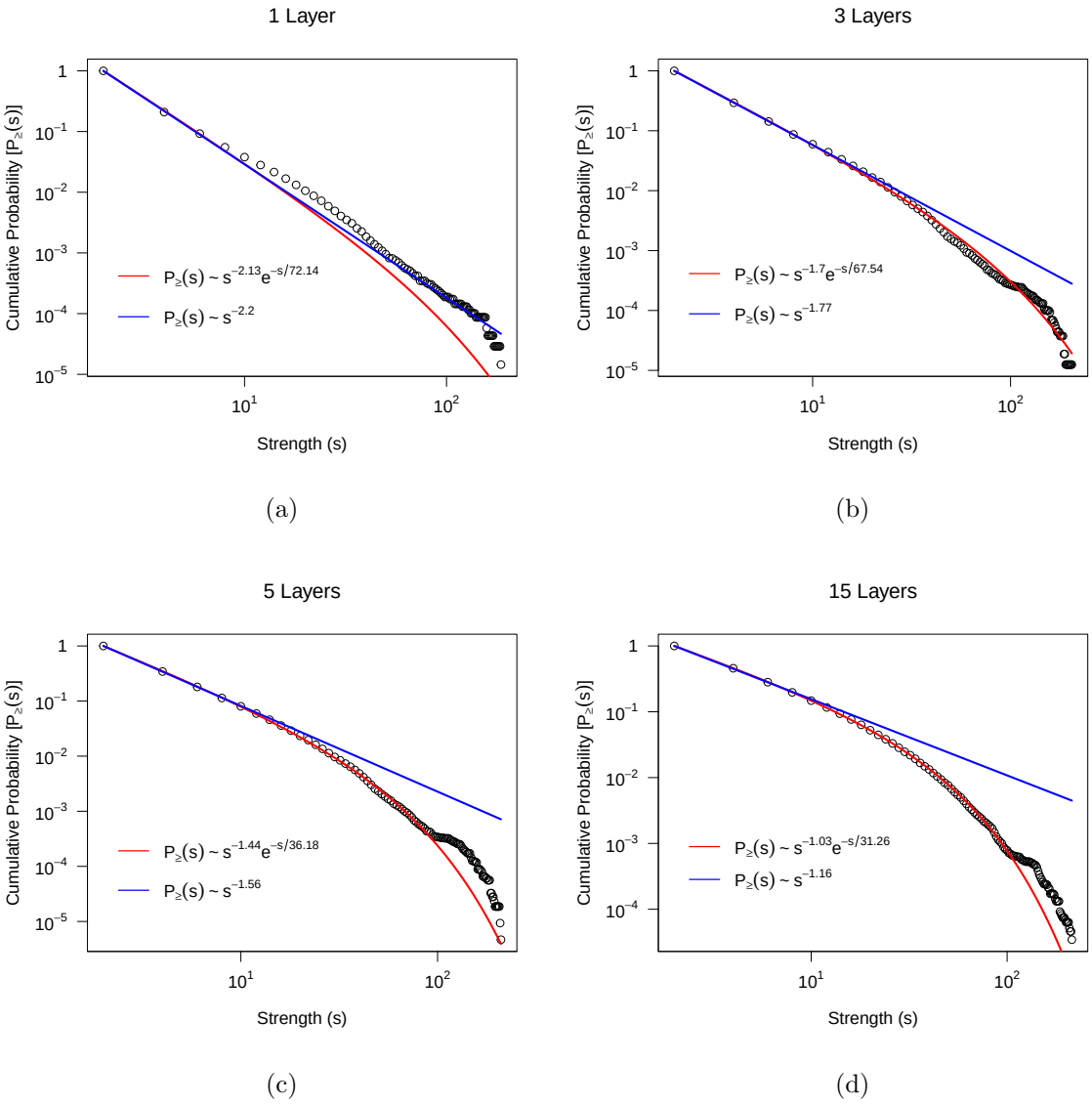

Fig. 4.11: Distribuições log-log de probabilidade acumulada de *strength* das redes temporais *multiplex* de terremotos rasos, considerando (a) 1 camada, (b) 3 camadas, (c) 5 camadas e (d) 15 camadas. É possível observar que com o aumento do número de camadas da rede as distribuições passam a apresentar um comportamento de lei de potência com corte exponencial (ajustes em vermelho). Em todos os casos, foram ajustadas leis de potência pura para comparação (ajustes em azul). O destaque é o gráfico obtido para 3 camadas [(b)], pois o regime em lei de potência é maior do que nas outras redes. Os valores encontrados para os parâmetros em cada ajuste estão presentes nas figuras.

madas considerado é $M = 3$ (Fig. 4.11(b)), a distribuição acumulada de *strength* possui um regime em lei de potência maior que em todos os outros casos (seja nas redes temporais com outros valores de camadas ou na rede agregada). Isso significa que ao analisarmos redes de terremotos rasos a partir da abordagem *multiplex* de 3 camadas, o comportamento livre de escala é mantido para maiores valores de *strength*, sendo um comportamento mais próximo do encontrado em estudos re-

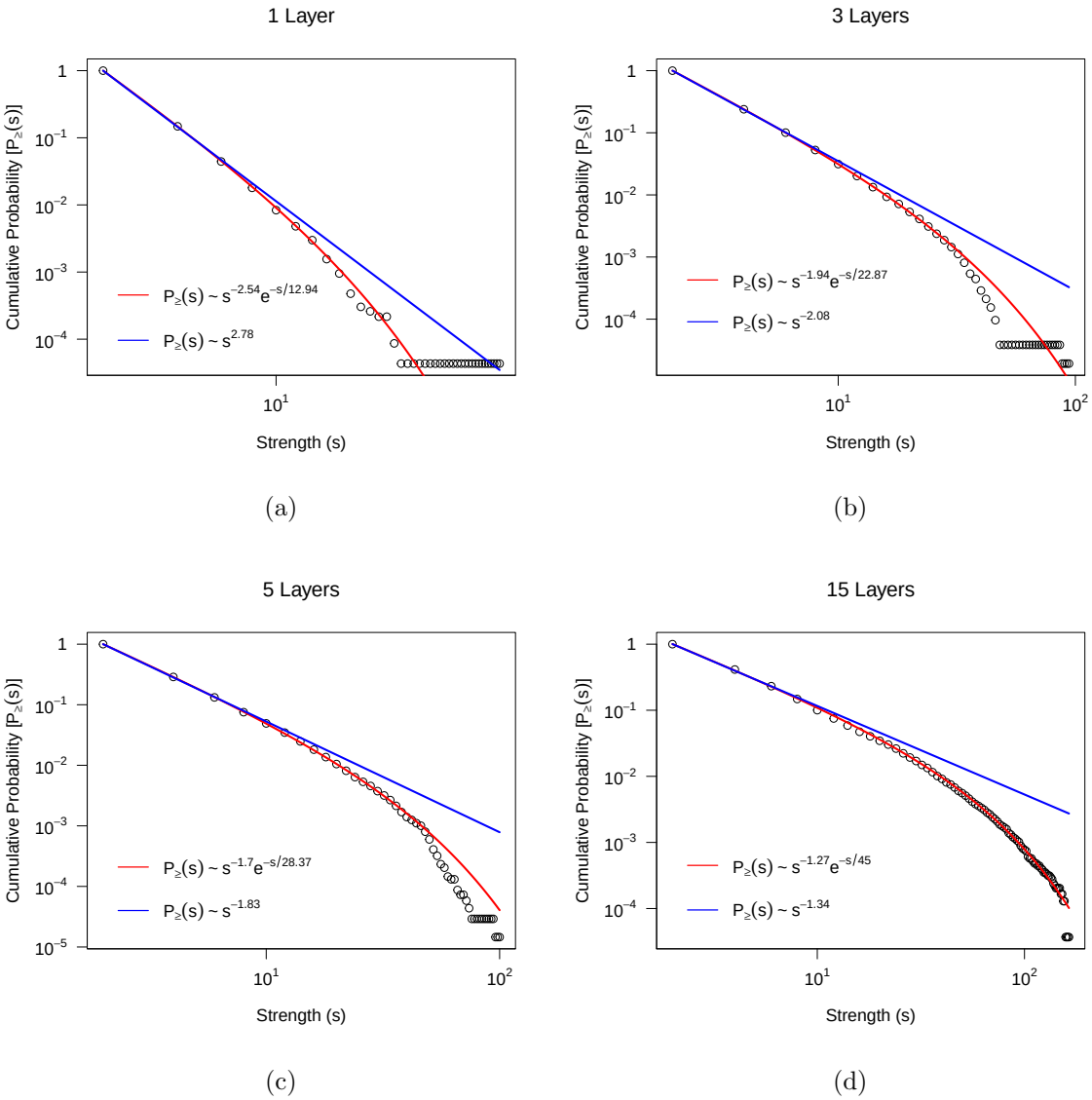

Fig. 4.12: Distribuições log-log de probabilidade acumulada de *strength* das redes temporais *multiplex* de terremotos profundos, considerando (a) 1 camada, (b) 3 camadas, (c) 5 camadas e (d) 15 camadas. As distribuições são bem ajustadas por leis de potência com corte exponencial (ajustes em vermelho), apresentando um corte exponencial ainda maior conforme o número de camadas cresce. Em todos os casos, foram ajustadas leis de potência pura para comparação (ajustes em azul). O destaque é o gráfico obtido para 5 camadas [(c)], uma vez que o regime em lei de potência é maior do que nas outras redes. Os valores encontrados para os parâmetros em cada ajuste estão presentes nas figuras.

alizados para redes monocamadas de terremotos de locais específicos do planeta [17, 22, 23, 24, 25]. Este fato se torna ainda mais relevante uma vez que para $M = 1$ e $M = 2$ (o gráfico deste último não está representado) o comportamento em lei de potência é praticamente inexistente. Ou seja, este comportamento se inicia em $M = 3$, sendo máximo neste mesmo valor. Destacamos ainda que a rede temporal de 15 camadas (Fig. 4.11(d)) apresenta uma distribuição muito similar à encontrada

para a rede agregada.

Outro ponto a ser observado nos resultados para terremotos rasos é o fato de que o valor máximo de *strength* é sempre próximo de 200, seja considerando a rede agregada de 20 anos (Fig. 4.10(a)) ou redes temporais com diferentes quantidades de camadas (Fig. 4.11). Esse resultado é interessante pois mostra que existem vértices com um elevado número de ligações que ocorrem em um período de tempo menor que um ano. Ou seja, para terremotos rasos, construir as redes utilizando dados de vários anos não produzem como consequência imediata altos valores de *strength*, uma vez que alguns eventos, mesmo em um curto período de tempo (menor que um ano), têm um grande efeito na ocorrência de outros terremotos. Tal fato pode ser entendido como um tipo de "clusterização temporal" nos terremotos rasos. Vale salientar que esse fato só foi observado devido à utilização do método de multicamadas, uma vez que ao construir uma única rede agregada essa informação detalhada seria "mascarada". A mesma quantidade de camadas foi considerada em um trabalho de rede temporais *multiplex* de terremotos do Irã e da Califórnia, regiões com predominância de terremotos rasos [7]. Contudo no referido trabalho os autores não fazem um estudo para diferentes quantidades de camadas, nem apresentam justificativa para a utilização de 3 camadas.

Com relação aos resultados para terremotos profundos, também foi observado que as distribuições de probabilidade de *strength* seguem uma lei de potência com corte exponencial. Na Fig. 4.12 é apresentado como esse comportamento varia ao serem adicionadas mais camadas na rede. Assim como nas redes temporais de terremotos rasos, as distribuições possuem comportamentos que apresentam maior similaridade com a função da eq. 4.13 conforme se aumenta a quantidade de camadas na rede. Para a rede criada com 15 camadas o comportamento do gráfico já apresenta grande semelhança com a distribuição da rede agregada (Fig. 4.10(b)). No entanto, diferentemente dos terremotos rasos, observamos que o comportamento em lei de potência pura se mantém para maior quantidade de dados quando o número de camadas é igual a 5 (apesar da distribuição sofrer pouca alteração no intervalo desde $M = 3$ até $M = 5$).

Outro destaque ocorre para o valor máximo de *strength* das redes *multiplex* de terremotos profundos, que possui características distintas das encontradas para dados rasos. Ao observar a Fig. 4.12, é possível notar que o valor máximo de s da rede cresce com o aumento do número de camadas. Ou seja, conforme é considerado uma maior quantidade de anos na construção da rede *multiplex*, os *hubs* da rede também acumulam uma maior quantidade de ligações. Dessa forma, os valores máximos de *strength* para essas redes são diretamente dependentes da quantidade de dados da atividade sísmica profunda nas regiões ao longo de anos, fazendo com que o fenômeno de "clusterização temporal", seja menos claro neste tipo de terremotos.

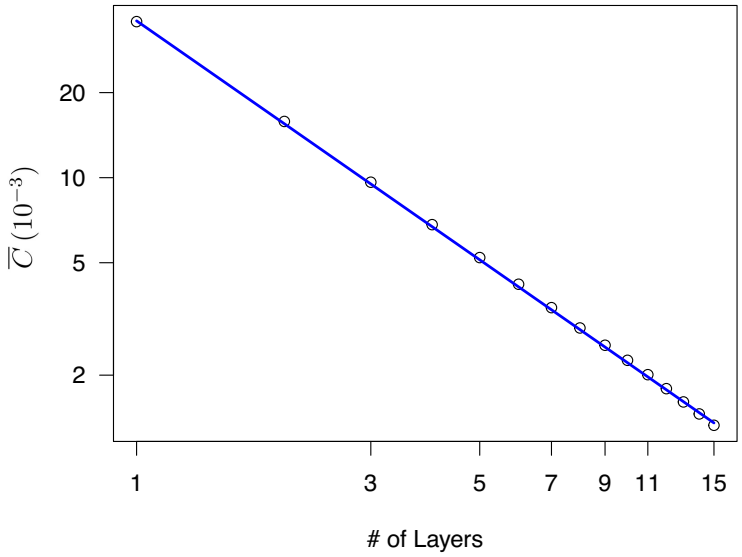

(a)

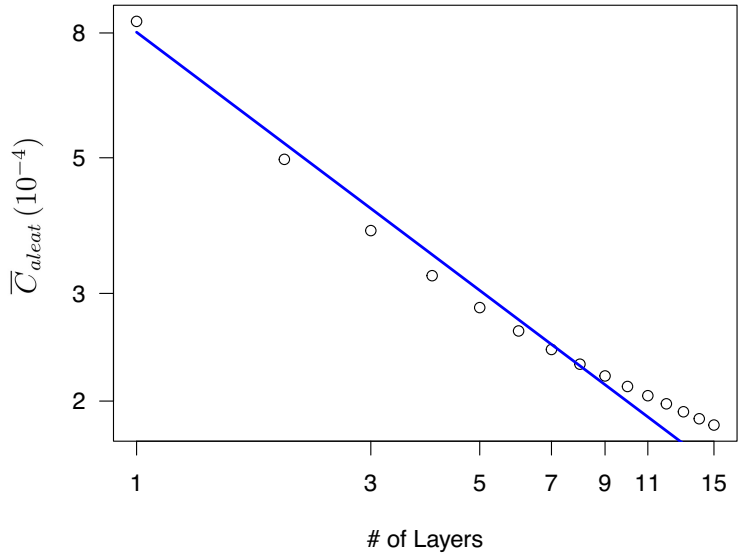

(b)

Fig. 4.13: Distribuição log-log de coeficiente de aglomeração global médio em função do número de camadas (a) para redes *multiplex* de terremotos rasos. O gráfico apresenta decaimento em lei de potência ($\overline{C} \sim M^{-\eta}$), com parâmetro $\eta = 1,21$ (linha sólida em azul). (b) Mesma distribuição, porém para uma rede aleatória similar. O ajuste em lei de potência serve como um guia para os olhos (linha sólida em azul). Como pode ser visto, essa rede não possui o mesmo comportamento que a rede original.

Além das distribuições de *strength*, foram investigados os valores de coeficiente de aglomeração global (C) e comprimento de menor caminho médio (ℓ) das redes temporais *multiplex* criadas. Para cada conjunto de M camadas, com M variando de 1 a 15 ($1 \leq M \leq 15; M \in \mathbb{N}$), foram calculadas as médias dos valores de C e ℓ a partir das equações Eq. 4.10 e 4.11, respectivamente. Vale ressaltar que para esses cálculos as redes foram simplificadas, isto é, foram retiradas auto-ligações (ligação de um vértice a si mesmo) e arestas repetidas foram consideradas como tendo peso igual a 1.

Como pode ser observado nas Figs. 4.13(a) e 4.14(a), tanto para terremotos rasos quanto profundos, o valor médio do coeficiente de aglomeração global, $\overline{C}$, das redes diminui consideravelmente com o aumento do número de camadas utilizadas. Contudo, o comportamento dos gráficos é diferente. Para as redes de terremotos rasos (Fig. 4.13(a)), encontramos um comportamento com excelente concordância entre os dados e uma função em lei de potência do tipo $\overline{C} \sim M^{-\eta}$, indicando uma invariância de escala no sistema. A fim de analisar se este comportamento é uma característica inerente às redes de terremotos rasos, ou se é uma característica aleatória do sistema, calculamos os valores dos coeficientes de aglomeração médios para redes aleatórias similares ($\overline{C}_{aleat}$), isto é, redes com a mesma quantidade de vértices e arestas que as redes originais de terremotos rasos, porém com suas ligações distribuídas aleatoriamente entre os vértices. Como pode ser observado na Fig. 4.13(b), o comportamento em lei de potência desaparece ao se utilizar as redes aleatórias, o que mostra que a propriedade de invariância de escala é característica do sistema de terremotos rasos, e não uma consequência do método de construção das redes de terremotos.

Uma observação a ser feita é que uma assinatura similar à que encontramos aqui também surge ao se estudar a relação entre coeficiente de aglomeração de redes monocamadas de terremotos no Irã e o tamanho das células consideradas para a definição dos vértices [23]. Nesse trabalho, os autores variaram a resolução das células espaciais que definem os vértices, e notaram um decaimento em lei de potência nos valores de coeficiente de aglomeração com o aumento da resolução. Dado esse resultado obtido para terremotos do Irã (local com predominância de terremotos ocorridos em baixas profundidades) e os encontrados no presente trabalho para redes temporais de terremotos mundiais rasos, é possível argumentar que os terremotos rasos possuem uma aglomeração com comportamento em lei de potência tanto em termos de uma resolução espacial quanto temporal.

No que concerne aos terremotos profundos, o comportamento do coeficiente de aglomeração global médio, $\overline{C}$, em função do número de camadas da rede temporal *multiplex* é mostrada na Fig. 4.14(a). Nota-se no gráfico um decrescimento rápido até o valor de 5 camadas, mantendo-se um decaimento mais suave a partir desse valor, não sendo encontrado portanto um comportamento em lei de potência, como

ocorre no caso das redes de terremotos rasos. Além disso, destacamos que o comportamento do coeficiente de aglomeração global médio de uma rede aleatória similar à rede de terremotos profundos possui comportamento semelhante ao obtido para as redes de terremotos profundos originais (vide a Fig. 4.14(b)). Tal resultado aponta para diferenças na formação de grupos de vértices nas redes construídas para eventos sísmicos rasos e profundos.

Além do coeficiente de aglomeração, outra medida topológica que foi investigada nas redes temporais *multiplex* de terremotos globais é o comprimento de menor caminho médio (ℓ). Na Fig. 4.15 são apresentados gráficos dos valores médios de ℓ em função do número de camadas consideradas nas redes de eventos rasos e profundos. Como pode ser observado, ambas as distribuições seguem um comportamento linear crescente com o número de camadas. Vale destacar que este resultado é coerente, uma vez que quanto mais camadas são consideradas, maior é o número de vértices da rede *multiplex*, e portanto maior é o valor de ℓ, uma vez que muitos vértices só conseguem ser alcançados por caminhos que utilizem de múltiplas camadas (como no exemplo da Fig. 4.6)

No trabalho realizado para redes monocamadas de terremotos do Irã [23], em que a resolução das células espaciais foi investigada, os autores também obtiveram um crescimento linear para o valor do comprimento de menor caminho médio, ℓ, com o aumento da resolução. Isso mostra mais uma evidência de que o fenômeno sismológico possui características espaciais e temporais similares.

Conforme comentado em capítulos anteriores desta dissertação, trabalhos prévios encontraram características livre de escala e mundo-pequeno em redes monocamadas (simples) de terremotos locais e globais [14, 15, 16, 17, 22, 23, 24, 25]. Para classificar uma rede mundo-pequeno, são investigados os valores de seu coeficiente de aglomeração e comprimento de menor caminho médio [8]. Redes com propriedade mundo-pequeno possuem um alto coeficiente de aglomeração, comparado ao valor para uma rede aleatória similar, e um baixo comprimento de menor caminho médio, quando comparado ao número de vértices na rede.

Assim, no presente estudo, a fim de analisar possíveis características de mundo-pequeno, essas propriedades foram analisadas para as redes *multiplex* de terremotos rasos e profundos. Para terremotos rasos foi considerada a rede de 3 camadas ($M = 3$) e para terremotos profundos a rede de 5 camadas ($M = 5$). Na Tabela 4.1 são apresentados os valores médios dessas métricas. Analisando os valores obtidos, nota-se que ambas as redes (terremotos rasos e profundos) fornecem um valor de comprimento de menor caminho médio com a mesma ordem de magnitude que o logaritmo do número de vértices ($\overline{\ell} \sim \ln \overline{N}$), sendo uma das característica necessárias para que uma rede seja definida como do tipo mundo-pequeno [26]. Contudo, os valores do coeficiente de aglomeração encontrados para essas redes são próximos

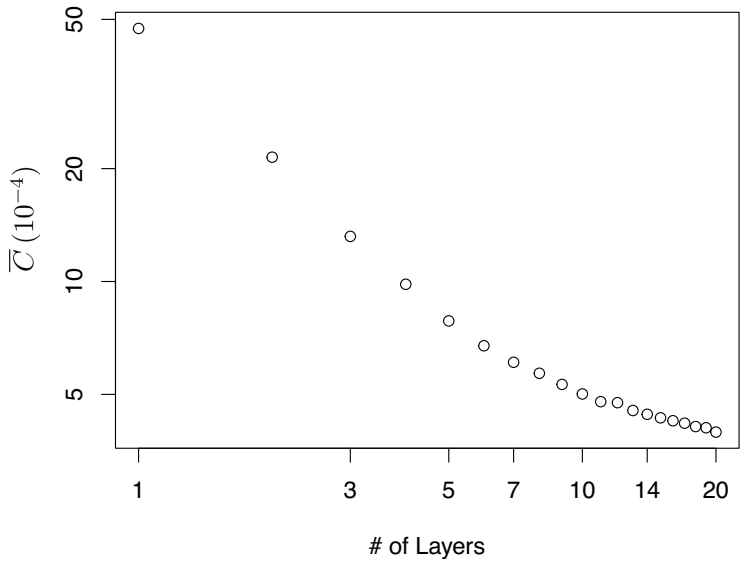

(a)

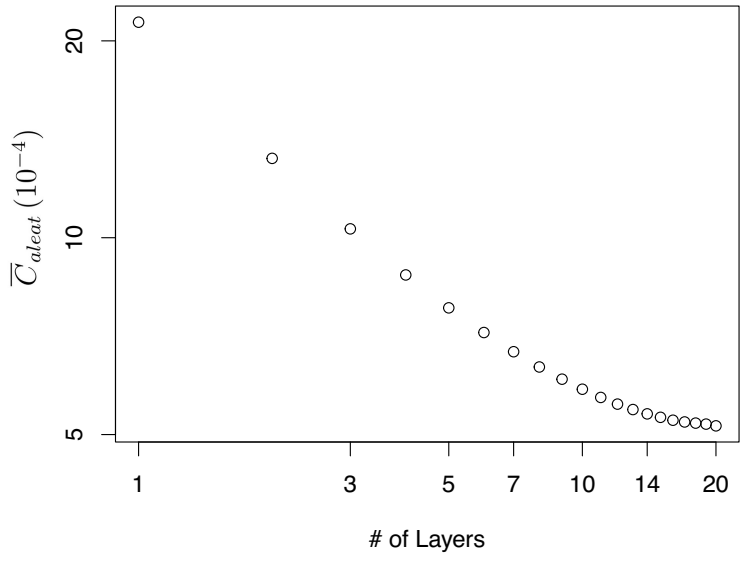

(b)

Fig. 4.14: Distribuição log-log de coeficiente de aglomeração global médio em função do número de camadas para (a) redes *multiplex* de terremotos profundos, e (b) redes aleatórias similares. Ambos os gráficos possuem um decaimento rápido até a camada de valor 5, apresentando um caimento mais suave a partir desse valor.

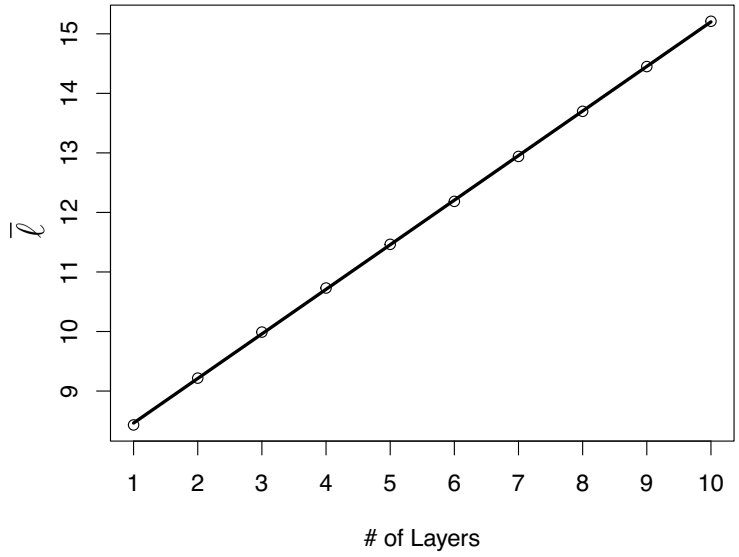

(a)

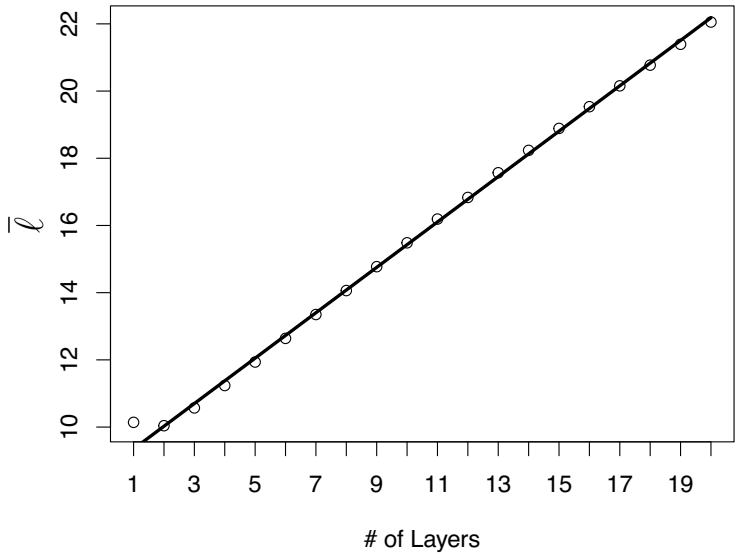

(b)

Fig. 4.15: Distribuição da média dos valores de comprimento de caminho médio, $\overline{\ell}$, em função do número de camadas nas redes *multiplex* (a) de dados sismológicos rasos e (b) dados sismológicos profundos. Em ambos os casos, é observado um comportamento crescente linear (linha sólida preta), dado por (a) $\overline{\ell} = 0,75\,M + 7,71$ e (b) $\overline{\ell} = 0,68\,M + 8,67$, em que M é o número de camadas.

Tabela 4.1: Valores de coeficiente de aglomeração ($\overline{C}$), coeficiente de aglomeração de redes aleatórias equivalentes ($\overline{C}_{aleat}$), comprimento de menor caminho médio ($\overline{\ell}$) e número médio de vértices ($\overline{N}$) para as redes temporais *multiplex* utilizadas neste trabalho.

Terremotos	$\overline{C}$	$\overline{C}_{aleat}$	$\overline{C}/\overline{C}_{aleat}$	$\overline{\ell}$	$\overline{N}$	$\ln \overline{N}$
Rasos (3 camadas)	0,00964	0,000380	25,4	9,99	8904	9,09
Profundos (5 camadas)	0,000785	0,000781	1,0	11,94	4298	8,37

dos valores obtidos para redes aleatórias de mesmo tamanho, isto é, não temos $\overline{C} \gg \overline{C}_{aleat}$. Dessa forma, tais redes não possuem propriedade de mundo-pequeno no sentido convencional utilizado para redes monocamadas.

Contudo, é importante salientar que estudos anteriores de redes monocamadas, tanto para terremotos rasos quanto profundos [15, 16], apontaram para o fato de que o método de criação de arestas conectando apenas epicentros de terremotos sucessivos não parece ser o mais adequado. Isto se deve ao fato de que esta modelagem acaba por minimizar propriedades de longo-alcance das redes. Desta forma, uma possibilidade para a falta de evidências de características de mundo-pequeno em nossas redes, pode ser a modelagem utilizando, sendo portanto necessária a aplicação de modelos de construção de redes mais robustos. Deste modo, os resultados obtidos no presente trabalho também colaboram com a ideia de que o modelo sucessivo utilizado na criação de arestas intracamadas apresenta limitações quando aplicado a redes *multiplex* de terremotos mundiais.

Por fim, é notável destacar que a abordagem multicamadas em redes de terremotos se apresenta promissora, uma vez que ela permite aumentar o refinamento das análises e também concede informações mais detalhadas sobre a evolução das propriedades das redes.

4.5 Conclusões

Neste capítulo foram investigadas propriedades topológicas de redes multicamadas de terremotos globais. Foram construídas redes temporais do tipo *multiplex*, sendo cada camada definida por uma rede sucessiva criada com dados sismológicos de 1 ano. As análises foram realizadas separadamente para dados de terremotos rasos e profundos, tendo em vista o pressuposto de que são mecanicamente diferentes [12, 19].

Primeiramente, foram criadas e analisadas imagens geoespaciais das redes em multicamadas, onde alguns pontos interessantes foram observados. A abordagem de redes *multiplex* permitiu observar características em redes de terremotos que não

eram visíveis ao utilizar uma única rede agregada. Na representação das redes o tamanho das células é proporcional ao número de conexões que a célula possui em cada camada. Nas redes temporais *multiplex* de terremotos rasos algumas regiões se destacam com relação ao tamanho das células nesses locais. Exemplos desses destaques são as regiões do Japão, Ilhas Sumatra, Tonga e Chile. Dado o elevado índice de ocorrência de terremotos nessas regiões, faz sentido que os *hubs* das nossas redes se encontrem nesses locais, indicando que a aplicação de redes complexas no estudo desses fenômenos apresenta resultados coerentes.

Tomando como exemplo o terremoto de grande magnitude ocorrido em 2004 em Sumatra, notou-se que antes do evento há o aumento de atividade sísmica em localidades próximas, e que esses eventos geram nos anos seguintes um elevado número de ligações entre essas células e outras do planeta, não apenas em lugares próximos, mas também a milhares de quilômetros de distância.

Por outro lado, as redes temporais de terremotos profundos mostraram que, independentemente da ocorrência de terremotos de magnitude elevada, não há uma variação tão evidente na atividade sísmica profunda ao longo do tempo, apresentando uma constância maior do que os terremotos rasos. Além disso, as células das redes estão localizadas, em sua grande maioria, em zonas de subducção, concordando com os conhecimentos geológicos existentes. Os vértices (células) de maior tamanho se encontram na região de Tonga, que é conhecida pela atividade sísmica profunda.

Esses resultados obtidos pela visualização espacial das redes em multicamadas apontam para diferenças na dinâmica de terremotos rasos e profundos. Vale ressaltar que esta caraterística de dinâmica temporal não é possível de ser observada ao se analisar as redes de forma agregada.

Com relação às distribuições de probabilidades dos *strengths* das redes, foi observado que tanto para terremotos rasos quanto profundos o melhor ajuste é dado por uma lei de potência com corte exponencial, e quanto maior o número de camadas na rede, menor é o comportamento da parte em lei de potência, e maior é a parte exponencial. O surgimento do corte exponencial sugere a existência de um fator limitante nas redes para grandes valores de *strength*, tendo sido encontrado esse resultado também em estudos de redes monocamadas sucessivas de terremotos mundiais [14]. Apesar disso, foi observado que existe um valor de número de camadas para o qual o regime em lei de potência é maior. Os valores de camadas que forneceram esse resultado foram 3 camadas para dados rasos e 5 camadas para dados profundos. Esse resultado mostra uma outra vantagem na utilização de redes multicamadas quando comparadas às redes monocamadas. Esta vantagem consiste no fato de permitir a análise dos mesmos 20 anos de dados (2000 a 2019) mas com uma análise mais detalhada.

Outras propriedades topológicas analisadas neste trabalho foram o coeficiente de aglomeração global (C) e o comprimento de menor caminho médio (ℓ). Em relação ao primeiro, características diferentes foram encontradas para os terremotos rasos e profundos. Para as redes temporais multiplex de terremotos rasos, o valor médio do coeficiente de aglomeração global variou com o número de camadas na rede seguindo uma lei de potência decrescente, o que é um resultado muito interessante, uma vez que essa função aponta invariância de escala em relacionamentos entre diferentes parâmetros. Para mostrar que esse resultado é inerente ao fenômeno e não somente um resultado aleatório, foram calculados os valores dos coeficiente de aglomeração de redes aleatórias similares. Nestas redes aleatórios, apesar de o coeficiente de aglomeração médio também decrescer com o tamanho do número de camadas, os resultados não possuem concordância com uma lei de potência.

Vale destacar que em [23] os autores utilizaram redes monocamadas de terremotos do Irã [23]. Neste trabalho também foi encontrada uma relação de lei de potência para o coeficiente de aglomeração da rede em função da resolução das células espaciais definidas como vértices. Visto que a abordagem de redes temporais aplicadas no presente estudo pode ser entendida como uma análise temporal da ocorrência de terremotos, pode ser argumentado que a formação de triângulos na rede de terremotos rasos (isto é, a informação do coeficiente de aglomeração) possui invariância de escala tanto espacial quanto temporalmente. Um estudo futuro mais detalhado dessa característica seria interessante para resultados mais aprofundados.

Por outro lado, as redes temporais de terremotos profundos não apresentaram uma relação em lei de potência entre os valores de coeficiente de aglomeração e o número de camadas da rede, tendo fornecido um comportamento similar ao de redes aleatórias de mesmo tamanho, e valores de coeficiente de aglomeração muito próximos, indicando (como explicitado em [16]) que o modelo de construção de redes sucessivas pode não ser o mais adequado para o estudo de determinadas propriedades mais refinadas.

No caso do comprimento de menor caminho médio, em ambos os conjuntos de dados (terremotos rasos e profundos) os valores encontrados apresentaram um crescimento linear com o número de camadas. Comportamento similar foi observado em redes monocamadas de terremotos do Irã [23], ao serem variados os tamanhos das células espaciais que definem os vértices. Assim, observa-se semelhança entre propriedades temporais e espaciais dos terremotos, sejam eles ocorridos em locais específicos do planeta ou em uma visão global.

Os valores de C e ℓ calculados para as redes *multiplex*, com número de camadas $M = 3$ para terremotos rasos, e $M = 5$ para terremotos profundos), foram usados para investigar a característica de mundo-pequeno nestas redes. Foi observado que apesar de possuírem um valor de ℓ proporcional ao logaritmo do número de vértices,

as redes não possuem um valor de $C \gg C_{aleat}$. Por conseguinte, essas redes *multiplex* não são do tipo mundo-pequeno.

Por fim, em [15] os autores propuseram uma metodologia aprimorada para a criação das ligações entre os vértices e, como foi apresentado no estudo, ela foi capaz de recuperar o regime livre de escala das distribuições de *strength* de redes monocamadas de terremotos globais. Além disso, ela forneceu características de mundo-pequeno não apenas para redes simples de terremotos regionais, como também para aquelas considerando eventos sísmicos de todo o globo. Assim, um dos trabalhos futuros será a aplicação desse modelo mais robusto para criar as ligações intracamadas e investigar a possibilidade da existência de propriedades livre de escala e mundo-pequeno.

Referências Bibliográficas

[1] Stefano Boccaletti, Ginestra Bianconi, Regino Criado, Charo I Del Genio, Jesús Gómez-Gardenes, Miguel Romance, Irene Sendina-Nadal, Zhen Wang, and Massimiliano Zanin. The structure and dynamics of multilayer networks. *Physics reports*, 544(1):1–122, 2014.

[2] Mikko Kivelä, Alex Arenas, Marc Barthelemy, James P Gleeson, Yamir Moreno, and Mason A Porter. Multilayer networks. *Journal of complex networks*, 2(3): 203–271, 2014.

[3] Manlio De Domenico. Multilayer networks: Analysis and visualization. *Introduction to muxViz with R. Cham: Springer*, 2022.

[4] Xianghua Li, Jingyi Guo, Chao Gao, Zhen Su, Deng Bao, and Zili Zhang. Network-based transportation system analysis: A case study in a mountain city. *Chaos, Solitons & Fractals*, 107:256–265, 2018.

[5] Yong Zhuang and Osman Yağan. Information propagation in clustered multilayer networks. *IEEE Transactions on Network Science and Engineering*, 3(4): 211–224, 2016.

[6] Petter Holme and Jari Saramäki. Temporal networks. *Physics reports*, 519(3): 97–125, 2012.

[7] Nastaran Lotfi, Amir Hossein Darooneh, and Francisco A Rodrigues. Centrality in earthquake multiplex networks. *Chaos: An Interdisciplinary Journal of Nonlinear Science*, 28(6):063113, 2018.

[8] Duncan J Watts and Steven H Strogatz. Collective dynamics of 'small-world'networks. *nature*, 393(6684):440–442, 1998.

[9] Marton Posfai and Albert-Laszlo Barabasi. *Network science*. Cambridge University Press, 2016.

[10] Manlio De Domenico, Albert Solé-Ribalta, Emanuele Cozzo, Mikko Kivelä, Yamir Moreno, Mason A Porter, Sergio Gómez, and Alex Arenas. Mathematical formulation of multilayer networks. *Physical Review X*, 3(4):041022, 2013.

[11] Emanuele Cozzo, Mikko Kivelä, Manlio De Domenico, Albert Solé-Ribalta, Alex Arenas, Sergio Gómez, Mason A Porter, and Yamir Moreno. Structure of triadic relations in multiplex networks. *New Journal of Physics*, 17(7):073029, 2015.

[12] Cliff Frohlich. The nature of deep-focus earthquakes. *Annual Review of Earth and Planetary Sciences*, 17:227, 1989.

[13] Cliff Frohlich. *Deep earthquakes*. Cambridge university press, UK, 1 edition, 2006.

[14] Douglas SR Ferreira, Andrés RR Papa, and Ronaldo Menezes. Small world picture of worldwide seismic events. *Physica A: Statistical Mechanics and its Applications*, 408:170–180, 2014.

[15] Douglas Ferreira, Jennifer Ribeiro, Andrés Papa, and Ronaldo Menezes. Towards evidence of long-range correlations in shallow seismic activities. *EPL (Europhysics Letters)*, 121(5):58003, 2018.

[16] Douglas SR Ferreira, Jennifer Ribeiro, Paulo SL Oliveira, André R Pimenta, Renato P Freitas, and Andrés RR Papa. Long-range correlation studies in deep earthquakes global series. *Physica A: Statistical Mechanics and its Applications*, 560:125146, 2020.

[17] Sumiyoshi Abe and Norikazu Suzuki. Small-world structure of earthquake network. *Physica A: Statistical Mechanics and its Applications*, 337(1-2):357–362, 2004.

[18] Gavin P Hayes, Emma K Meyers, James W Dewey, Richard W Briggs, Paul S Earle, Harley M Benz, Gregory M Smoczyk, Hanna E Flamme, William D Barnhart, Ryan D Gold, et al. Tectonic summaries of magnitude 7 and greater earthquakes from 2000 to 2015. Technical report, US Geological Survey, 2017.

[19] Cliff Frohlich. *Deep Earthquakes*. Cambridge University Press, 2006.

[20] Sumiyoshi Abe and Norikazu Suzuki. Complex-network description of seismicity. *Nonlinear Processes in Geophysics*, 13(2):145–150, 2006.

[21] Denisse Pasten, Sumiyoshi Abe, Victor Munoz, and Norikazu Suzuki. Scale-free and small-world properties of earthquake network in chile. *arXiv preprint arXiv:1005.5548*, 2010.

[22] Sumiyoshi Abe and Norikazu Suzuki. Scale-free network of earthquakes. *EPL (Europhysics Letters)*, 65(4):581, 2004.

[23] Nastaran Lotfi and Amir Hossein Darooneh. The earthquakes network: the role of cell size. *The European Physical Journal B*, 85:1–4, 2012.

[24] Denisse Pastén, Felipe Torres, Benjamín A Toledo, Víctor Muñoz, José Rogan, and Juan Alejandro Valdivia. Non-universal critical exponents in earthquake complex networks. *Physica A: Statistical Mechanics and its Applications*, 491: 445–452, 2018.

[25] D Chorozoglou, Eleftheria Papadimitriou, and Dimitris Kugiumtzis. Investigating small-world and scale-free structure of earthquake networks in greece. *Chaos, Solitons & Fractals*, 122:143–152, 2019.

[26] Duncan J Watts. Networks, dynamics, and the small-world phenomenon. *American Journal of sociology*, 105(2):493–527, 1999.

Capítulo 5

Considerações Finais

Nesta dissertação, aplicamos métodos de redes complexas e física estatística para investigar propriedades de terremotos ocorridos em escala mundial, sendo concluídos os pontos abordados a seguir.

Do ponto de vista da Mecânica Estatística Não-Extensiva, foram encontradas relações de escala em distribuições de distância, tempo e velocidade entre terremotos sucessivos gerados com um modelo OFC de topologia mundo-pequeno e terremotos globais, tanto rasos quanto profundos. Os gráficos apresentaram excelente concordância com uma função da família de funções de Tsallis, q-exponencial, que apresenta comportamento assintótico em lei de potência. Uma vez que essa função surge em sistemas de interações de longo alcance espaço-temporal, tal fato é um indicativo do comportamento não-extensivo no fenômeno sismológico.

Além disso, a concordância entre os resultados de terremotos sintéticos e reais sugere a presença da propriedade de criticalidade auto-organizada nesse sistema. Ademais, nossas descobertas apoiam a ideia de que a crosta terrestre acumula energia lentamente e a libera rapidamente por meio de falhas. O estudo realizado demonstrou ainda que o modelo OFC modificado fornece resultados melhores e mais consistentes do que o modelo *spring-block* 2D original, sendo uma excelente opção para se analisar propriedades de terremotos reais. Estes resultados estão apresentados no Capítulo 2 e foram publicados em *Chaos, Solitons & Fractals, 165 (2022) 112814, DOI: 10.1016/j.chaos.2022.112814.*

Em relação às redes complexas, foram utilizadas duas abordagens: redes monocamadas (simples) e redes multicamadas. No estudo de redes monocamadas de terremotos foram investigadas suas propriedades de correlação, considerando dados de terremotos reais rasos e profundos, e catálogos de terremotos simulados com o modelo OFC modificado. Os métodos de construção das redes foram dois: o modelo sucessivo e o modelo de janela de tempo.

As redes construídas para terremotos rasos usando ambos os modelos são assortativas, ou seja, *hubs* da rede tendem, em média, a estar mais ligados entre si do

que com outros vértices. Isso significa dizer que regiões do mundo onde ocorrem terremotos de grande magnitude possuem uma correlação entre si muito maior, do que com outras regiões, independentemente da distância entre elas. Foi observado que a rede criada com o modelo de janela de tempo apresenta comportamento muito mais assortativo. Resultados semelhantes foram encontrados para redes de eventos sísmicos na Califórnia e no Japão, em trabalhos prévios.

Em contraste, as redes de terremotos profundos não mostraram correlação entre a conectividade (grau) dos vértices, tanto para o modelo sucessivo quanto o modelo de janela de tempo. Ou seja, locais onde terremotos profundos ocorrem em todo o planeta não possuem um tipo de correlação específica, sendo encontrado comportamento neutro (aleatório). Os resultados permaneceram consistentes ao considerar diferentes restrições, como limites de magnitude e exclusão de eventos com profundidades fixas.

Essas descobertas sugerem que terremotos rasos e profundos têm diferentes propriedades de correlação temporal e espacial. Além disso, a rede criada para dados sintéticos do modelo OFC com topologia mundo-pequeno apresentou comportamento assortativo, assemelhando-se aos terremotos rasos. Estes resultados estão apresentados no Capítulo 3 e foram publicados em *Brazilian Journal of Geophysics, v.40, n.1. DOI: 10.22564/brjg.v40i1.2134.*

Finalmente, como mostrado no Capítulo 4, a aplicação de redes temporais *multiplex* construídas com o modelo sucessivo revelou propriedades em redes de terremotos que não eram visíveis em redes agregadas. As redes de terremotos rasos mostraram que certas regiões, como Japão, Ilhas de Sumatra, Tonga e Chile, são constantemente destacadas devido à alta ocorrência de terremotos. O terremoto de Sumatra, em 2004, demonstrou o aumento da atividade sísmica em locais próximos antes de um grande evento, resultando em um grande número de conexões entre as células nos anos subsequentes, mesmo a milhares de quilômetros de distância. Em contraste, as redes temporais de terremotos profundos exibiram menos variação na atividade sísmica ao longo do tempo, e as células se apresentaram localizadas, principalmente, em zonas de subducção.

As distribuições de *strength* dessas redes apresentaram comportamento de uma lei de potência com corte exponencial, sendo esse corte maior quanto maior o número de camadas. No entanto, foi observado que para determinado valor de camada as redes possuem maior regime livre de escala. O coeficiente de aglomeração global das redes *multiplex* rasas apresentou decaimento em lei de potência com o valor de camadas na rede, indicando invariância de escala nas relações entre esses parâmetros. Esse resultado não foi encontrado, entretanto, para as redes de eventos sísmicos profundos, tendo, na verdade, comportamento semelhante aos fornecidos por redes aleatórias similares. O comprimento de menor caminho médio em redes de terremo-

tos rasos e profundos demonstrou crescimento linear com o número de camadas.

Os resultados apontam similaridades e diferenças entre terremotos rasos e profundos, em diferentes situações. Ademais, notou-se que o modelo sucessivo possui limitações ao se analisar redes de epicentros. Dessa maneira, como perspectivas futuras, e continuação do presente trabalho, deve-se realizar análises e investigações de redes de terremotos utilizando diferentes modelos de criação de redes, de forma a produzir um melhor mapeamento do sistema de terremotos e suas características. Realizando então estudos de medidas topológicas e dinâmicas de redes para um melhor entendimento desse sistema, e a formulação de métodos de redes multicamadas mais robustos, que não seja somente *multiplex* (variação de camadas por profundidade dos terremotos, por exemplo).